Plasmonics (2024) 19:1303–1357
https://doi.org/10.1007/s11468-023-02034-1

REVIEW

Plasmonic Copper: Ways and Means of Achieving, Directing, and Utilizing Surface Plasmons

A. R. Indhu[1] · C. Dharanya[1] · Gnanaprakash Dharmalingam[1]

Received: 26 July 2023 / Accepted: 28 August 2023 / Published online: 5 October 2023

Abstract

Copper has been reclusive with regard to its plasmonic investigations among the founding plasmonic metals. With the advent of technology and the associated improvements in understanding of plasmonics, copper has been able to make a stand for itself among its peers and even outshine them in a few aspects such as dielectric loss, cost, and a more intricate and facile tuning of the near and far field intensities of the plasmon-enhanced distributions. This review is aimed at highlighting the different classes of plasmonic copper (PC), ranging from its pristine version to the array of composited and alloyed compositions. The focus is on an all-encompassing review of PC with regard to its shortcomings and merits, its exploration for plasmonic applications, and emerging phenomena discovered due to the plasmonic virtue. We aim to bring about a comprehensive treatise of the investigations on PC, where the major discussions are on the topics of a generic treatise on surface plasmons (both localized and propagating), pristine copper and its potential for different applications, the almost inescapable phenomenon of oxidation, and the associations that copper has been made to form in order to be exploited for multiple uses such as chalcogenides, silicides, alloys, and other metamaterial architectures. Specific outcomes of the changes to the near and far-field distributions of PC in various conditions such as oxidized/alloyed/composited and stabilized have been discussed, highlighting the changes to PC in lieu of these modifications. The concluding sections highlight some fascinating compositions including multi-elemental copper and its atomic clusters and cursorily studied compositions which are among the few materials that could offer untapped capabilities which will be made evident from brief glimpses of their plasmonic character. The outlook for plasmonic copper has never been more promising, ranging from the need for comprehensive investigations of emerging material compositions and configurations (of both pristine and composited copper) to the realm of commercialization. Copper has, thus, been projected to be a viable alternative to existing options including the poster children of plasmonics, namely, silver and gold.

Keywords Pristine Cu · Chalcogenides · Composites · Fluorescence · Oxidation

Introduction

Plasmonic nanoparticles have wide applications due to their fundamental virtue of being light manipulators, such as in sensing, catalysis, switches, waveguides, heaters, and theranostic agents [1]. Among the coinage metals, Cu has often had to take a back seat with regard to its promise in plasmonic applications due to the superior properties of the other two, among which stability and low optical loss are often attributed to be the reasons for their being frontrunners for plasmon-enhanced properties. As an example of the potentially inferior nature of Cu compared to Au and Ag, the degree of overlap between the inter-(excitonic) and intra-(plasmonic) bands of Cu nanoparticles (NPs) (≈ 0.03 eV) is much higher than Au and Ag, causing the LSPR absorption to be fundamentally less intense. This is all the more evident while considering the energy spacing between the 3 days and 4 s orbitals for Cu in comparison with Au and Ag [2]. Yet, plasmonic copper has rekindled the interest of researchers recently due to its promise as a replacement for Au and Ag in a myriad of applications such as for enhanced scattering, catalysis, and even non-linear optical (NLO) properties. In this review, we discuss how this has become possible with the advent of nanotechnology and nanomaterials. Specifically, with the evolution of synthesis techniques and

✉ Gnanaprakash Dharmalingam
dgp@psgias.ac.in

[1] Plasmonic Nanomaterials Laboratory, PSG Institute of Advanced Studies, Coimbatore, India 641004

fabrication technologies, delicate control of the oxidation of Cu is one such enabler, allowing the blooming of investigations aimed at replacing expensive plasmonic metals such as Au and Ag with Cu. We have attempted to highlight the prospect of Cu as a plasmonic metal by discussing its applicability towards every aspect of plasmonic research to the best of our reach of published literature.

We start with a discussion on plasmonics in general and the factors to be mindful of while trying to manipulate plasmonic behavior, with a restriction that only surface plasmon resonance (LSPR) is dealt with and not its companion, bulk plasmon resonance. We then discuss the two themes of research of pristine Cu plasmonics, viz., plasmonic Cu nanoparticles (CuNPs) and films. Attempts to be comprehensive in terms of the prospects of both these configurations have been made by a review of their promise for a wide array of applications. The very interesting and quintessential part of Cu plasmonics, that is, oxidation, is discussed subsequently. Oxidation can be avoided and completely reversed, as multiple investigations have revealed, and can even be beneficial when control is achieved of the oxidation rate and if permanent termination of the oxidation process can be intentionally induced. We then discuss the extensive avenue of Cu composites such as chalcogenides, carbides, silicides, alloys, multi-elemental composites, and other hitherto unexplored (from a plasmonic angle) compositions of Cu. Comprehensive discussions on often explored plasmon-enhanced properties, such as the use of this enhancement for theranostics, catalysis, energy storage, and Raman scattering along with unexplored/rarely explored aspects such as multi-elemental compositions (composed of Cu clusters with more than three elements) and applications such as NLO and electron emitting plasmonic sources, are attempted. As will be demonstrated from this review, the property of Cu being less expensive (and hence amenable for unconventional explorations in terms of composition and for mass production) and having a dielectric function that can be easily (due to inherently high reactivity) and intricately varied for manipulations of the plasmonic profile can make it the metal of choice for plasmonic applications. We conclude this review with a discussion of the myriad of aspects that are unaddressed/those that need a more rigorous confirmation and the avenues that are yet untouched by plasmonic Cu nanostructures, highlighting the conclusion that Cu plasmonics is an increasingly expanding area of the broader field of plasmonics.

SPP vs LSPR: A Brief Treatise

The collective excitation of free electrons at a metal–dielectric interface in response to an electromagnetic field is termed as plasmon resonance. The excitation being dependent intricately on the electronic structure of the material, the material constants such as the dielectric constant, rate constant of different types of excitations that can induce a plasmonic resonance etc. are important, and excellent reviews can be found elucidating the same [3]. This resonant oscillation can be very different when induced in continuous films compared to induction in discrete nanoparticles. In films, this excitation can lead to the generation of a propagating wave of plasmons (the surface plasmon polariton wave or SPP), whereas due to the localization of the excitation within the boundaries of a nanoparticle, it is termed as localized surface plasmon resonance (LSPR) when induced in them. We give here an overall understanding of the theoretical calculations which can help predict the defining attributes of the plasmon resonance such as the damping, the frequency, propagation constant, and the dielectric constants.

For a propagating wave at the interface between a dielectric and the metal, we can consider the situation illustrated in Fig. 1 [4], where 1 denotes the dielectric and 2 is the metal.

From classical electrodynamics defining the conditions for continuity of a wave between 1 and 2 and from Maxwell's equations which when solved allow computation of the fields created by the oscillating plasma of electrons, we get the relation between the wave vectors of the SPP in the metal and the dielectric as [4]

$$\frac{k_{1,Z}}{\varepsilon_1} = \frac{k_{2,Z}}{\varepsilon_2} \tag{1}$$

where k_1, k_2 are wave vectors and ε_1, ε_2 are the dielectric constants.

From this relation, it is evident that the plasmon wave can exist at the interface only for the condition of $\varepsilon_1 = -\varepsilon_2$, that the wave exists only at frequencies of negative values of the dielectric function, and that the wave can exist only at the interface on the assumption of an exponential decay away from it, as shown in Fig. 2 [4].

The propagation constant of the SPP is given as [5]

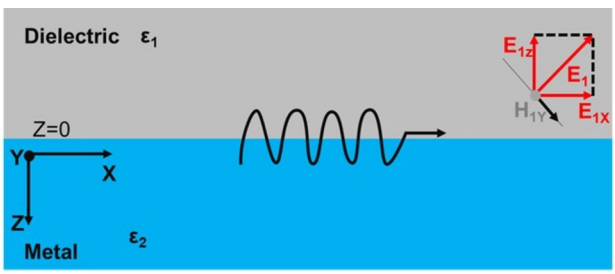

Fig. 1 Propagating SPP wave at the interface between a metal and a dielectric

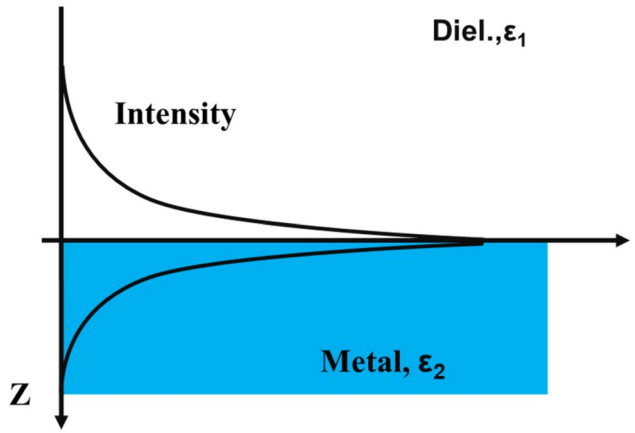

Fig. 2 The field of the propagating plasmon wave at the interface where it decays with different degrees into the respective media

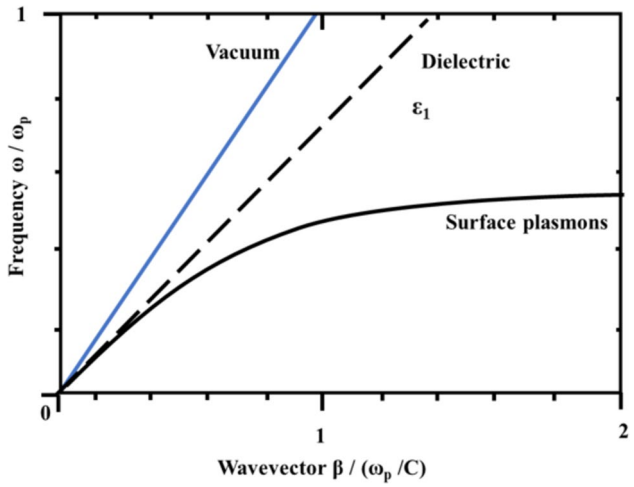

Fig. 3 Dispersion relation between wave vector and frequency of light in a vacuum, in a dielectric, and of surface plasmons

$$k_{sp} = \frac{\omega}{c}\left[\frac{\varepsilon_r \varepsilon(\omega)}{\varepsilon_r + \varepsilon(\omega)}\right]^{1/2} \tag{2}$$

where k_{sp} is the wavenumber of surface plasmon polariton, $\varepsilon(\omega)$ is the dielectric constant as a function of frequency, and c is the speed of light.

As briefly mentioned, the condition for the SPP constrained to the interface dictates an exponential decay away from it. The penetration depth of the evanescent field of the SPP away from the interface is hence different for the dielectric and the metal, where this distance is referred to as the skin depth for the latter. The value of this propagation length (L_{sp}) is arrived at from the imaginary part of the SPP wavenumber [5]

$$\frac{1}{L_{sp}} = 2Imk_{sp} = \frac{\omega}{c}\frac{\varepsilon_1^{\frac{3}{2}}\varepsilon_2(\omega)}{|\varepsilon_1(\omega)|^{\frac{1}{2}}(|\varepsilon_1(\omega)| - \varepsilon_1)^{3/2}} \tag{3}$$

The discussion so far defining the nature of the SPP once induced, it is important that the SPP also needs to couple with the incoming electromagnetic wave for resonant excitation and hence requires both frequency and wave vector matching with it (in contrast to localized surface plasmons (LSPs) which do not as they are not a propagating wave). This can happen only when the condition of momentum matching is satisfied between the two waves. It is to be kept in mind that the momentum of the SPP is always greater than that of a free space photon, as shown in Fig. 3 [4] which illustrates the dispersion relation of the plasmon wave. Various means of achieving this coupling exist and are broadly classified as through photon tunneling (through the configurations pioneered by Otto and Kretschmann) and through diffraction coupling (through the employment of scattering features such as gratings on the metallic films), although other unconventional methods such as through electron tunneling and LSP scattering have also been reported.

With the defining attributes of the SPP being described until this juncture, we will attempt to describe similar attributes for the second type of resonating plasmons, i.e., LSPs. LSPs are electrostatic oscillations in contrast to propagating SPPs and can arise both in films (on confined areas such as roughness features) and in bound geometries such as nanoparticles. The location and width of LSPs are defined by the particle size/shape, composition, and the dielectric environment around it. In deriving the characteristic oscillation frequency of the LSPs, one starts with calculating the displacement of the collective plasmon oscillation (termed as dielectric displacement, D) in relation to the incident electric field (E) of the incident electromagnetic wave as [6]

$$D = \varepsilon_0 E + P \tag{4}$$

where P is the polarization density which is

$$P = nex \tag{5}$$

The number density being (n) and e is the charge of the electron, and the value of x is arrived at by solving the equation of motion of a free electron with mass m, given by [4]

$$m\ddot{x} + m\gamma\dot{x} = -eE \tag{6}$$

Solving the equation and inserting the displacement x into the equation for D gives the expression for the bulk plasma frequency (ω),

$$D = \varepsilon_0\left(1 - \frac{\omega_p^2}{\omega^2 + i\gamma\omega}\right)E \tag{7}$$

where $\omega_p = \sqrt{(\frac{e^2 n}{\epsilon_0 m})}$ is the natural frequency of oscillation of the electron cloud (the plasma frequency), γ the damping parameter, and ε_0 the dielectric permittivity of free space.

One of the constitutive relations of linear isotropic materials with a permittivity ε is that [7]

$$D = \varepsilon_0 \varepsilon E \tag{8}$$

On comparing the relations for D, we get

$$\varepsilon(\omega) = (1 - \frac{\omega_p^2}{\omega^2 + i\gamma\omega}) \tag{9}$$

For frequencies close to ω_p, the temporal duration of damping events is quite low (approaching femto seconds and thus, close to 10^{15} Hz), leading to an often-made approximation that damping can be ignored, leading to [8]

$$\varepsilon(\omega) = (1 - \frac{\omega_p^2}{\omega^2}) \tag{10}$$

This relation can be modified to incorporate the dielectric permittivity of the material around the plasmonic entity by establishing the relation between the dielectric constants of the two. For this purpose, the extinction of light by a nanoparticle at the resonance condition needs to be examined. The quantification of this extinction is through the calculation of the extinction cross-section (a combination of the scattering and absorption cross-sections). For a spherical nanoparticle and under the quasistatic approximation (of a homogeneous polarization or a dipolar resonance), the absorption cross-section is given by [9]

$$c_a = \frac{4\pi^2 R^3 N \varepsilon_s^{3/2}}{\lambda} \frac{\varepsilon_i}{(\varepsilon_r + 2\varepsilon_s)^2 + \varepsilon_2^2} \tag{11}$$

where ε_s is the dielectric function of the surrounding medium, $\varepsilon_r, \varepsilon_i$ are the real and imaginary parts of dielectric constants of the material (nanoparticle) exhibiting SPR, N is the conduction electron density of the nanoparticle, and R is the radius of the nanoparticle.

For resonance to occur and hence the maximization of absorption [10], the condition

$$\varepsilon_1 = -2\varepsilon_s \tag{12}$$

can hence be arrived at for spherical nanoparticles. Equation (10) then becomes

$$\omega = \frac{\omega_p}{\sqrt{2\varepsilon_s + 1}} \tag{13}$$

which intimately ties the resonance frequency with the free electron density and the dielectric constant of the surrounding material. It is to be noted here that the value of 2 is only valid for spherical nanoparticles, and for other morphologies, it needs to be modified accordingly. For example, the case of nanorods changes the value to $((1\text{-}p_f)/p_f)$, where p_f is the depolarization factor that is determined from the nanorod aspect ratio. In actual materials, there is often an overlap between the energies at which inter-band transitions occur and the SPR. To account for this and the fact that the damping of the resonance is not negligible and is contributed to by scattering from lattice entities (phonons, defects, impurities, other fermions (Γ_b)), the surface (for particle sizes approaching the mean free path of the material ((Γ_s))), and radiative damping (Γ_r), the relation (10) is written as [11]

$$\epsilon_r = \epsilon_{\text{inter}} + 1 - \frac{\omega^2}{\omega_p^2 + (\Gamma_b + \Gamma_s + \Gamma_r)^2} \tag{14}$$

where $\varepsilon_{\text{inter}}$ is the interband transition, and damping constants are given by

$$\Gamma_b = {}^{\nu_F}/_{l_\infty} \tag{15}$$

$$\Gamma_s = \gamma_0 + \frac{A\nu_F}{R} \tag{16}$$

$$\Gamma_r = 2hkV \tag{17}$$

where ν_F is the fermi velocity of electrons, l_∞ is the mean free path of the conduction electrons in bulk, γ_0 is the bulk damping constant, A is a theory-dependent parameter which is dependent on the type of the scattering process, R is the radius of the metal nanosphere, h is Planck's constant, V is the volume of nanoparticle, and k is a constant that can be arrived at from the graph relating the resonance energy of the plasmon with the measured experimental linewidth. The plasmon frequency hence changes to [12]

$$\omega = \sqrt{\frac{\omega_p^2}{1 + \varepsilon_{ib1} + 2\varepsilon_s} - \gamma^2} \tag{18}$$

where ε_{ib1} denotes the contribution of interband transitions to the real part of the nanoparticle permittivity.

It is to be kept in mind that for obtaining the cross-sections for non-spherical particles (such as nanostars and nano dendrites), computational methods tuned to sufficiently simulate complex shapes are often necessary. Methods based on the discrete dipole approximation (DDA) such as the finite-difference time-domain (FDTD) analysis have been typically used to simulate the optical properties [13] that arise in such non-spherical plasmonic structures. FDTD algorithms solve the differential form of Maxwell's equations by assuming appropriate boundary conditions and discretizing the space and time domain to

find the electric and magnetic fields at different positions and time steps of the structure under examination.

The brief treatise in this section on the characteristics of surface plasmons enables multiple insights to be arrived at. The prediction of the plasmonic property has reached a level of maturity that lattice-level manipulations of materials and the resulting changes/induction of plasmonic virtues can be simulated knowing the equations above and incorporating appropriate boundary conditions, as will be discussed in subsequent sections. An intuitive conclusion from the comparison of SPPs and LSPs is that the latter can be much more amenable in terms of tuning compared to the former, considering the ease of excitation (due to no requirement of frequency as well as wave vector matching), the number of variables that exist for the tuning investigations, the inherent stability of discrete nanostructures than continuous films (one reason for which is the requirement of lattice matching for plasmonic films in order to have a reasonable durability when subjected to practical conditions), and the ease of synthesis (with films requiring in many cases cost prohibitive equipment). However, SPPs are worthy on their own, especially in terms of achieving resonances that are hybrids with other similar modes possible on manipulating the configurations of the films, as will be shown in later sections. It stands that the application dictates in almost every instance the choice between a film vs nanoparticle configuration, as other dictating entities such as difficulties in fabrication and compositions usually do not exist due to the rapid evolution of technology.

Plasmon-Enhanced Properties due to Nanostructured Copper

This section has been elaborated with the contextual flow of an introductory section on synthesis of CuNPs followed by the different investigations that have reported pristine as well as modified plasmonic Cu nanostructures.

Synthesis Techniques of Plasmonic Copper

A brief description of the methods and their evolutions for the synthesis of structured/morphologically controlled copper nano/microparticles and the associated changes to the LSPR properties is relevant to understanding the achievement of tuned light absorption. Simple solution-based methods such as chemical reduction [14, 15] often lead to the problems of agglomeration and the coupled loss/deterioration of the absorption properties. Oxidation in particular is a significant problem for CuNPs, with Cu_2O or CuO forming as a result depending on whether the medium is alkaline or acidic/neutral, the processing conditions, and the use of capping agents. Plasmonic properties are lost as a result due to the transition from metallic Cu to a semiconducting oxide [16]. Capping agents such as polyvinylpyrrolidone (PVP) and polyethylene glycol (PEG) can help in this regard, although differences in dispersion/agglomeration based on the choice of such agents must be kept in mind. For example, PVP has been reported to stabilize CuNPs against oxidation in a considerably better manner than PEG [17]. Techniques such as anodic stripping voltammetry can reveal the ease with which capped nanoparticles are oxidized, and analogous studies on Ag NPs which also oxidize readily report that PVP is better at preventing oxidation than PEG [18]. We have included an explicit section of how oxidation in Cu can be detrimental/prevented/exploited for and in various applications. Distinct morphologies such as nanorods and spheres, with differing degrees of sizes, oxidation, and agglomeration are possible by modifying the Cu precursors (such as $Cu(DS)_2$ instead of $CuSO_4$) and surfactant concentrations [19]. It is also possible to control agglomeration and oxidation through the use of halides such as iodine and bromine, with CuI demonstrating the best colloidal stability due to stronger attraction between Cu and I atoms and hence a more dispersed colloid (the product solubility constant quantifies this comparison between halides such as Cl, Br, and I as stabilizers) [20].

With the purpose of this review being on the different plasmonic investigations on Cu, the discussion on the synthesis modalities has been given a very cursory treatment. However, an exhaustive but incomplete summary of the shapes and sizes of Cu nano/microparticles and the methods of synthesis is presented in Table 1, and review articles on the synthesis methods for Cu [21] are also referred to the reader for a more comprehensive/specific list.

Plasmon-Enhanced Properties from Discrete and Pristine Copper Nanoparticles

Cu Plasmons for Photoemission

Sub-wavelength features are frontrunners of the need for tuned LSPR and SPP. They have been reported to enhance multiple properties such as Raman scattering, fluorescence, second harmonic generation, catalysis etc. due in major part to the coupling between the enhanced electromagnetic field resulting from the plasmons with the phenomena responsible for the individual properties [71–74]. As an example of the probing into such features, a 100-fold increase in the charge density extracted due to photoemission of electrons from a nanostructured Cu surface has been reported. The surface consisted of patterned (through ion beam milling) nanoholes on a single crystalline Cu surface. Tuning of the absorption wavelength was pronounced while changing the spacing between the holes and much lesser while changing their dimensions and/or shapes, allowing

Table 1 Summary of a few morphological investigations on Cu nano/microparticles with the SPR peak locations and the synthesis method

S. no.	Synthesis method	Morphology (nano)	Dimensions (nm)	SPR wavelength (nm)	Ref.
1	**Chemical reduction**	Spheres	43–45	561–572	[17]
2		Spheres	1.3–4.7	587	[22]
3		Spheres	4–7	–	[23]
4		Spheres	10	573	[24]
5		Flowers	2–4	554	[25]
6		Spheres	2.5	600	[26]
7		Spheres	1000	–	[27]
8		Shells	Core: 63; shell: 30	550–720	[28]
9		Spheres	2–20	560	[29]
10		Plates	Dia: 48; thickness: 17	600	[30]
11		Spheres	23	576	[31]
12		Cubes	Edge length = 28	700	[32]
13		Cubes	Edge length = 30	620	[33]
14		Wires	24	591	[34]
15		Spheres	5–25	591	[35]
16		Spheres	2500–2800	–	[36]
17		Spheres	100	570	[37]
18		Spheres	40	580	[38]
19		Wires	Aspect ratio = 5700	–	[39]
20		Spheres	1500	–	[40]
21		Spheres	5.1	577	[41]
22		Spheres	1.3–1.8	570	[42]
23		Wires	Aspect ratio = 350–450	590	[43]
24		Hexagon	Edge length = 50	565	[44]
25		Cubes	100	610	[45]
26		Clusters	1	443	[46]
27		Rods	Dia = 20	695	[47]
28		Rods	Aspect ratio = 2.8–35	762–2201	[48]
29	**Supramolecular assembly**	Disks, prisms, cylinders	Dia: 14.8	650	[49]
			Size: 13.5	650	
			Aspect ratio: 1.7	560,650	
30		Spheres	16	580	[50]
31		Cluster	1.4–2.8	570	[51]
32	**Polyol**	Spheres	65	–	[52]
33		Spheres	45	–	[53]
34	**Pulsed laser ablation**	Spheres	1–7	609–626	[54]
35		Spheres	10–14.3	595–626	[55]
36	**Electron beam irradiation**	Spheres	25	–	[56]
37		Spheres	30–70	670–730	[57]
38	**Hot injection**	Cubes	Edge length = 75	588	[58]
39		Spheres	108–300	–	[59]
40	**Wet chemical**	Wires	Aspect ratio: 4	620–626	[60]
41	**Hydrothermal**	Hexagons	600–900	608	[61]
42		Tubes	Length = 30–80; dia = 8–12	550–650	[62]
43	**Microwave**	Spheres, rods	10–70	–	[63]
44		Spheres	7.2	560	[64]
45		Spheres	3	278	[65]
46		Crystals	2.3	275	[66]

Table 1 (continued)

S. no.	Synthesis method	Morphology (nano)	Dimensions (nm)	SPR wavelength (nm)	Ref.
47	**Microemulsion**	Clusters	3	450	[67]
48		Spheres	4	570	[68]
49		Truncated triangular nanoplates	Size = 60; width = 22	565–585	[69]
50		Spheres	300–500	430–630	[70]

close as well as a wide control of the absorption wavelength. Since photoemission can occur through multiple processes such as the three-step process and field-assisted emission, the Keldysh parameter was used to justify that photoemission was due to enhancements to the three-step process of electron emission from a surface rather than due to field emission. Limitations of a reduced damage threshold necessitated the reduction of the input laser fluence by five times compared to a flat surface [75]. The reason for the enhanced photoemission was postulated to be due to the efficient absorption of the incident photon energy and the transfer of this energy through plasmon decay to the ejected electrons. Such manipulations of metallic surfaces promise their usability as sources of electron beams despite their intrinsically low quantum efficiencies.

Cu Plasmonics in Energy

The concept of solar energy harvesting using nanomaterials has become increasingly relevant with time, with applications that utilize this energy including current generation, anti-reflective coatings, and heating [76]. The process of solar energy utilization through increasing carrier generation in conventionally employed materials (such as through plasmonic absorption as well as energy transfer) is a highly researched one. Briefly, the absorbed solar energy by the plasmonic oscillation is transferred to hot electron–hole pairs (in the regime of femtoseconds) from the plasmon decay [77]. Cu and Au have advantages as attractive materials in this regard as both intraband and interband transitions can be excited by visible light (the latter being 2.14 eV for Cu and 2.4 eV for Au), a major part of the solar spectrum [78]. The lower interband transitional energy of Cu generates hot electrons (inner shell electrons in the vicinity of the plasmons) of higher energy due to the close overlap. Additionally, comparing these two, Au has a higher work function (5.1 eV) than Cu (4.65 eV) [79], and Cu, therefore, can form lower energy barriers (for e^- transfer) with electron-accepting materials such as TiO_2. Indeed, Cu plasmonic systems in both film and NP configurations have been extensively investigated for photocatalysis when composited with TiO_2 for example [80]. Additionally, theoretical calculations of the hot carrier energies that can result from plasmon decay through direct vs phonon-assisted processes predict that the hot carriers can have a higher energy than the decaying plasmon energy due to the higher density of states (DOS) in the *d* bands of Cu [81]. All of these reasons make Cu a theoretically promising material for solar photovoltaics and for energy harvesting and storage applications. A detailed analysis of this comparison between Au and Cu has confirmed that the predictions are true in terms of the photocurrent generated as a result of hot carrier injection from Au vs from Cu. Cu exhibited photocurrent increases due to contributions to hot carrier injection from both the inter (550 nm) and intraband (675 nm) transition regimes, whereas Au exhibited this increase for only the plasmonic excitation due to the higher barrier Schottky barrier that the interband transition generated hot electrons could not overcome. Care must be taken however in designing the interface between plasmonic Cu and the matrix, as the distance between the plasmon-generated hot carriers (confined to near surface regions) and the electron acceptor must be at the maximum the mean free path of the hot electrons (~ 30 nm) to prevent their thermalization within Cu itself [82]. With regards to PC for energy applications, the intricacies in the processes of thermalization and scattering have been an important focal point, as summarized in Fig. 4.

Notably, the higher imaginary component of Cu in comparison to Au and Ag at wavelengths corresponding to the dipolar resonance means that the plasmon peak is significantly damped at these wavelengths, compared in Fig. 5, adapted from the excellent work of Barbara et al. [88].

A tuning in LSPR location and intensity has been reported by a simple switching of the anions used for controlling solution pH between Cl^- and SO_4^{2-}, wherein the former was able to selectively adsorb on the growing CuNPs and cause variations in the final morphologies and crystallinities. These variations led to an optimal temperature increase of 40 °C when used for LSPR-based PT heating, with a resulting promise for use as an antibacterial agent [93]. It is important to note here that the depression of the melting point of nanoparticles compared to their bulk counterparts (depending on parameters like strain, morphology, defect chemistry, crystallographic orientation of the surface, size, and shape) must be taken care of while designing them for PPT applications. Multiple studies have investigated the same, reporting significant differences from the bulk melting point of approx. 1358 K.

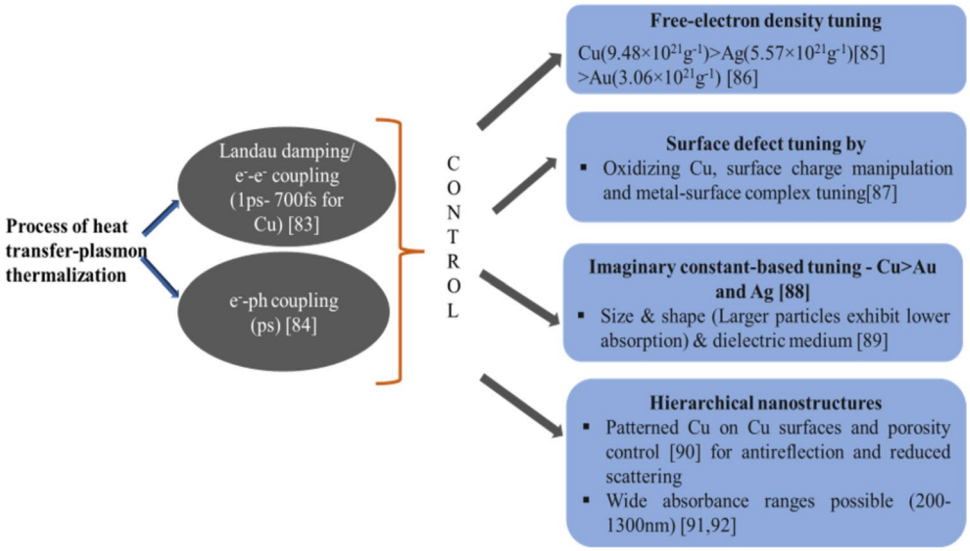

Fig. 4 Summary on the investigations on PC for energy applications [83–92]

Spheres of diameters 30 nm have their melting points as low as 450 K [94], and rods of dimensions undergo melting transitions at 673 K [95]. The PPT property can intuitively be also employed for therapy, wherein highly localized increases of temperature can kill cancerous/malignant cells [96]. The tunability of the plasmonic property is almost mandatory for such applications, as the ability to synthesize nanomaterials that absorb in the biological transparency window (650–1350 nm) is vital for in vivo therapy. CuNPs, either present alone in pertinent morphologies such as nanowires (NWs) [97] or along with a biocompatible support that helps in dispersion, have been

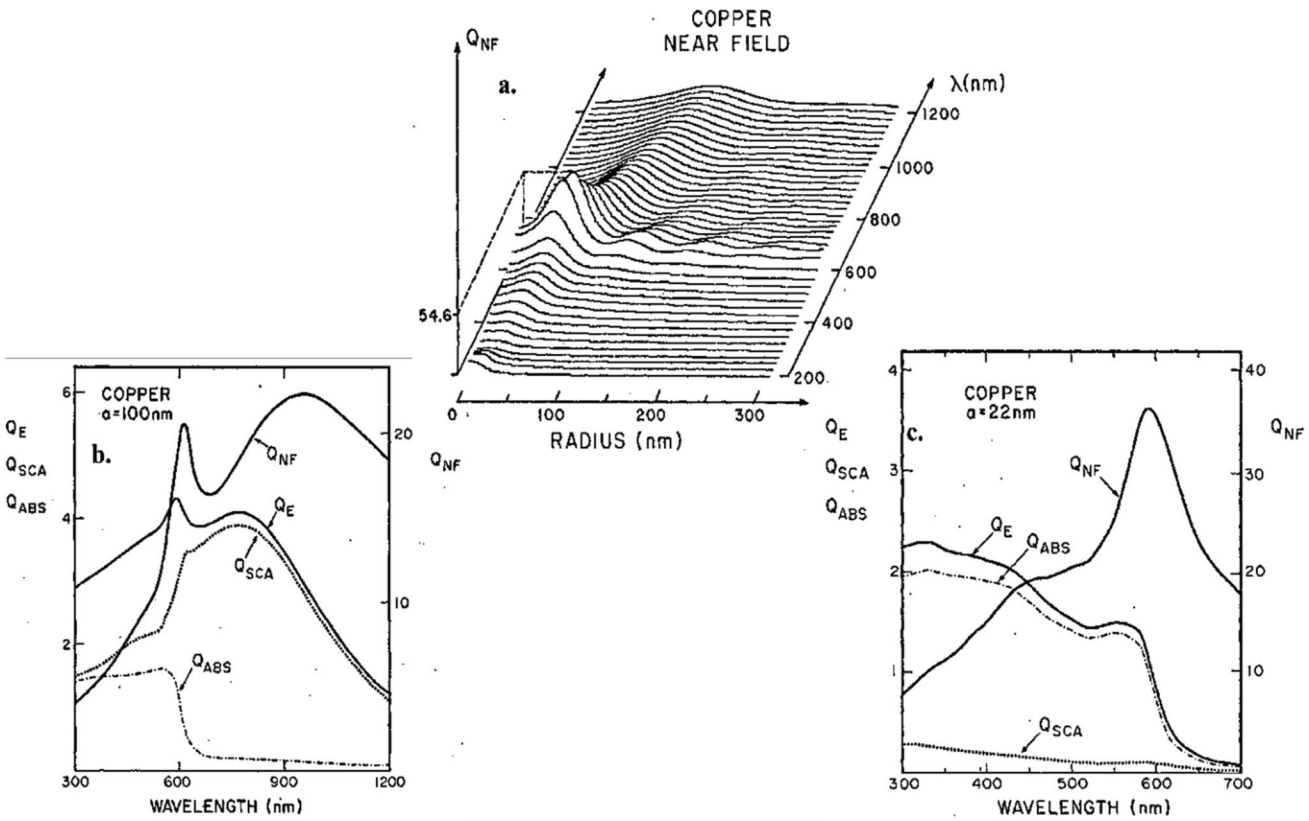

Fig. 5 **a** Near-field scattering efficiency of Cu-water interface for different radii of spherical particles. Extinction, far-field scattering, and absorption efficiency of Cu spheres with different radii; **b** 100 nm and **c** 22 nm in water (reproduced with permission from [88])

explored with this motive. Where a temperature difference of a few degrees can be the difference between live tissue and one that can be neutralized, plasmonic heating with CuNPs can easily achieve temperature increases of 20–35 degrees [98]. A comprehensive summary of the different morphologies of Cu and Cu systems investigated exclusively for PPT applications can be found in [99].

Cu Plasmonics for Catalysis

The concept of PT heating is also of use in catalysis, termed photocatalysis, or PT catalysis [100, 101]. The obvious increase in reaction rates with temperature makes plasmonic materials that convert light into heat suitable candidates here. An important advantage of plasmonic nanomaterials in catalysis is the ability to achieve selectivity, as the energy of the hot carriers that are generated from plasmon decay depends on the plasmon characteristics [102]. All the three mechanisms of plasmon damping, viz., radiative damping into photons, Landau's damping, and non-radiative hot electron–hole pair generation can lead to enhancements in catalytic rates. Indeed, these mechanisms have been shown in founding research wherein the photo-induced oxidative switching between Cu_2O/Cu resulted in the increase in epoxidation of propylene, an important reaction in simplifying plastic manufacturing. The energy deposition by the plasmons into the Cu_2O shell was shown to convert it into pristine Cu and restore the catalytic property. The only requirement seemed to be that of the irradiation power, where only intensities above 550 mW/cm^2 could cause this change in oxidation state [103]. Cross-coupling (C-C) reactions are a class of catalytic process in which complex products are formed from simpler entities. Core–shell nanocubes of Cu@Ni were able to catalyze and improve the yield by 62% of the C-C reaction of boric acid, due to the enhancement in the reaction rate provided by the absorption of light by plasmonic Cu and its conversion into heat. Compared to conventional methods of providing heat such as through a thermal transfer-based process, plasmonic heating was found to be more efficient [104]. A summary of the investigations on mechanistic aspects of PC catalysis has been compiled and presented in Fig. 6. Ag and Cu nanoparticles were compared for their catalytic enhancement rates in the oxidation of ferrocyanide, with the observation that CuNPs had an order of magnitude higher catalytic activity than Ag, yet with an accompanying limitation of a much higher oxidation-induced rate loss and leaching from the support material. Deconvolutions of the photocatalytic vs PPT mechanisms of enhancements were not performed (although possible with specialized techniques such as scanning electrochemical microscopy [105]), which would have allowed discerning the results in terms of the PT efficiency of Ag and Cu [106].

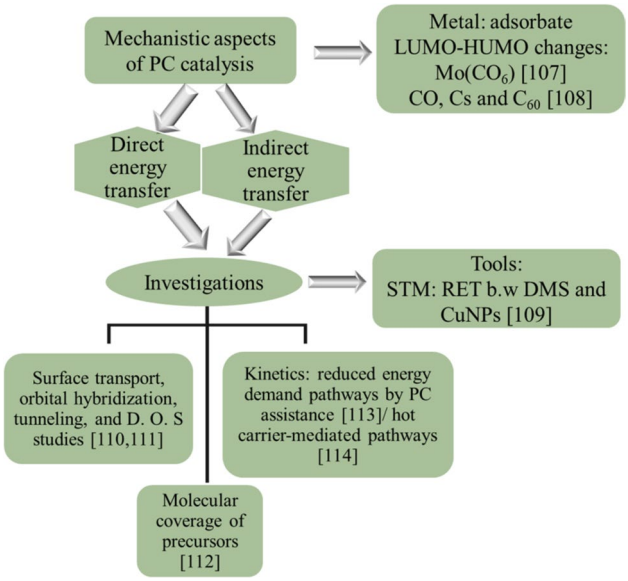

Fig. 6 An overview of different reports on the employment of PC for catalysis [107–114]

CuNPs for Enhanced/Directed Scattering of Photons: Fluorescence, Enhanced Raman Studies, and Luminescence

Since LSPR and SPP predominantly talk about absorption and scattering of light, one can intuit that the property of luminescence by materials distal to plasmonic materials can be significantly enhanced and/or altered. Properties such as fluorescence [115, 116], phosphorescence [117], and chemiluminescence [118] have been reported to be enhanced due to coupling of the fluorophores' scattering transitions with surface plasmons and their oscillating electromagnetic field. The enhancements to fluorescence are conventionally examined through two material systems. One is where Cu alone is studied for changes in scattering as a function of particle size/environment/film thickness, roughness, and material composition. The second approach is to study the enhancements to the emission of fluorophores that are used for a myriad of applications, as a function of extremely varied parameters such as the size/shape/dielectric/composition of the Cu or the composition/distance and conjugation intensity of the fluorophore. Cu alone when present at sizes down to 12 nm exhibited an enhancement in fluorescence yield by 4 orders of magnitude (5 for 30 nm particles) compared to bulk Cu in one study [87], due in part to the enhanced local electromagnetic fields that increased the quantum yield by coupling with the incoming and outgoing photons and in part to the second harmonic generation (SHG) of LSPR [119]. Another study revealed that roughened films can enhance the emission only when the excitation energy is close to the LSPR that occurs at the local roughness features, and that the enhancement is absent for the higher energy

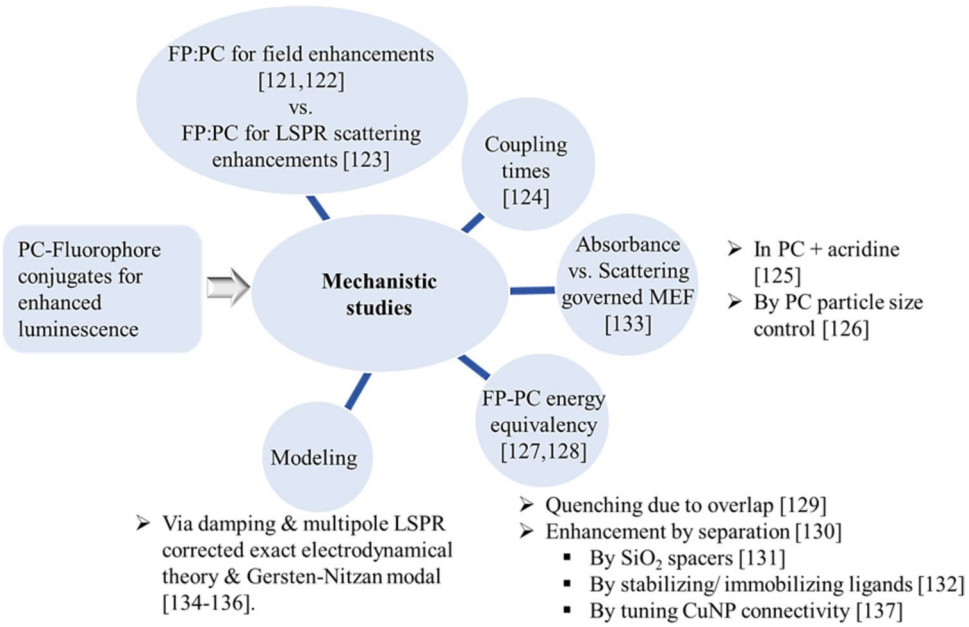

Fig. 7 Investigations revealing enhancements to photon scattering using PC [121–137]

emissions (such as the emission from the second d band of Cu centered at 3.50 eV [120]. An important observation from this study was that this absence in enhancement for the rough surface was due to the quenching of the emitted photons by the roughness features themselves, although it is probable that the absence of coupling between the LSPR (occurring at approx. 2.15 eV) and the 3.50 eV emission could be the primary cause. Enhancements to the luminescence property in particular of different PC conjugates have been compiled in Fig. 7.

A simple but excellent illustration clarifies the reasons to the observed enhancements, as shown in Fig. 8 [134]. Multiple studies that have explored PC exclusively for enhancements to scattered Raman profiles have been illustrated in Fig. 9 along with a few unusual explorations of PC for display applications.

As shown in Fig. 10, drastic changes could be achieved in the absorbance wavelengths when PC was explored as a candidate material for displays [149].

Plasmonic CuNPs for Non-Linear Optics

One of the manifestations of the nonlinearity in optical properties (NLO) is second harmonic generation (SHG), which is the frequency doubling of photons when passed through a non-linear material and has huge potential, for example, in realizing high-energy lasers, specifically those with tailored wavelengths (instead of only the typically available wavelengths that are limited in terms of their length by the material's electronic structure). Local field enhancements are a crucial reason for the enhancements to both SHG and SERS, and measurements of the same can be helpful in comparing and choosing the appropriate plasmonic material of choice. In this regard, the drastic drop in field enhancements for excitation wavelengths below approx. 650 nm (due to an increased damping of the resonance from inter-band excitons) necessitates this as a limit for plasmon-enhanced SHG from Cu [158]. Of the very few studies that have explored the NLO potential of Cu, that of PVP-protected CuNPs revealed third-order nonlinear susceptibilities equivalent to that of AuNPs, leading to their prospective potential in four-wave mixing. The plasmonic component being the reason for this observation was not discussed; however, it is probable that the LSPR excitation played a part here as

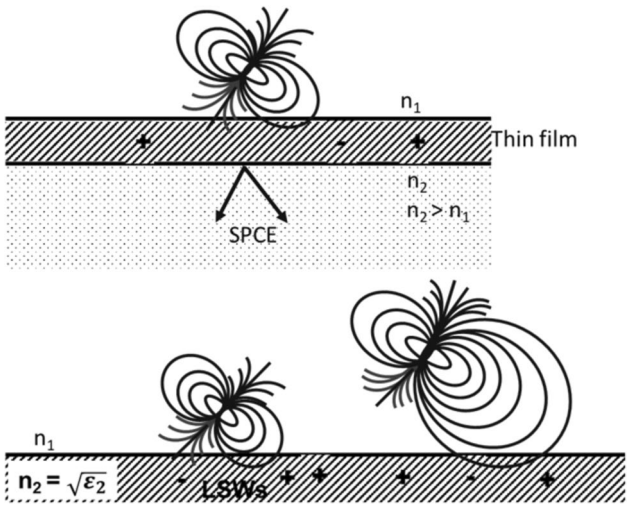

Fig. 8 Enhanced fluorophore interacting with a metal surface via the near-field or the far-field for the cases of region 1 (~50 nm) or distant (≥500 nm)

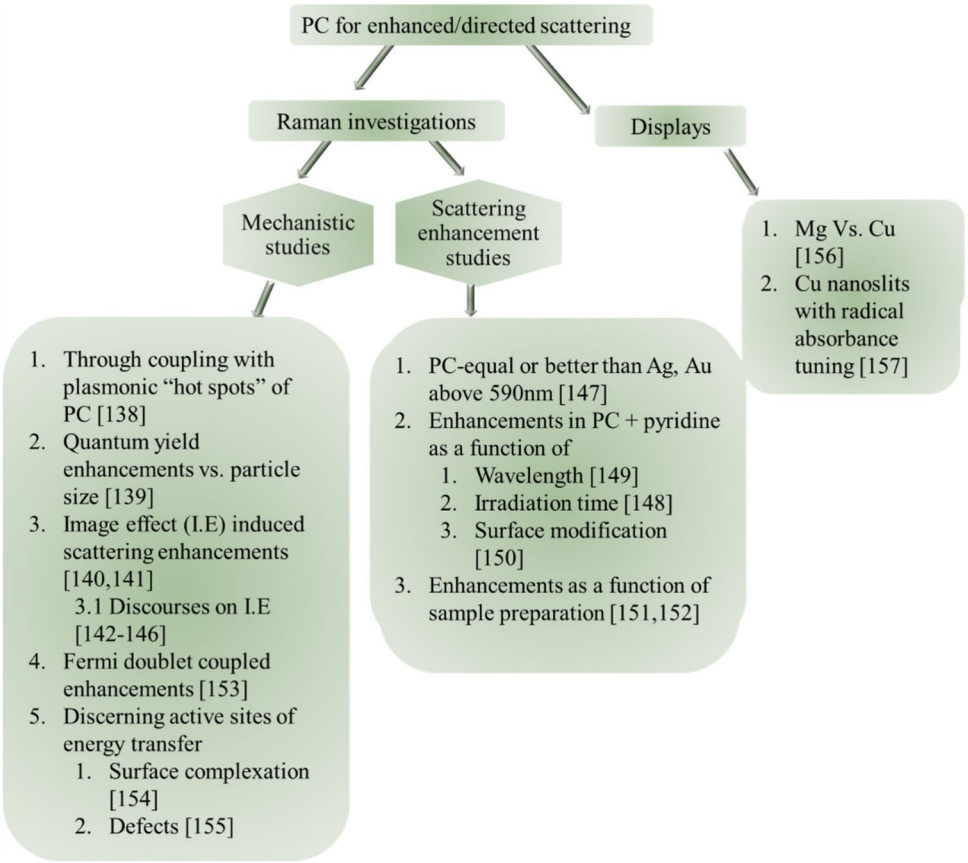

Fig. 9 PC studied exclusively for enhanced Raman scattering applications as well as those rare studies on PC for displays [138–157]

the excitation wavelength used close to that of the LSPR of CuNPs [159]. From the myriad of investigations that report the possibilities of non-linear SHG on multiple plasmonic materials [160–165], it is proposed that the potential of Cu for the same is at a very nascent stage of study.

Cu Plasmonics for Sensing

Sensing with CuNPs alone without a protective layer presents problems in terms of oxidation, as will be discussed in subsequent sections. However, different architectures incorporating Cu in the nanometer sizes have been explored regardless. An example is the use of thickness-controlled deposited Cu shells on a SiO_2 island, with the prediction of a higher refractive index (compared to air) and bio-compatible SiO_2 being more suitable for a red-shifted and stable plasmon. The influence of thickness was detrimental post 30 nm, for which the highest intensities of absorption were observed. The use of these capped Cu shells for DNA sensing was investigated, and sensitivities down to 10 fM were reported [166]. A general comment here is that for sensing with CuNPs formed from film deposition and annealing, the relation between the thickness of films and the observed plasmonic attributes such as intensities, positions, peak widths, and stability is not always universal, as other factors such as packing density (which controls light penetration) and surface faceting of the islands of Cu that are finally achieved also play a role. CuNPs have been investigated for colorimetric sensing as well, with

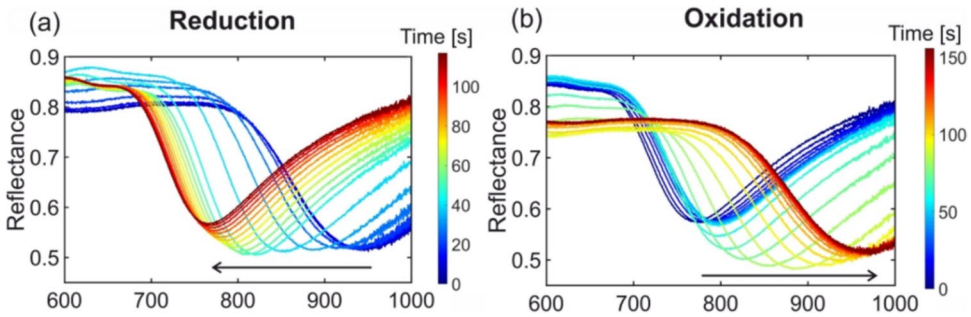

Fig. 10 Spectral response of the nanostructured plasmonic copper film with thickness, length, and width of the slits is 30 nm 140 nm, and 60 nm respectively, and periodicity in *x*- and *y*-direction 300 nm during **a** reduction and **b** oxidation (reproduced with the permission from [148])

the ability to detect sulfide ions at concentrations between 12.5 and 50 μM. Interestingly, the oxidation of the synthesized nanoparticles did not happen for a few days, attributed to being stored in airproof vials and the protective nature of the CTAB ligands used during synthesis [167]. These are among the few studies that have explored the potential of discrete nanoparticles of Cu for sensing, more investigations being limited mainly by the tendency for oxidation and probably difficulties in achieving unique morphologies that can be better in terms of the plasmonic properties compared to conventional spherical ones.

We have so far presented an overview of the different purposes for which Cu has been explored in the nanoparticle form for plasmonic applications and explorations. The other construction of plasmonic Cu is the Cu film, wherein interesting plasmonic phenomena can be invoked apart from the traditional SPP wave. The different applications, limitations, solutions, and outlook on the use of Cu films exploiting in particular the SPP characteristics are discussed in the subsequent sections.

Copper Plasmonics in Films

Plasmonic Cu Films for Sensing

The field of sensing is a prime area of application for plasmonic films, due to the inherent interface sensitivity of the plasmon to charge interactions. Films of Cu have also been explored in this regard, although with the consideration that a protective dielectric be deposited on the film to avoid oxidation. With this ideology of fabrication, films of Cu protected by SiO_2 or Al_2O_3 with a graphene oxide linker have been reported for studying neutravidin-biotin interactions. The refractive index sensitivities for the Cu films with these layers were found to be 55% and 75% higher than for even Au films with no dielectric on top, attributed to the significantly lower optical losses in the energies investigated for Cu compared to Au [168]. The Langmuir–Blodgett films of copper phthalocyanine have been shown to be a potential sensor material for NO_2 [169]. An issue with multi-elemental protective films is their deterioration over time and use due to the high probability of the presence of defects including pores at the time of deposition, which can serve as diffusion paths for oxygen to access the underlying Cu, oxidizing it over time and eliminating the plasmonic effect. Close-packed and conformal films can hence be inherently better at protection, and graphene has been attempted as a protective layer with this reasoning on Cu films. The atomic thickness with which graphene can be worked with aids in reducing the extent of shielding of the plasmonic field compared to the thicker layers of the multi-elemental materials as well, aiding in enhanced sensitivities than other thicker films. The defect density in graphene is again vital here, and graphene grown elsewhere and transferred onto Cu was better at protection than in situ grown graphene due to a higher defect presence in the latter films, arising from surface effects from lattice mismatch during film growth. The resulting protected Cu films were promising for the sensing of graphene hydrogenation, as well as waveguides for light transmission [170]. With this investigation as proof, a subsequent study has revealed the prospect of this Cu/graphene layer composition deposited on a photonic fiber as an effective sensing configuration with a sensitivity of 2000 nm/RIU. An increase in sensitivity was achieved through intentionally incorporating appropriately sized holes (300 nm diameter) on the fiber surface prior to Cu/graphene deposition, leading to the coupling between the SPP mode and the LSPR of the holes. The number of layers of graphene had a profound impact on the sensitivity, as more than two layers led to a significant damping of the SPP. Due to the attenuation of the SPP into the metal being much stronger than the dielectric, a higher refractive index dielectric as an intermediate layer can be intuitively understood to be better for sensing due to the resulting improved accessibility of the plasmon field to interactions happening on the surface. With this understanding and with regard to improving the sensing performance of Cu films, materials amenable to deposition as a continuous film with a high refractive index and a low thermo-optic coefficient along with minimal lattice mismatch can be ideal. An investigation of the use of III-V nitrides which have a low thermo-optic coefficient, similar lattice configuration to graphene (hexagonal) high refractive index, and a near-zero extinction co-efficient (and hence unwanted incident light attenuation) at the Cu SPP wavelength of 633 nm has proven to enhance the sensitivity of simpler Cu/graphene films with this reasoning [171]. The theoretical study revealed that the higher optical quality (judged from obtaining the best evanescent field enhancement and sensitivity) of InN among the other nitrides resulted in the best performing composite film.

Native oxides of Cu have also been investigated as the easiest to form protective layer for Cu in sensing applications. A study on the best thickness of Cu and an intentionally created oxide layer (through annealing) revealed that for the maximum sensitivity of the film when the refractive index was changed between that of air and water, the optimal thickness of Cu was 44 nm and that of the oxide was 1 nm for a film deposited on a glass prism [172]. A similar investigation in terms of the sensitivities between air and aqueous phases but with the objective of comparing the sensing configuration has been performed, in which the configurations of Cu films deposited on prisms, those with periodic corrugations (the grating configuration) and those deposited directly on optical fibers were fabricated. Results revealed that the prism configuration exhibited the best sensitivities, but that this was primarily due to difficulties associated with the other two configurations, viz., the

inhomogeneity of films for the fiber configuration and the loss of a significant portion of the incident light due to diffraction in the grating configuration. A thin layer of Au was deposited to prevent oxidation of the films [173]. A similar finding of a lower refractive index sensitivity, when films in the Kretschmann configuration and those with a grating configuration were studied, has been reported, wherein Cu was found to be more sensitive than an Au film. The reason for the grating configuration being an order of magnitude less sensitive could be due to inefficient evanescent wave coupling to the plasmon, as the evanescent wave is not entirely restricted to the metal/dielectric interface in this configuration [174]. Refractive index sensitivity studies with water and glycerol with Cu films prepared through chemical deposition and protected by a layer of benzotriazole molecules led to values of up to 131 nm/RIU depending on the film deposition parameters [175]. The choice of materials that can improve the sensitivity is more critical with regards to sensing with films rather than the film parameters themselves, such as protecting/permittivity enhancing over layers and the use of adsorption enhancing molecules, as revealed by a study employing Cu films with Fe_2O_3 and antimonene over layers on Cu configured in the Kretschmann geometry. Fe_2O_3 improved the permittivity, and antimonene was used for a more efficient binding molecule due to its highly customizable functional group chemistry. Refractive index sensitivities of up to 398 nm/RIU were reported from the simulations [176].

Cu Films as Plasmonic Waveguides

It is of note here that the loss of the Cu plasmon wave is significantly dependent on the surface quality (against impurities) and surface crystallinity (against a high concentration of grain boundaries) as well, significantly impacting the propagation length which can reach values of up to 65 μm at 750 nm for oxide-free but polycrystalline films [177]. These values are of significant importance in the field of subwavelength optical guides, of which plasmonic materials are deemed as frontrunners. Cu is especially relevant for wave-guiding applications due to its compatibility with existing CMOS processes. But Cu by itself is not preferred for wave-guiding among the coinage metals due to lower propagation lengths stemming from high ohmic losses, albeit having a smaller mode confinement volume [178]. However, lengths > 40 μm at the telecommunication wavelength of 1550 nm for 170 nm thick films protected by SiO_2 and SiN layers have been observed [179]. Of importance here is that the propagation length is not only governed by the material but also by the construction of the waveguide.

Waveguides can be made significantly more efficient in terms of propagation lengths by sandwiching a low-permittivity material between the metal and the conventional dielectric as the propagating mode is pushed out of the metal into the sandwiching dielectric [180]. Interesting to note here that the selection of the intermediary dielectric is opposite here (with regards to permittivity) than when one is selected for sensing. The resultant coupling between the SPP mode in the metal-low permittivity dielectric and the fundamental mode in the higher permittivity dielectric leads to a strong confinement (within areas down to $1/100^{th}$ of the diffraction-limited area for the wavelength) of the propagating hybrid mode, significantly enhancing the propagation distances [181]. A common configuration of this hybrid plasmonic waveguide is Cu-SiO_2-Si [182–184], which has also been reported as the first experimental configuration to demonstrate polarization splitting in the hybrid waveguide configuration. This splitting results in the TM excitation being able to propagate along the device, whereas the TE is not [185]. The same configuration has also been demonstrated as a compact electro-optic modulator with very low waveguide insertion loss [186]. Cu-TiO_2-Si was a configuration investigated as a waveguide-based resonator due to the negative thermo-optic coefficient of TiO_2 [187]. Spoof surface plasmons, waves propagating in the 1×10^9–11×10^9 Hz regime, have been realized with staggered waveguides made of Cu films. Propagation distances over 150 times the wavelength have been reported with features that were in the form of squared bars, and the distances depend on the staggered separations between the bars [186].

Cu Films in Non-Linear Optics

Films designed for non-linear optics are of benefit for example in making neutral density filters, as lasing materials, as emission sources of up converted photons, and as other light manipulators. Cu films exhibiting one such NLO characteristic of reverse saturable absorption (RSA) have been fabricated through pulsed laser deposition. RSA is the increase in absorption of the excited state electron population in comparison to the ground state electron population, which is notably contributed to not only by plasmon absorption but also by inter-band transitions. Manifestation of this behavior was found to be closely associated with the particle size in one study, which for sufficiently small particles related directly with the hot carrier generation efficiency from plasmonic decay. The line between calling the deposited structures films vs particles was very thin in this study, as although the deposition was described as a film, the plasmonic behavior (observation of a broad absorbance) was attributed to discrete and polydisperse nanoparticles [188]. The standing of a particular material composition/configuration for non-linear RSA applications is quantified by the non-linear absorption coefficient, which was on the order of 10^{-4} cm/W for these laser-prepared CuNPs. Other studies have examined different compositions and configurations, and the analogous coefficients were $2–6\times10^{-5}$ cm/W for

Cu-SiO_2 films [189], 0.01–1×10^{-8} cm/W for ion-exchanged Cu nanocomposite glass [190], and 10^{-6}–10^{-7} cm/W for Cu implanted silica glass nanocomposites [191], demonstrating the possibilities for such materials for optical attenuation in high power lasing applications for example. Towards another investigation of NLO from Cu, an unconventional and novel study on the excitation of tip-induced plasmons (TIP) due to energy transfer between electrons tunneling between the tip of a scanning tunneling microscope (STM) and a Cu phthalocyanine (CuPh)/Au film has reported an enhancement in the emission of up-converted photons from this configuration. An enhancement in the inter-band electronic transition-induced photon emission at a wavelength of 720 nm from the CuPh was observed. The up-conversion was confirmed from the fact that the bias voltage of the tunneling electrons (< 1.7 V $\approx$ 720 nm) was lower than the energy of photons emitted (720 nm) [192]. The use of nanopatterned Cu films as cathode sources for electron emission has been reported. The enhancements of such a surface composed of spherical holes (and localized resonances hybridizing with the SPP mode) to the electron yield was 1200 times that of a flat surface which does not exhibit localized resonances. The emitted electrons had a narrow energy distribution (judged from the value of the Keldysh parameter), and the enhancements originated from SP assistance, confirmed through simulations and calculations of expected enhancements assuming the changes occurred only due to a lower reflectivity of the patterned films (the Fowler-Dubridge theory was used for quantifying the enhancements due to lower reflectivity). The angular spread, emission time scales, and the damage threshold of laser fluence of the nanohole array cathode were comparable to the most efficient metallic cathodes [193].

Cu Films for Enhanced Scattering

Scattering of light by plasmons being a dominant field of study and Raman scattering being a major benefactor from plasmonic enhancements, Cu films have also been explored along these lines, albeit to a much lesser extent than Au and Ag due to the high oxidation instability and often comparable or inferior enhancements to the latter two. SERS of Cu phthalocyanine molecules deposited on Cu resulted in a 23-fold enhancement when excited at the SPP wavelength of 632 nm of Cu, compared to the 50-fold enhancement observed for Au. The collection efficiency of the scattered light from the SPP was improved using a Weierstrauss prism and in the Otto configuration (the latter for control over the angle of reflectance) [194]. The coupling of propagating SPPs and LSPRs can be very interesting due to the intense electromagnetic fields concentrated at the interfaces between the NPs and the films. In this regard, islands of Ag with their LSPR have been investigated as a coupled system with the propagating SPPs of Cu films for enhancements to the fluorescence of dye molecules. Both emissions of photons into free space by the proximal dye molecules of rhodamine, as well as plasmon-coupled fluorescence (PCF-detected at the back of the Cu films), increased with the presence and increasing coverage of the Ag islands, and at coverages approximating Ag films instead of NPs, the enhancements diminished considerably indicating the beginning of the loss of the metal-enhanced fluorescence property. A narrowing of the emission angle of the PCF was also a consequence of the presence of the Ag islands [195]. Similar observations were made in one of the other rare investigations of MEF on Cu films, with 40 nm thick films exhibiting the highest increase in PCF by 1.39 times of sulforhodamine fluorophores [196]. While it is intuitable that such films may not stand the test of time due to their oxidation-prone nature, it is probable that thin protective layers such as graphene as discussed earlier in this article can be a viable approach for realizing durable and plasmonic fluorescence enhancing Cu films.

SERS being dependent on the hotspots created and the extreme field localizations at these locations, films of plasmonic materials empowered with surface roughness and/or roughness features such as other nanoparticles can be interesting. The role of the hotspot in SERS studies (which can also be used to monitor scattering from molecules created at the hotspot assisted by plasmons) can be confirmed for example from two separate studies. The first used a film of Cu on which Ag nanoparticles were and were not present on the surface, for which the latter morphology catalyzed the reaction (the dimerization of 4-nitrobenzenethiol) and the former did not on the excitation of SPP/LSPR, respectively [143]. The second study was also on photocatalysis (for the conversion of 4-aminothiophenol to p,p′-dimercaptoazobenzene) but employed CuNPs which could readily cause the reaction [197].

Optical Nanoparticle Trapping by Cu Plasmons

Optical trapping is the phenomenon of exertion of forces on an agent (example: an NP) for its manipulation by virtue of its interaction with light. A coherent/concentrated EM field is required for this to be possible, such as from a laser. Plasmons intrinsically can be of applicability in this field and have been explored for this property. The tuning of the separation distance and geometry of one such Cu plasmonic nanoantenna for the manipulation of polystyrene nanoparticles resulted in the intense EM fields exerting forces up to a few femtonewtons on them. It is important to note here that the enhancements to the EM fields that resulted in the trapping were due to excitation at 1064 nm and not the plasmonic wavelength of Cu, which should be equal to if not better for optical trapping if investigated due to the inherently magnified and localized fields during resonance. The

potential use of polystyrene for biological applications led to the choice of this wavelength for the study, wherein in vitro applications can benefit from this manipulation [198].

On the Oxidation of and Changes Thereby to the Plasmonics of Copper

The Nature of Oxidation of Cu

Many theories and supporting evidence exist for the highly detrimental (from a plasmonic view) phenomenon of metal oxidation [199, 200]. However, we restrict the discussion on this topic to reports specific to the observation and investigation of oxidation to plasmonic Cu films and nanoparticle structures. Copper has an extremely high tendency for oxidation, with the dominant oxidation product being Cu_2O [201] and also CuO (with intermediate phases such as CuO_x where $x = 0.67$ [202] present). It is to be noted however that a range of stoichiometries of CuO_x is possible depending on temperature, film porosity, thickness, and particle diameter with X values from 0.67 to 1 [203, 204]. The growth of the oxidized layer is linear depending on the ambient and the nature of the film/NPs, at an oxide film formation rate of 0.004 nm/day when stored at ambient temperatures (23 °C) and atmospheric pressure for example [205] (contradicting numbers exist here for the oxidation rates depending on particle sizes and ambient conditions such as the rate of 0.034 nm/day for 100–140 nm spherical CuNPs [206]). These numbers predict a continuous growth of an oxide film, whereas other reports observe a saturation in oxide formation to the tune of 13 nm thick films after a few hours irrespective of oxygen pressure. Multiple mechanisms have been proposed as to the oxidation mechanism such as the uniform passivation of the CuNPs surface by oxygen to form the oxide [207] which was superseded later by the observation where oxide islands nucleate on the surface and coalesce to form the film [208]. Nevertheless, the quick oxidation of pristine Cu with a resulting layer not exceeding a thickness of ~ 15 nm (composed of Cu_2O) followed by the occurrence/conversion of other species such as CuO and CuO_xH_2O [209] is the inference from research on this subject, post which further diffusion of oxygen into the oxide becomes a limiting step for oxidation of the underlying pristine Cu. The self-limiting nature of this process (when exposed to air for example) has been reported to disappear even at 50 °C, post which complete oxidation of NPs occurs [210]. The resulting oxide is composed of mostly Cu_2O with CuO moieties present in proportions that depend on temperature. Although the amount of formation of Cu_2O is largely near the surface of the bare metal [211], significant differences can occur in the plasmon oscillation as this is a phenomenon confined to the surface, leading to a gradual loss of the property due to a decrease in the free electron density. This loss and changes to the plasmonic properties of Cu in general have been studied in detail by multiple researchers [212–214]. Conflicting reports thus exist in this continuing field of CuNP oxidation research as revealed by the discussion so far, to be added to the prediction and confirmation (through theoretical modeling of the barrier energy for continued Cu diffusion for oxidation) of a maximum self-limiting oxide shell thickness of only 0.56 nm. Although, in this letter study, theoretical calculations considered the various barriers to diffusion of Cu atoms at the core towards the surface, it was observed that for shell thicknesses up to 0.56 nm, the barrier to Cu diffusion from the bulk to the surface was low enough for oxidation to proceed [206]. It stands that the phenomenon of oxidation while considering Cu fluctuates highly in terms of the time required and the extent of self-limitation depending on factors such as purity, morphology, temperature, and surface characteristics (such as crystallinity, roughness, porosity, etc.) and the ambient environment (with its own decisive parameters such as pressure and nature of the oxidizing species) [215] but cannot be unaddressed unless stabilized or isolated against even the mildest of oxidizing environments.

Prevention/Reversal/Utilization of Cu Oxidation as Relevant to Plasmonics

Reversal

Oxidation in Cu can be prevented/reversed by a few procedures. For example, the treatment of oxidized Cu with acetic acid was found to remove the oxide layer through the formation of cupric acetate and a resulting return of the plasmonic metallic Cu [57, 216]. There was no loss of the thus exposed Cu due to etching, rendering it safe for such procedures. Adoption of appropriate post treatment procedures such as drying with inert N_2 instead of a water rinse/air drying is essential [217], to avoid the reformation of the various oxide species. Although these species reappear once exposed to ambient conditions, this method presents a solution where devices based on plasmonic Cu can be prepared where vacuum transfer between fabricating equipment can minimize this re-occurrence. If avoiding hydrated environments is not a possibility, vapor phase etchants such as 1,1,1,5,5,5-hexafluoro-2,4-pentanedione (H + hfac) can give similar results of removing the oxides [218]. The oxidation can also be reversed for example by subjecting to a strongly reducing atmosphere such as H_2 where all the phases of oxide were observed to change into elemental form. This study has investigated only CuNPs and not films, and hence, the redox behavior of films can be expected to be different based on porosity, thickness, etc. [204]. Yet another method of reversal seems to be direct irradiation with the light of oxidized Cu. With regards to deposited Cu nanoclusters,

the facet design of the clusters can be useful in prevention. Preparing clusters through gas phase aggregation such as through physical vapor deposition leads them to typically have a monocrystalline nature {(111)}, with these facets having a higher coordination compared to polycrystalline NPs. This results in fewer reaction sites for oxidation. Combined with a process such as plasma ozone treatment which resulted in the formation of a Cu (II) oxide compared to Cu (I) and where the Cu core-Cu (II) shell was found to be much more stable against further oxidation than when Cu (I) forms (typically when exposed to ambient conditions during storage), this methodology of CuNP production can be a prospective solution to the oxidation problem of plasmonic Cu, as shown in Fig. 11 [219].

Prevention

In terms of prevention, the obvious choice of stabilizing ligands is the most straightforward solution. Multiple ligand types and classes including thiols and acids have been tested for their effects on stabilizing CuNPs against oxidation, with thiols and oleic acid being those which lead to oxidation stability while simultaneously avoiding aggregation [220]. For thiols, longer chains resulted in more stability to oxidation but were also found to cause a rapid loss of plasmonic Cu due to thiolate formation with the help of atmospheric oxygen. This observation was not found with oleic acid, wherein the double bond in the oleyl chain was responsible for stabilizing the CuNPs [221]. Thiolate immobilization (which is usually self-assembled) can thus prevent oxidation, but probably at the cost of the plasmonic property of Cu [222]. The chain length and the composition of the thiol affect the stability provided against oxidation, with longer chains stabilizing better due to the reduced permeability of oxygen through the chains [223–225]. One-step synthesis techniques such as irradiation by high-energy γ rays of the matrix in which CuNP precursors are dispersed are also effective ways to realize NP synthesis (by ionized species generated by the irradiation) and to avoid oxidation simultaneously (as the dispersion matrix, PVA, is impervious to oxygen) [226]. Stabilizing ligands which contain multiple moieties that can bind to the CuNPs can be found in molecules such as polyethyleneimine, allowing enhanced stability and an alternative pathway to prevent oxidation compared to single- and double-molecule-capped CuNPs [227]. Prevention of CuNPs from oxidation to preserve SPR by various modalities has been reported in brief in Fig. 12.

Utilization

The oxidation of CuNPs leads to interesting effects as well due to the inherent nature of the LSPR property. For example, the commencement of the process does not immediately quench the plasmon oscillation, until the coupling of

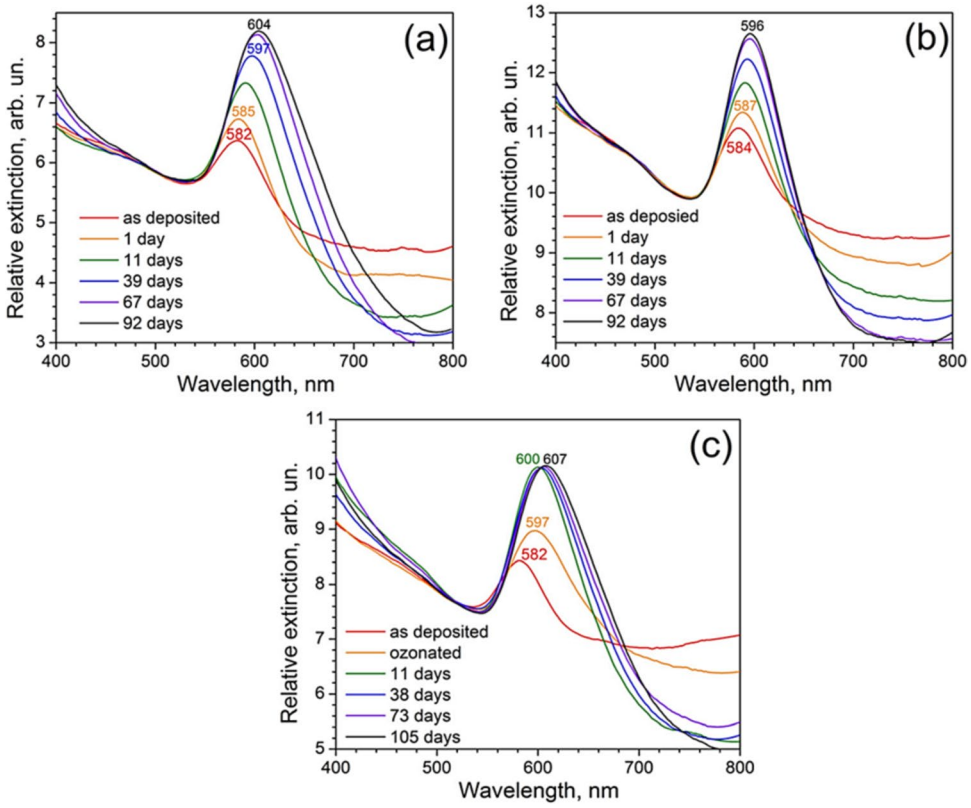

Fig. 11 LSPR band for large CuNPs at different times **a** kept in ambient air, **b** kept in a nitrogen atmosphere, and **c** ozonated and kept in ambient air (reprinted with permission from [219])

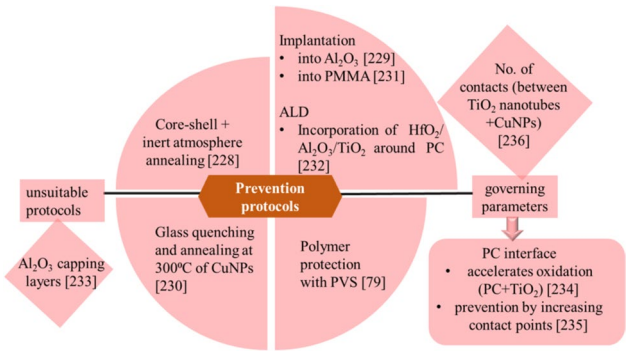

Fig. 12 Research on the prevention of PC oxidation towards LSPR preservation [228–236]

the photon to the valence electrons proximal to the surface is no longer possible due to the screening of the incident photon field from them [237]. In fact, depending on the nature of the solvents (i.e., whether they are capable of forming electron-sharing associations like pi- bonds), the plasmon intensity has been reported to increase if the solvents where the CuNPs are dispersed change from one that is not capable of pi-bonding to one that is. The eventual result is the attenuation of the plasmon peak and the appearance of the exciton peaks, depending on the rate of oxidation [238] in such solvents. Yet another prospect is the use of oxidized Cu as an electron scavenger, preventing recombination and leading to the generation of holes for catalyzing reactions. In a study with ZnO composited with Cu, the oxidized phase of Cu (CuO), which resulted very quickly on exposure to the ambient, was used as an advantage to scavenge electrons on photoexcitation of ZnO, wherein these electrons were used for reduction of the CuO, whereas the holes were used for catalyzing production of H_2O_2. For such an application, Cu is most beneficial compared to Au and Ag due to its lower half-cell potential (0.52 V) compared to Au (1.69 V) and Ag (0.80 V) [239]. A similar enhancement to the catalytic activity of Cu@CuO also points to the usability of an oxide shell, for catalysis at least [240]. Such studies reveal the prospect of achieving tailored absorption through facile manipulation of the CuNPs' environments and can be useful while trying to achieve NPs with a better shelf life for various applications.

From the discussion thus far, the phenomenon of oxidation in Cu need not always be viewed as a detrimental process. The intricate control of the parameters such as the proportion of the CuNPs that are oxidized, the thickness of the oxide layer, and its use for applications as pointed out so far leads to the postulation that Cu plasmonics can lead to a fruitful collaboration with oxidizing agents in terms of realizing specific goals for pertinent applications.

Plasmonics in Doped/Non-Elemental/Composite Copper Nanosystems

Pristine plasmonic nanomaterials gradually lose their plasmonic property on increasing the particle size, due to increasingly stronger damping of the plasmon with size. Moreover, the plasmonic properties of pristine metals are locked-in post deciding their size, shape, and composition. However, doped nanomaterials can have significantly different LSPR manipulative abilities, due to the possibility of making changes to the stoichiometry (and by extension the dielectric constant/free electron density) by doping, for instance. Apart from doping, temperature modulation (including thermal aging), phase transitions, oxidation, and field-assisted copper migration can also tune the LSPR of Cu [241, 242]. Doping can be achieved predominantly through two modalities, viz., inclusion of a different element and by self-doping [243], wherein the parent molecule is imbibed with vacancies to change the stoichiometry. Copper is particularly amenable to creating non-stoichiometric doped compositions due to its low chemical potential which leads to its release from the solid phase relatively easily, leading to the induction of LSPR due to self-doping. The former modality for inducing LSPR through doping/alloying is the compositing of pristine plasmonic materials with other materials such as semiconductors [244] and polymers with marked improvements in the resulting properties. Herein, we attempt as much a comprehensive discussion as possible on the different classes of Cu-based plasmonic nanomaterials, with a focus on the plasmonic aspects.

Copper Chalcogenides

Chalcogenides of Cu have been the major players among the different plasmonic Cu compounds, being extensively investigated for their plasmonic properties. Hence, the section on chalcogenides alone has been divided broadly into their origins and their applications.

Plasmonic Origins and Virtues of Chalcogenides and Their Applications

Summaries treating Cu chalcogenides as sub-sections of a broader perspective, for example, on doped semiconductors and metal oxides, as well as summaries of chalcogenides being explored for different applications such as theranostics and catalysis, have been published [245–250]. Broadly, the investigations on plasmonic copper chalcogenides have been centered primarily on Cu_2S and Cu_2Se, with compounds such as Cu_2Te and CuSSe also being investigated with a decreasing order of frequency. It is of

note that stoichiometric chalcogenides are not plasmonic due to the absence of sufficient free carrier density, while Cu-deficient compounds are plasmonic due to the presence of holes. Rigorous reviews on plasmonic Cu sulfides treat these compounds in terms of multiple viewpoints such as their compositional integrity in various situations, the limits of plasmonic manipulation, the applications where they can offer benefits, and the property enhancements possible by doping multi-valent ions into their lattice [251]. Their applicability to the control of solar radiation has also been widely investigated (through films deposited via chemical bath deposition on multiple substrates) as efficient reflectors of infra-red radiation while permitting visible light penetration [252–254]. On this perspective, only their light interaction properties of transmittance, reflectance, etc. are quantified, with the mechanisms behind the observations either attributed to their semiconducting nature or not discussed. Considering the focus of this work, only research that has discussed and discovered aspects in the plasmonic perspective and those that explicitly acknowledge/treat this perspective of Cu_xS have been included.

With regard to the plasmonic $Cu_{2-x}S$ family, these nanomaterials have had an interesting history of being identified as plasmonically active nanomaterials in the infra-red from being wrongly assigned as indirect band gap materials [255–257]. The validation of the LSPR property through assessment of the optical absorbance dependence on free carrier density (for Cu_2S) was the point from which plasmonic chalcogenide research took off [258, 259]. Of note is the fact that the confirmation of the LSPR property in the first study derived from comparisons of the observations of the optical absorbance of stoichiometric Cu_2S which did not exhibit LSPR absorbance [260]. Since then the investigations of this family have grown in terms of manipulating LSPR through various means, although in many instances continued attributions to the d-d transitions instead of plasmonic excitations in these materials [261–264] are made. The composition of $Cu_{2-x}S$ can accommodate large variations in Cu vacancies, leading to structures such as chalcocite ($Cu_{1.997-2}S$), djurleite ($Cu_{1.93–1.97}S$), digenite ($Cu_{1.8}S$), and anilite ($Cu_{1.75}S$). As cursorily mentioned earlier, LSPRs of non-stoichiometric Cu_2S are mediated by holes rather than electrons as they are the free carriers in this *p*-type molecule and are generated when CuS gets oxidized to the different non-stoichiometric forms. The relatively lower free electron densities that result lead to LSPRs in the NIR region, with high tunability in their position and bandwidth depending on free carrier density, shape, and the refractive index of the surroundings (such as stabilizing ligands/shells/solvents). To this extent, different shapes and sizes of $Cu_{2-x}S$ nanomaterials have been developed, including disks [265], spheres with precise manipulation and reversibility of the SPR property (through the reversible processes of oxidation in air /reduction with tetrakis hexafluorophosphate) [266], and spheres with biasing based modulation of the free carrier density [267]. It is worth noting that the LSPR of these chalcogenides can be controlled more drastically by controlling the transformations between the different phases rather than by controlling the morphology, and even then, within a phase, only a limited variation in non-stoichiometry exists. It is also established that the barrier for further transformations into other phases is higher than that for achieving variations in stoichiometry within a phase. Hence, by employing oxidizing conditions with suitable potencies, fine tuning of the LSPRs of chalcogenides can be possible [268]. A very useful equation that allows prediction of the LSPR energy (ω_{sp}) is given as follows [269]:

$$\omega_{sp} = \sqrt{\frac{\omega_p^2}{1 + 2\varepsilon_m} - \gamma^2} \tag{19}$$

The terms ω_p, ε_m, and γ are as explained in the previous sections. It is of importance to note here that the above equation is valid when the LSPR is separated from the band gap excitonic transitions. It is important as well that the linewidth γ is influenced by variations in vacancy density as well as the particle size distribution and that estimating the value of the hole effective mass in the calculations of ω_p is not always performed for the purposes of validation of the calculations. Accurate values of hole effective mass which can be arrived at from the valence band curvature are very important to be able to predict the location and the width of the resonance for hole-based LSPR materials such as chalcogenides. Indeed, substantial variations in the effective masses exist for the CuS family, ranging from 0.55 m_e for CuS to 0.8 m_e for $Cu_{1.96}S$ [270, 271]. With regard to how many free carriers are required for a plasmon oscillation, such estimations for a 6 nm QD of $Cu_{2-x}S$, for example, lead to a figure of approximately 200, ample enough to sustain LSPR which was confirmed by spectroscopic investigations. Care must be taken while dealing with interpreting the LSPR behavior of Cu_xS, as multiple studies have also revealed the possibility of Cu existing in monovalent or divalent states depending on the lattice coordination environment. It can be predicted then that LSPR tuning is possible for the latter than the former, and it is evident that the full potential of LSPR manipulation of CuS/Cu_2S is not always addressed [272, 273]. Indeed, the conversion between covellite (CuS) and chalcocite (Cu_2S) through reduction with Cu^+ ions is one of the transitions that have been well documented, although the manifestation of this transition on plasmonic virtues such as the study on band structure and temporal stability leaves room for discovery [274].

Since Cu is inherently unstable unless protected by various means as discussed in earlier sections, investigations on protecting CuNPs and films against oxidation while still

maintaining the electronic structure of the free carriers have been a continuing endeavor. A promising but less explored route of stabilizing the hole-free carriers, not by Cu vacancies, but by using anions adsorbed on the surface, has been realized in this approach. The compound of ferrocenium triflate was found to be a suitable valence hole stabilizing species by adsorbing as an anion on the surface while still preserving the Cu stoichiometry. This approach was, however, quantitatively less effective at stabilizing the holes (by approx. 300 mV) compared to the conventional approach of creating Cu vacancies to realize free holes. Interestingly, both modes of realizing free holes resulted in indistinguishable LSPR bands, indicating the suitability of this approach where Cu deficiency leading to phase transitions is not desired [275]. Plasmonic probes of reactions can be very sensitive to the refractive index (n_m) according to the following equation [276]:

$$\varepsilon_r(\omega) = -2n_m^2 \tag{20}$$

They can thus be used to monitor the reaction environment to determine parameters like the pH, charged species present and in general to ascertain the redox conditions. Specifically, the activities of oxidants such as alkylamines and iodine promote the creation of Cu vacancies whereas reductants like thiols and sodium biphenyl quench them, causing a blue and a red shift of the LSPR respectively, proving that the Cu plasmon can also serve as an indicator of the species present if the reverse approach (of interpreting the shift in LSPR as an indicator) is followed. Additionally, the mobility of Cu in CuS has been proven to be high and essentially without restriction (due to multiple theories one of which is the weak-electrolyte model) [277], thus not factoring as a rate-limiting step in these reactions and enabling them to be used as prompt probes of the reaction conditions [276].

Cu Chalcogenide Sulfides

The concept of PT catalysis due to plasmon-induced heating has also been investigated with plasmonic Cu chalcogenides. Anilite (Cu_4S_7) has been used with this motive for the cyclocondensation of 1,3-cycloheanedione and 3-methyl-2-butenal. The porous nature of anilite achieved helped in maximizing the absorption in the infrared, leading to enhancements of approximately five-fold of the catalytic rates. The crevices of the pores were also predicted to contribute to this enhancement by facilitating heat transfer through their increased surface area [278]. Analogously, enhancements to the catalytic reactions of the Suzuki coupling reaction, the oxidation of benzyl alcohol, and the hydrogenation of nitrobenzene have been reported to be due to the plasmon-enhanced performance of anilite@Pd nanoparticles. The infrared absorption of anilite compared to the UV–visible for Pd caused only anilite to be the contributor to the increased catalytic rates at NIR wavelengths. Separation of the contributions to this enhancement due to thermal heating (due to plasmonic absorption) and due to the photocatalytic channel was done through a simple experiment in the presence and absence of light (while still providing external heat when illumination was not present). The considerably reduced catalytic rates for the latter condition confirmed the LSPR route for photocatalytic enhancement. Corroboration with work function calculations leads to the mechanism of hot hole injection (due to LSPR-induced e–h pair generation) into Pd from Cu as the cause for this enhancement, whose resulting *p*-type nature served as the initiator for all the reactions such as the dissociation of H atoms [279]. The observations here support the theoretical band structure calculations for Cu from other studies, which report generation of hot holes with a considerably higher energy than hot electrons (by ~ 2 eV) and hence an easier injection into other materials, making them promising for such applications. This asymmetry in energy distributions of hot electrons and holes makes Cu an efficient material for hole injection and an attractive prospect in plasmon-driven hot carrier research [280]. Yet another hydrogenation reaction in which furfural was catalyzed by Cu-LSPR-mediated dissociated H_2 into furfuryl alcohol reports hot carriers as the energy source for the dissociation. The encapsulation of CuNPs in a thin film of carbon enabled oxidation-stable photocatalysis during the hydrogenation process [281]. The easier migration of free holes within plasmonic Cu_xS through creating this material with the help of a Cu_xS seed vs without has been studied. The observations indicate that the seed-based approach led to a much higher concentration of Cu vacancies and, hence, a better photocurrent density than the starting material of stoichiometric CuS. The increase in free hole density by approx. 2.5 times between materials achieved through these two processes was sufficient to cause a shift by approx. 1000 nm in the LSPR wavelength [282].

Theranostics, the field combining both branches of medicine of therapy and diagnostics, has evolved in a considerable manner with the advent of nanotechnology. In this regard, PT therapy of tumors has been a highly explored one, especially with plasmonic nanoparticles due to their widely tunable morphology and stability. The PT property of plasmonic digenite was found to be effective for cell destruction due to its plasmonic absorption in the NIR region. Comparisons with AuNRs led to the conclusion that they can be superior to the latter, although comparisons with optimally designed AuNRs for PT therapy were not done [283]. Materials with more than just the PT property, such as those that can also enhance the imaging component of the therapeutic methods, can be intuited to be better than those capable of a singular function. In this regard, with particles between 10 and 50 nm being ideal to have the best

retention times in vivo, magnetic Fe_3O_4@$Cu_{2-x}S$ nanoparticles with synergistic advantages of imaging (magnetic and thermal) and therapy (by infrared absorption induced heating and ablation) of tumors have been reported [284]. Regardless of the controversy surrounding the nature of the excitation of Cu chalcogenides, such composites with both magnetic and optical control have immense interest stemming primarily from their broad absorption, allowing exploitation of their absorbing nature at both the biological windows (808 nm and 1064 nm). The efficacy of the lower energy window was much higher than the higher energy, and the molar extinction coefficient was the reason. Specifically, the higher extinction coefficient for the lower energy allowed a higher temperature rise during irradiation, leading to a higher tumor-killing efficacy. The PT conversion efficiency was higher for the 1064 nm irradiation as well, determined from the formula in Eq. (21) [285]. Another composition is one where Au was composited with CuS, allowing excitation of the LSPR in both and possibly bettering the PTT metrics. Indeed, the absorbance intensity of the composite when in the same concentration as when either of the materials were present alone was quantitatively higher [286]. Previous research has shown that the field enhancement "tails" of the LSPR can extend to energies much beyond the peak LSPR energy, resulting in much higher absorbance intensities due to coupling between this tail (of the Au's LSPR) and the LSPR of the CuS. Specifically, the interparticle dipole coupling can create hotspots [287] in the enhanced fields, which can result in the observed effects. The killing of tumor cells was achieved at much lower laser powers in the Au/CuS study, the reason being attributed again due to the coupling between Au and CuS. This is likely (given that the excitation wavelength for the therapy was 980nm, much lower than the 530nm required for exciting the LSPR of Au), yet it is probable that other reasons are at play here, such as possibly a higher surface area for heat transfer of the composited particles which improved the killing efficacy. The NIR LSPR of CuS alone has also been explored for combined PT and positron emission tomography (PET) imaging by incorporating the radio isotope of ^{64}Cu into CuS which was synthesized in the nanodot morphology with an effective hydrodynamic diameter of less than 6 nm (controlled through the molecular weight and concentration of PVP). Irradiation at 808 nm resulted in a temperature rise to 50 °C, which along with the quick renal clearance (95% removed within 24 h) resulted in a composition that has a rare potential for dual modes of imaging and therapy of cancer [288]. Another commonly used radioisotope of ^{131}I was also investigated for the same purposes, also proving to be effective in NIR absorption-based PTT and imaging when incorporated with an effective diameter of 20 nm, albeit with a protective cap of PEG [289].

$$\eta = \frac{hS\left(T_{max} - T_{surr}\right) - Q_S}{I(1 - 10^{-A}\lambda)} \tag{21}$$

where η is the PT conversion efficiency, I is the laser power, A is a constant, λ is the wavelength of the laser, h is the heat transfer coefficient, S is the surface area of the well, T is the temperature of the solution, and Qs is the heat associated with the light absorbance of the well and solvent.

Insertion of different elements into the chalcogenide lattice leads to optical properties not possible with the chalcogenide lattice alone. Copper iron sulfide is a promising variant of CuS due to its extremely diverse LSPR bands. Plasmons absorbing from 486 to 1200 nm have been reported in this compound by a simple increase in the ratio of Cu: Fe from 1:1 to 10:1. High-resolution XPS studies revealed that the proportions of the cations and anions at the surface, the nature of the valence state of the surface atoms, and the nature and concentrations of the capping ligands decided the intensity and shift in LSPR position, determined directly by the Cu/Fe/S ratios used during synthesis [290]. The origins of the LSPR have hence not been explicitly dealt with in this study, and even a previous review on this composition only briefly ascribes that the possibility of the presence of side phases/Cu deficiencies is the reason for the plasmonic effect [291]. Clarifications in this regard were presented in a more recent work, wherein a changeover from an electron-based LSPR (at approx. 500 nm) to a hole-based NIR LSPR (at approx. 1200 nm) was observed wherein iron sulfates were produced during this transition, creating the hole carriers [292]. Yet another ternary composition is copper indium sulfide, whose Cu deficiency (resulting in $Cu_xIn_yS_2$) led to sub band-gap LSPR resonances in the NIR at around 1200 nm. The close energy spacing between the LSPR frequency and the excitonic band-gap (at 800 nm) makes this material promising for applications looking for light harvesting using both excitations such as light harvesting and catalysis [293]. Such ternary materials are often explored only for their band-gap tuning and seldom studied for their non-stoichiometric compositions [294]. Apart from the brief discussions on the possible elements that can be incorporated in the CuS lattice, a more comprehensive summary of others is presented in Table 3. The hitherto discussed possibilities of tuning the light absorption of the Cu_xS family by stoichiometry manipulation have been extended by an interesting investigation on this manipulation. The conversion between covellite and stoichiometric (non-plasmonic but fluorescent) chalcocite has been reported by electrochemical mediation. Specifically, the intercalation of Li ions into the chalcogen lattice led to this conversion, while Cu^+ intercalation led to a permanent conversion to chalcocite. The prospects of these results is attractive for applications such as optical

switching in the NIR and those involving fluorescent imaging such as sensing and other luminescence based applications [295].

The closing remarks of the CuS family of plasmonic materials are ironic with a review of a study attributing plasmonic absorption in stoichiometric CuS, which as a pristine material was not thought to not possess vacancy-originated hole plasmons. This study employed the discrete dipole approximation and the Drude-Sommerfeld model to account for the observed experimental spectra. The excellent fit between model and experiment was proof that the free holes necessary to exhibit the Drude-like behavior were constituents of the pristine lattice itself, with densities of up to 10^{22} cm^{-3}. Additional confirmations of the inherent resistance to stoichiometric changes of CuS were also reported as additional proofs for this phenomenon. The nano disk morphologies investigated in this work exhibited two resonances in the NIR corresponding to one in-plane and another out-of-plane resonance [273]. Few studies exist on the LSPR origins of covellite such as this that attribute the LSPR nature to inherent lattice free-holes. It can be predicted then that these free carriers can make CuS reactive. Similar to how an oxide layer of controlled thickness can help in stabilization, the incorporation of Pd into the CuS structure as a CuPdS shell tuned the LSPR along with increasing the stability. A limitation, however, was the increased broadening with the increase in Pd content, due to a reduced particle size (and a resulting higher surface scattering) [296]. It is hence evident that the CuS family although exhaustively investigated is still nascent in the aspects of studying and manipulating the origins of the LSPRs in it.

Cu Chalcogenide Selenides

Non-stoichiometric Cu_2Se is another interesting prospect in the plasmonic copper chalcogenide group. The absorptions in this material have been in multiple instances attributed to impurity level transitions similar to the sulfide family and have since been corroborated well with LSPR excitations [297–299]. Mechanisms of achieving non-stoichiometry involve commonly the use of oxidizing agents or atmospheres and reversal through reducing agents [250, 268]. Unusual techniques such as ligand exchange which allow for tuning over 200 nm of the LSPR peak position [300, 301] are among the different modalities of tuning. Remarkable tuning of the LSPR can be possible, as shown in Table 2.

Electrochemical redox reactions can give useful insights into the mechanism of LSPR tuning in Cu_2Se, wherein in situ tuning and LSPR observation are possible [312]. Influences of the potential sweeping voltages (magnitude/sweep rate), electrolyte concentrations/compositions, hysteresis in material composition between redox cycles, and dispersion of the plasmonic NPs in a secondary medium such as a membrane (which itself will influence LSPR through particle aggregation/charge transfer) are a few of the multiple factors that influence the LSPR of the resulting NPs. XPS measurements confirmed the contributions to LSPR of Cu vacancies rather than oxidation state changes, as no peaks corresponding to divalent Cu were observed.

Non-stoichiometric $Cu_{2-x}Se$ has also been explored for theranostics, such post encapsulation with a bio-compatible polymer that prevents cytotoxicity while still maintaining the particle sizes (10–50 nm) for longer retention within the body. The temperatures attained matched those when AuNRs were used, which makes them more suitable due to the better sizes (AuNRs were larger in order to be able to absorb at 808 nm) and the fact that the structure-directing agent of CTAB used for AuNR synthesis is cytotoxic [313]. The multifunctionality of plasmonic $Cu_{2-x}Se$ nanoparticles (with sizes in the sub-5nm range) wherein the purposes of imaging (PTT), Single Photon Emission Computed Tomography (SPECT) and Computed Tomography (CT) could be possible was fulfilled by these nanoparticles. With regards to the plasmonic role, the temperature increases achieved as a result of the PT effect could be precisely controlled between 25 °C and 75 °C by changing the concentration of the NPs keeping the irradiation power constant [314]. A similar objective of sensitive photoacoustic imaging (pulsed optical excitation leading to ultrasonic wave emission due to thermoelastic lattice expansions) has been reported with $Cu_{2-x}Se$ NPs for imaging lymph nodes, the usual paths of cancer progression. Highly sensitive imaging of the lymph nodes could be done with the concentrations of the phospholipid encapsulated NPs down to 1.7 pmol/ml while excited at 900 nm [315]. NPs are conventionally promoted as nano-sized carriers of drugs, and a composition of $Cu_{2-x}Se$ encapsulated by a SiO_2 shell has been used in this regard both as a PT and chemotherapeutic nanomaterial. The cancer drug doxorubicin was loaded onto the shells along with a PEG cap that added the property of hydrophilicity to the complex, and the drug released by the heat generated on NIR radiation of the NP raised the temperature to 45.3 °C [316]. In place of an encapsulated shell, heterogeneous NPs (heterodimers) composed of Au and $Cu_{2-x}Se$ have been reported for the combined possibilities of dark-field as well as photoacoustic imaging. The dark-field imaging was feasible due to the scattering of light by the AuNPs at 566 nm (red-shifted from the expected peak at 520 nm due to hole transfer from the $Cu_{2-x}Se$), enabling highly localized imaging of the infected lymph node. The PTT potential of the approx. 10 nm diameter NPs were not investigated, however, which should have been a possibility considering other research that has done very similar explorations into this aspect [317].

The plurality of the CuS/Se family in terms of applicability has been investigated with a rare perspective of their suitability for non-linear absorption. Specifically,

Table 2 Plasmonic copper chalcogenide selenides and the mechanisms of tuning their morphology and plasmonic properties

S. no.	Chemical compositions	Morphology (nano)	Dimensions/LSPR (nm)	Prospective applications	Method of tuning LSPR	Novel findings	Ref. no.
1	$Cu_{2-x}Se$	Spheres	Dia = 4 to 5/1000–1600	Photothermal therapy	Oxidation time or by the addition of Ce(IV)	Oxidation at ambient exposure/with Ce(IV)/reduction by Cu (I)	[266]
2	$Cu_{2-x}Se$	Spheres	Dia = 2.8–16.5/1000–1350	Microelectronic devices and field effect transistors	Oleic acid concentration	Oleic acid/oleylamine mediated size and crystal phase tuning	[300]
3	$Cu_{2-x}Se$	Spheres	Dia = 9.2/590, 950	Sensing	Ligand concentrations	Post-synthesis ligand exchange-mediated LSPR tuning	[301]
4	Cu_3Se_2	Cubes	Edge length = 18/900–1100	Optoelectronics	Absorbance tuning was not a focus of this study	Al^{3+} ions catalyzed Cu_3Se_2 nanocubes/nanocube seeds' formation	[302]
5	Cu_2Se	Spheres	10/500–560	Photovoltaics	Absorbance tuning was not a focus of this study	One-pot synthesis of stoichiometric Cu_2Se NPs without the initial presence of the sub-stoichiometric phase	[303]
6	$Cu_{2-x}Se$	Nanosheets	6/840	Sensors, solar cells	Absorbance tuning was not a focus of this study	Phase-controlled synthesis of 2D nanomaterials	[304]
7	$Cu_{2-x}Se$	Nanocrystals	13/1050	Chemical sensors	Absorbance tuning was not a focus of this study	Ultrafast optical response of colloidal $Cu_{2-x}Se$ nanocrystals excited at the plasmon resonant energy	[305]
8	$Cu_{2-x}Se$	Nanocubes	13/1000–1750	Theranostics and optoelectronic devices	Different Cu ion concentrations	Carrier populations and NP composition and crystallinity interpreted through NMR	[306]
9	$Cu_{2-x}Se$	Sphere	2–6/1000–1500	Electro-optic switches	Increasing oxidation time	$Cu_{2-x}Se$ is a solid with a peculiar ionic structure at the smaller size	[307]
10	CuSe	Nanospheres	150/438	Photothermal therapy and photodynamic effect	Absorbance tuning was not a focus of this study	Monodispersed NPs were prepared with mild solution-phase synthesis method at room temperature	[308]
11	$Cu_{2-x}Se$	Nanospheres	Dia = 16.4/1600	Sensing and SERS	Absorbance tuning was not a focus of this study	Plasmonically-driven chemical conversion using degenerately doped semiconductor	[309]
12	$Cu_{2-x}Se$	Nanospheres	Dia = 53/1000	Cancer therapy	Absorbance tuning was not a focus of this study	RBC-coated $Cu_{2-x}Se$ NPs with high PT conversion efficiency	[310]
13	$Cu_{2-x}Se$	Hollow spheres	160–180/800–1100	Photocatalysts and photothermal therapy	Changing the $Cu_{2-x}Se$ concentrations in an aqueous solution	High photostability and photothermal conversion efficiency of 48%	[311]

the enhancements to the two-photon emission intensities from these materials catalyzed by LSPR have been studied, wherein the LSPR provides a virtual state for excitation. The mechanism of enhancement of this emission has been shown in Fig. 13 [318]. The explicit role of LSPR in enhancing this intensity was confirmed by tuning its absorption close to the two-photon absorption edge (by substituting Se for S at an atomic percent of 2.6), which was at 950 nm. A significant enhancement was observed for LSPR at this energy, compared to 1145 nm for stoichiometric CuS [318].

Similar to CuS, insertions of elements in the Se-based Cu chalcogens have also been studied. Such ternary compounds exhibit variations in their LSPR based on their size and shape as can be intuited, but an additional modality of compositional tuning was achieved with varying the Se precursors with the same Cu and Sn precursors (leading to differing LSPRs due to differing free carrier densities). Specifically, the reason for this was the differing abilities of the different Se precursors to incorporate Sn into the lattice, which ultimately controlled the Cu:Sn ratio and hence the LSPR position and width, apart from the differences in morphology [319].

Plasmonic Cu Chalcogenide Sulfide Selenides

Plasmonic chalcogenide compositions of both S and Se have been reported in the interests of discovering the tunability possible in the optical properties for applications such as diodes. In this regard, compositions of Cu_{2-x} (S_ySe_{1-y}) were synthesized, and observations of the different stoichiometries indicated that the plasmonic behavior was predominantly controlled by the Cu deficiency and, to some extent, the phase of the materials (cubic vs hexagonal), and not the S/Se stoichiometry. The particle sizes were not found to be a governing parameter, as they were in regimes where the quasistatic approximation (predominantly dipolar contributions only and no multipolar contributions) holds as well as where surface dephasing was not an issue as well [320]. Another study of these compositions revealed an observation of variation in the direct band gap with S/Se ratios, although the changes to the free carrier absorbance were not investigated here. The purely cubic nanowire morphologies were synthesized maintaining the Cu ratios constant and tuning the S/Se ratio [321]. The tunability of the phase and the free carrier absorbance with the S/Se ratio was, however, reported through the synthesis of these compositions with different precursors and processing agents [322]. Achieving monodisperse particles as well as a broadly tunable (from 1350 to 1600 nm) LSPR of this composition was possible while using a specific complex capped precursor, while changing the specific complexes did not result in the same level of tuning [323]. One of the more comprehensive investigations of the insertion of Se into a CuS chalcogen through anion exchange corroborated the influence on the effective mass of free carriers, band gap, and the LSPR peak position with this insertion. The trends of decreased electron density, effective mass, and increased bulk plasma energy as well as LSPR were all attributed to the insertion of the larger Se atom which led to a more diffused setting of the lattice. However, experimentally little influence (a change of only 0.1e V in LSPR energy) was found on the insertion of Se, as unaccounted for effects such as the surface capping ligand and a decrease in free carrier density due to an increase in Cu content during synthesis were attributed to be more influential in reality [324]. It could be concluded then (at least from the reports from the majority of studies on Cu/S/Se) that the Cu deficiency and phase predominantly influence the free carrier absorbance, whereas the S/Se ratios influence the direct band gaps in these materials.

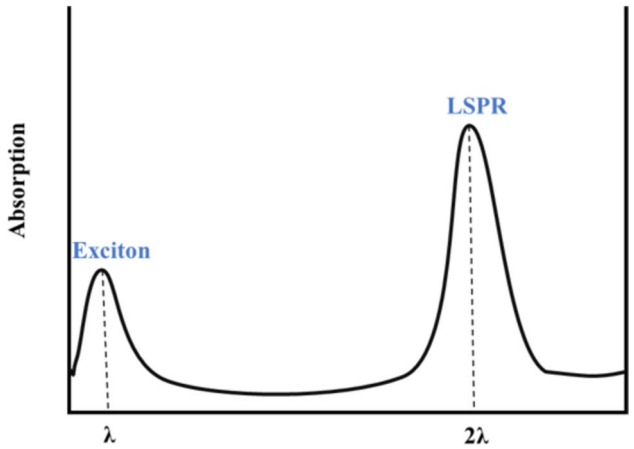

Fig. 13 Absorbance profile for plasmon-assisted two-photon-absorbing inorganic nanoparticles

Plasmonic Cu Chalcogenide Tellurides

The enhanced scattering properties of either molecules in the proximity of LSPR active nanomaterials or of the LSPR nanomaterials themselves have been well established, including in reports in this review. In consideration of one of the mechanisms of this enhanced scattering, SERS, the distance between the molecule under study and the LSPR nanoparticles is of considerable importance for the enhancements. The ideal molecule will have moieties that can directly bind with the LSPR nanoparticle. With this purpose, the poster children of SERS (Au and Ag) have electronegativities which prevent their binding for example with –OH moieties which are a predominant part of many SERS active molecules. An alternate LSPR composition in this regard is CuTe, wherein the electropositivity of Te allows probing of molecules with –OH groups, enabling and extending the classes of molecules that can be investigated. The LSPR of

CuTe being in the NIR is an added benefit in terms of the coupling between the LSPR mode and the Raman modes of molecules. Although comparisons of SERS enhancements between Au, Ag, and CuTe are not possible in most cases due to the inability to match the proximity between the molecule and the plasmonic material, considerable enhancements (approx. 10^6) were observed with CuTe nanocubes and found to be the highest in comparison to nanoplates and nanorods of CuTe [325]. Interestingly, pump-probe spectroscopic measurements concluded that the time constants for LSP thermalization are lesser for $Cu_{2-x}Te$ than $Cu_{2-x}S$ and $Cu_{2-x}Se$ by a factor of 3 and 2, respectively, potentially indicating their applicability for PT purposes as well [326]. It remains an observation that the plasmonic properties of CuTe through experiments and for different applications remain largely unexplored, though multiple reports on its synthesis exist [327]. Insights into field enhancements [328] are often used to validate the potential for a material for a certain application, and from one such investigation, $Cu_{2-x}Te$ having morphologies of spheres, rods, and tetrapods were studied. Revealing insights on the distribution and excitation of the LSPR for these shapes indicated that the enhancements were found to be strongest for elongated shapes (rods and tetrapods) compared to spheres. However, the low carrier density (compared to Au for example) and possibly localized (and not collective) oscillations resulted in a lower enhancement magnitude of the field compared to similar morphologies of Au. The localized nature of carriers in $Cu_{2-x}Te$ is also reported in Ab initio structure calculations, wherein vacancy channels of 0.3×0.7 nm were revealed to be alternatingly formed along the {001} layers connected by low-density areas between them as shown in Fig. 14 [329].

The lack of a database for the material constants of this chalcogenide is also an issue here [330], as it is quite possible that the enhancements are not reflective of the actual numbers due to the difference in the LSPR peak positions of the calculations vs the synthesized nanoparticle, and hence, the field enhancement magnitudes are quite possible to be revised as research progresses on these materials. This is indeed made clear from a previous report [217], wherein field enhancements comparable to many if not the best coinage metals have been observed.

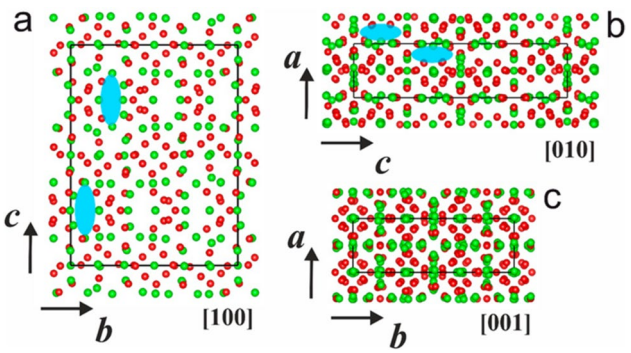

Fig. 14 $Cu_{1.5}$ Te structure determined and refined by electron diffraction tomography (EDT). **a** View along [100] and [100] highlighted in blue. **b** View along [010]. HAADF-STEM images are highlighted in blue. **c** View along [001]. Te represented by green, Cu atoms by red (reprinted with permission from [329])

Combining the optoelectronic properties of semiconductors and metals can be of immense benefit, as both excitonic and plasmonic properties can be exploited. To this end, compositions of CdTe-$Cu_{2-x}Te$ have been investigated. An interesting behavior of the Auger-mediated recombination between excitons in CdTe with the free carrier holes in $Cu_{2-x}Te$ was reported, resulting in a quenching of the PL of the CdTe subunit although the investigators were careful not to rule out the changes to PL as due to the different surfaces and proximities for the CdTe vs $CdTeCu_{2-x}Te$ compositions. Another observation was the unexpectedly low shifts in resonance frequency between the two materials, which was ascribed to the fact that the free carriers were localized more in comparison with the conventional free electron-based resonance exhibiting materials wherein the delocalization results in a wider influence on the plasmon resonance. This degree of localization was alluded to as the reason that the environment had a lesser impact on the resonance of the composite in terms of the shift despite the markedly higher refractive index. The carrier dynamics were found to be significantly altered for the composite than pristine CdTe material, ascribed also due to the faster Auger route of exciton relaxation. Such interesting combinations can be used for manipulating the decay dynamics and other interactions between these absorptions, which have been proven to lead to new phenomena such as Fano resonances [331].

The reports reviewed so far have been chosen to reflect the differences possible in terms of observations and applications of the predominant plasmonic chalcogenides of Cu. We present a comprehensive summary on the different chalcogenides of Cu used for plasmonic investigations in Table 3. Studies on the optical metrics of such Cu deficient chalcogenides aimed at revealing the absorption and scattering cross-sections, dependence of them on particle morphologies and the dielectric environment, and changes to them based on the myriad of possibilities present in terms of lattice alterations are vital to take these group of materials forward for such applications. Research such as reviewed here reveal the fundamentally interesting prospects of non-stoichiometric plasmonic chalcogenides, with regards to tuning their optoelectronic behavior in accordance with LSPRs as well as the coupling between them and excitonic transitions. This coupling for example leads to changes in the excitonic band-gap as well and is often reconciled by pertinent theories such as the Moss-Burstein effect, AC Stark effect, and the Purcell effect. Phenomena such as enhanced two-photon absorption, dynamical Stark shifts, up-conversion,

Table 3 Copper chalcogenides and mechanisms of tuning morphology and plasmonic properties

S. no.	Chemical compositions	Morphology	Dimensions/LSPR (nm)	Prospective applications	Method of tuning LSPR	Novel findings	Ref. no.
1	$Cu_{2-x}S$	Nanodisk	Aspect ratio = 4.6–7.1/1650 to 1860	Photovoltaics, photocatalysts, and chemical sensing	Reaction time & temperature	Independent tuning of morphology and carrier density	[333]
2	$Cu_{2-x}S$	Nanodots	Dia = 2/600–1100	Photoacoustic imaging and Photothermal therapy	Changing the Cu concentrations	PA imaging and PTT along with EPR capability	[334]
3	$Cu_{2-x}S$	Nanospheres	Dia = 15/1000–1350	MRI, thermal, photoacoustic multimodal imaging	Changing the Cu concentrations	Improved contrast through NIR imaging for multimodal imaging and therapy	[335]
4	$Cu_{2-x}S$	Nanospheres	Dia = 6.5/1400	Photothermal and photodynamic therapy	Absorbance tuning was not a focus of this study	Dual PTT and PDT cytotoxic effects on NIR illumination	[333]
5	$Cu_{2-x}S$	Nanorods	Aspect ratio = 4.5/1200	Photothermal therapy	Phase and composition	I_2 is a switch between cation exchange and shell deposition during synthesis	[333]
6	$Cu_{2-x}S$	Nanocrystals	5–51/300–650	Mineralogy	Different methods of synthesis	Spectra of $Cu_{2-x}S$ indicate direct band gap character	[258]
7	$Cu_{2-x}S$	Nanosphere, Dodecahedron	72–115/350	Electrocatalyst	Tuning the precursor concentration and reaction conditions	Controlling the size and morphology by tuning the precursor concentration	[336]
8	$Cu_{2-x}S$	Spheres	2.4–5.9/200–516	Nanophotonic circuitry and terahertz imaging	Changing refractive index	LSPRs and quantum-confined excitons within the same nanostructure made strong coupling of photonic and electronic modes	[269]
9	$Cu_{2-x}S$	Sphere	13.7/1250	Sensors, nanomedicine, catalysis, and energy conversion	Absorbance tuning was not a focus of this study	Fermi level of the $Cu_{2-x}S$ nanocrystals as measured through electron equilibration	[337]
10	$Cu_{2-x}S$	Spheres	12–20/700	Photodynamic	Absorbance tuning was not a focus of this study	Metal chalcogenides could act as smart light-driven sterilant	[338]
11	$[^{64}Cu]CuS$	Nanospheres	Dia = 11/930	Positron emission tomography and photothermal therapy	Varying the ligand type	PT active and theranostic $[^{64}Cu]$ CuS NPs with intrinsic nuclear and LSPR characteristics	[339]
12	CuS	Nanodisk	Thickness = 15/1250	Generic optical applications	Changing the dielectric of the surrounding medium using different solvents	Ligand exchange mediated LSPR recovery with oleylamine	[333]

Table 3 (continued)

S. no.	Chemical compositions	Morphology	Dimensions/LSPR (nm)	Prospective applications	Method of tuning LSPR	Novel findings	Ref. no.
13	CuS, $Cu_{1.96}S$, $Cu_{7.2}S_4$	Nanodisk	Aspect ratio = 4–5/500–700	Infrared plasmonics, and for light-matter interactions at the nanoscale	Generating non-stoichiometric vacancies	The geometry of nanodisk assemblies produces a dramatic change in LSPR coupling	[270]
14	$Cu_{1.75}S$	Nanocapsules	Dia: shell = 199–438; core = 153/600	Drug delivery and photothermal therapy	Varying the cross-linker dosage	Mild irradiation and low a dosage sufficient PT + chemotherapy	[104]
15	CuS	Nanospheres	Dia = 2.7–7.2/500–950	Tumor imaging	Increasing the reaction time	Small particles enable contrast-enhanced tumor imaging	[340]
16	$Cu_{1.8}S$	Nanospheres	Dia = 6.6–17.3/1000–1250	Optoelectronic devices	Increasing the reaction temperature	Gram-scale synthesis	[341]
17	$Cu_{7.2}S_4$	Nanospheres	Dia = 20/1000	Photothermal therapy	Varying I_2 exposure time and duration	Enhanced photostability and reduced dosage sufficient for tumor ablation	[342]
18	$Cu_{1.94}S$	Nanocrystals	20/1125	Photothermal therapy and sensing	Absorbance tuning was not a focus of this study	A negligible fraction of Cu species could be detected in the solution phase	[343]
19	CuS	Nanodisk	Dia = 19, h = 5/1112–1300	–	By changing the refractive index using different solvents	Coherent excitation of symmetric radial breathing modes are observed at LSPR wavelengths	[273]
20	$Cu_{1.1}S$	Nanodisk	Dia = 13, Thickness = 5.3/1100–1700	–	Generating non-stoichiometric vacancies of Cu	Chalcogen – chalcogen bonds holding the layers for intercalated metals, while their overall anion sublattice does not change	[274]
21	Cu_2S	Nanorods	Length = 30; dia = 5/1200	Photocatalysis	Absorbance tuning was not a focus of this study	Reducing the potential of electrons in the conduction band of CdS s to fabricate $Cu_{2-x}S$ nanorods	[344]
22	Cu_2S	Nanorods	5/1240	Optoelectronic devices	Absorbance tuning was not a focus of this study	Cation exchange route to synthesize epitaxial heterogeneous nanostructures	[345]
23	CuS	Triangular prisms	Edge length = 23–56/700–1100	Chemo-photothermal therapy, bioimaging, and biosensing	Increasing the reaction time	Presence of halide ions binding interactions between oleyl amine and the CuS surface	[346]

Table 3 (continued)

S. no.	Chemical compositions	Morphology	Dimensions/LSPR (nm)	Prospective applications	Method of tuning LSPR	Novel findings	Ref. no.
24	Cu_2S	Sphere	6.9–11.9/800–1200	Sensing and photocatalytic	Absorbance tuning was not a focus of this study	Cu_2S nanocrystals were prepared by two methods to give surfaces capped by crystal-bound and surface-bound	[347]
25	$Cu_{31}S_{16}$	Tetradecahedra	Dia = 23, thickness = 29/1250–2250	SERS sensor	A high density of Cu vacancies	$Cu_{31}S_{16}$ converted to more copper-deficient roxbyite by the heat treatment	[348]
26	Cu_2S	Spheres	4.5–5.7/800–1100	Photovoltaic	Using capping agent	Surface ligands prevent oxidation	[349]
27	CuS	Spheres	10–12/1000	Solar cells, photocatalysts, smart windows, superionic materials, and chemical sensors	Varying the concentration of capping agent	The aggregated CuS NPs could form large particles, thereby reducing the intrinsic LSPR	[350]
28	CuS	Sheets	Size = 30–50; thickness = 3–5/1200–1500	Photovoltaics	Varying the concentration of precursor	shape and size control CuS tuning the precursor concentration	[351]
29	CuS	Plates and prism	38/1000–1750	Solar cell and sensing	Increasing the reaction temperature	The crystallinity of the surfactant coating affects LSPR	[352]
30	Er@$NaGdF_4$:Yb@ $NaNdF_4$@$mSiO_2$-CuS	Core–shell	Dia: shell = 3; core = 30/–	Chemo and photothermal therapy	Absorbance tuning was not a focus of this study	Cancer imaging and ablation by synergistic PTT	[353]
31	PEG-GO/CuS	Nanocomposites	Dia = 13/980	Photothermal therapy	Varying the ligand type	High loading efficiency with photo and chemotherapeutic capabilities	[354]
32	CuS@$mSiO_2$-PEG	Core–shell	Dia: shell = 13; core = 37/700–1100	Chemo and photothermal therapy	Changing the pH	DOX release by NIR PTT and pH	[355]
33	Au@$Cu_{2-x}S$	Core–shell	Dia = 150/980	Chemo and photothermal therapy	Changing Cu concentration	The size of the Au core @ $Cu_{2-x}S$ controls LSPR	[356]
34	$Au-Cu_9S_5$	Nanospheres	Dia = 10/1064	X-ray CT imaging and photothermal therapy	By alloy formation	$Au-Cu_9S_5$ hybrid NPs have a higher absorbance than Cu_9S_5	[357]
35	$Cu_{1.94}S$-CdS, $Cu_{1.94}S$-$Zn_xCd_{1-x}S$	Nano disk	Dia = 41.7; thickness = 115.9/490	Heterojunction solar cells	Composition	Monoclinic wurtzite structures by thermal decomposition	[358]
36	$Cu_{1.94}S$-ZnS, $Cu_{1.94}S$-ZnS-$Cu_{1.94}S$, $Cu_{1.94}S$-ZnS-$Cu_{1.94}S$-ZnS- $Cu_{1.94}S$	Nano screw, nanodumbell, and nanospheres	Length = 60; dia = 30/800, 2000	Optoelectronic, solar cells, optical sensing	Concentration of Zn cations	Hetero nanostructures of metal chalcogenides with unique morphologies	[359]
37	CuCdS	Fusiform, nanorods, nano hexagon	Length = 44; width = 24/960–1067	Photovoltaics, photoelectric	Varying the molar ratios of Cu/Cd	Temperature and precursor-controlled morphologies	[360]

Table 3 (continued)

S. no.	Chemical compositions	Morphology	Dimensions/LSPR (nm)	Prospective applications	Method of tuning LSPR	Novel findings	Ref. no.
38	Au@ZnS, Au@CdS, Au@AgAuS, Au@Ag_2S	Nanocubes, polyhedrons, nanorods	Polyhedron dia = 43; edge length = 50; dia of nanorod = 14; length = 58 nm/500–700	Photovoltaics, photovoltaics	Varying the metal sulfides	Water-dispersible gold–Cu sulfide heterostructures	[361]
39	Au@ $Cu_{2-x}S$	Core–shell	Core = 100; shell = 10/700–1000	Photothermal	Varying the concentration of precursor	Coupled resonance peaks from the coupling SPR of $Cu_{2-x}S$ shell, and the two plasmon resonances of Au NRs	[362]
40	$Cu_{2-x}S$@Pt	Nanospheres	8.5/1050	Cancer therapy	Absorbance tuning was not a focus of this study	CT imaging and chemo-photothermal therapy can be achieved by injecting $Cu_{2-x}S$:Pt(0.3)/PVP NPs in a single dose	[363]
41	$Cu_{1.84}S$, $Cu_{1.9}S$, Cu_2S @ ZnS	Nanocrystals	R = 20; thickness = 15/1300	Photovoltaic devices, superionic materials, battery electrodes and photocatalysis	Absorbance tuning was not a focus of this study	Solid − solid phase transformation of the copper sulfide phase in heterostructure NC	[364]
42	$Cu_{2-x}S$	Spheres/ Disks	Dia = 4; aspect ratio = 3–6/1800–3100	Thermal imaging, IR-responsive coatings, and telecommunication	Increasing thermal treatment time and temperature	Shape tuning for manipulation of LSPR/subwavelength EM radiation	[265]
43	$Cu_{2-x}S_ySe_{1-y}$	Nanowires	Dia = 200–500/565–760	Chemical sensors, Solar cells, optoelectronic devices	Different molar ratios of Cu/S/Se	Synthesis of cubic phased $Cu_{2-x}S_ySe_{1-y}$ compounds	[321]
44	$Cu_{2-x}S$, $Cu_{2-x}Se_yS_{1-y}$, $Cu_{2-x}Te_yS_{1-y}$	Spheres	Dia = 3 to 10/1270, 1300, 800	Optoelectronic and biomedical	The concentration of oxidizing agent	Common synthesis of water-soluble plasmonic CuE (E = S, Se, Te)	[268]
45	$Cu_{2-x}Se$, $Cu_{2-x}S$	Crystals	Length = 12; width = 5/1000–1500	Optoelectronic	Different morphologies	vacancy-doped copper chalcogenide NCs with NIR optical resonances	[330]
46	$Cu_{2-x}S$, $Cu_{2-x}Se$, $Cu_{2-x}Te$	Nanocrystals	5–12/900–1400	Photovoltaic	Generating non-stoichiometric vacancies of Cu	$Cu_{2-x}Te$ shows similar properties of $Cu_{2-x}S$, $Cu_{2-x}Se$ in the NIR region	[326]
47	CuTe	Rods	Length = 15–40/1000	Photonics, photovoltaics, photothermal therapy	Absorbance tuning was not a focus of this study	Explains the crystallographic structure of complex nanocrystals containing defects	[365]
48	$Cu_{2-x}Te$	Nanospheres/hollow nanospheres	Dia = 8.8; dia = 16.5/1150, 1200	Optoelectronic devices	Increasing the reaction time	LSPR of hollow-type $Cu_{2-x}Te$ NS more sensitive to the refractive index	[366]

Table 3 (continued)

S. no.	Chemical compositions	Morphology	Dimensions/LSPR (nm)	Prospective applications	Method of tuning LSPR	Novel findings	Ref. no.
49	$Au@Cu_{2-x}S$, $Au@Cu_{2-x}Se$, $Au@Cu_{2-x}Te$	Coreshell	Shell = 24–54 /500–900	Photocatalysis	Varying the concentration of Au	Au and CuS exhibit two LSPR peaks at Vis and NIR region	[367]
50	$Au@Cu_{2-x}S$, $Au@Cu_{2-x}Se$	Core–shell	Shell = 2.2–13.5; Core = 19–27/490 nm	Photoacoustic, X-ray computed tomography, photothermal therapy	Changing core thickness	Low non-specific interaction and high photothermal stability	[368]
51	$Cu_{2-x}S_ySe_{1-y}$	Spheres	8.8–9.6/1500	Optoelectronic	Varying the concentration of Cu/S	$Cu_{2-x}S_ySe_{1-y}$ NCs blue-shift from 0.90 to 1.00 eV with the increase of Se content from 11 to 66% related to the effective mass of free carriers	[369]
52	$Cu_{2-x}S$, $Cu_{2-x}Se$, $Cu_{2-x}Te$	Spheres	2.8–13.5, 6–16.5/1000–1300	Printable field-effect transistors and micro electronic devices	Increasing the reaction temperature	Surface interaction of the deprotonated carboxyl group controls both the size and the cationic deficiency	[300]

and plasmon generation by quantized exciton generation are a few examples of potentially rewarding investigations in such plasmonic systems [332].

Plasmonics of Composited/Ligand Stabilized Cu Nanoparticles

We discuss here the design, synthesis, and study of materials and devices based on combining plasmonic Cu with various moieties as ligands, stabilizers, and generically as additives. The concept of MEF has been introduced already, and the use of metallic alloys composed in part of Cu has been investigated for their enhancements to the fluorescence of suitable fluorescent molecules. In this regard, the effect of adding Cu to the most commonly used AgNPs for fluorescent enhancement has been investigated. The result was that the CuNPs quenched the fluorescence when present in increasing mole fractions, as new channels of non-radiative decay of the absorbed photons were created in Cu. The overlap of the emission peak of the tested fluorophore (Cy3) with the inter-band transitions in Cu can be intuited to be a problem as well, as it will further quench the emission intensities. However, engineering the particle sizes to tune the scattering vs absorption (i.e., radiative vs non-radiative channels) percentages can help, as it was found that alloy particles of 60 nm diameter were found to cause MEF when present as spheres and in a dielectric of polyvinyl alcohol [370].

The composite of graphene/Cu has been projected to be one of the better prospects for photonic applications, due to reasons like a strong confinement of the plasmon at the interface, an effective protection against oxidation, and minimal interference with the plasmonic field enhancements due to the monoatomic thicknesses possible. As grown Cu/graphene can be advantageous (albeit having a higher defect density as a result of the lattice mismatch during growth) compared to transferred graphene grown in a separate CVD process wherein a better level of intimate electrical contact and adhesion is possible with the former. To overcome this limitation, CuNPs were formed post deposition of a continuous film simultaneously during the deposition and growth of Graphene with methane as the carbon source. The resulting capped composites exhibited a tenfold enhancement in the fluorescent intensity of a DCM dye due to strong coupling and energy transfer between the plasmonic and dipolar modes [371]. Graphene-protected Cu was also studied as a fluorescence-enhancing combination for a single crystalline material. BP3T modified with this combination exhibited a marked increase in PL intensity when compared with either BP3T/Cu or BP3T alone. The contribution from graphene was not explicitly addressed (apart from improvements to oxidation stability), while the enhancements to the intensity were attributed due to the coupling of the LSPR of Cu to the emission from the dye and a reduction as a result of the

emission lifetimes. Directional emission studies measuring the polarization of the emitted light could have shed more light on the causal reasons for the enhancements [372]. An interesting aspect to be mindful of while designing graphene-protected Cu is the presence, concentration, and nature of defects. Comparing the defects present in sheets vs in graphene powders led to a change in the intimacy in contact between them. The result was a lower H_2 evolution (through H^+ reduction on graphene defect sites) when Cu alone was used and when graphene with lower concentrations of defects was used. The mechanism of hot carrier generation through plasmon decay and the crucial subsequent step of their separation (electrons to graphene and holes to lactic acid) was proposed as the causal mechanism for the observations. Hence, it can be stated that graphene with defects can be beneficial too, as evidenced by this example [373]. Graphene has hence become a strong associative combination with Cu for a myriad of purposes and enhanced phenomena.

Mimicking natural processes has been an ongoing effort for a diverse range of purposes [374]. One such process which when mimicked can give efficient results is photosynthesis, in which utilization of CO_2 forms a part. This begins with conversion of CO_2 into for example the CO_2 radical anion or CO, which can initiate multiple reactions such as fuel production from biowaste. For the catalytic reduction of CO_2, plasmonic materials are of benefit due to the generation of hot carriers during thermalization. If the hot electrons and hot holes can be separated, reactions can be catalyzed [375]. In this research on hot carrier generation and separation, the contributions to the hole population (when for example d-holes are generated) by plasmonic decay are crucial [376], as the energies of these holes critically dictate their lifetimes and hence probabilities to participate in reactions. This dependence of the d-hole energy on its lifetime is directly tied to the DOS which for Cu varies steeply with energy as shown in Fig. 15 [376] compared to for example Au, as the hybridization between the d and sp bands is stronger for the latter leading to a broader DOS and hence a lower dependency on energy. The result is that for d-holes created at levels at increasing distances from the Fermi energy, the lifetimes increasingly reduce due to this nature of the DOS in Cu [377].

Meticulous calculations of the lifetimes confirm this trend, with 250 fs observed for hot electrons excited to energies of 0.1 eV above the Fermi level whereas for those excited to 2 eV a drastically reduced lifetime of 20 fs [378]. In this field of hot carrier separation catalysis, the natural tendency of Au NPs to be more inert than Cu has made it

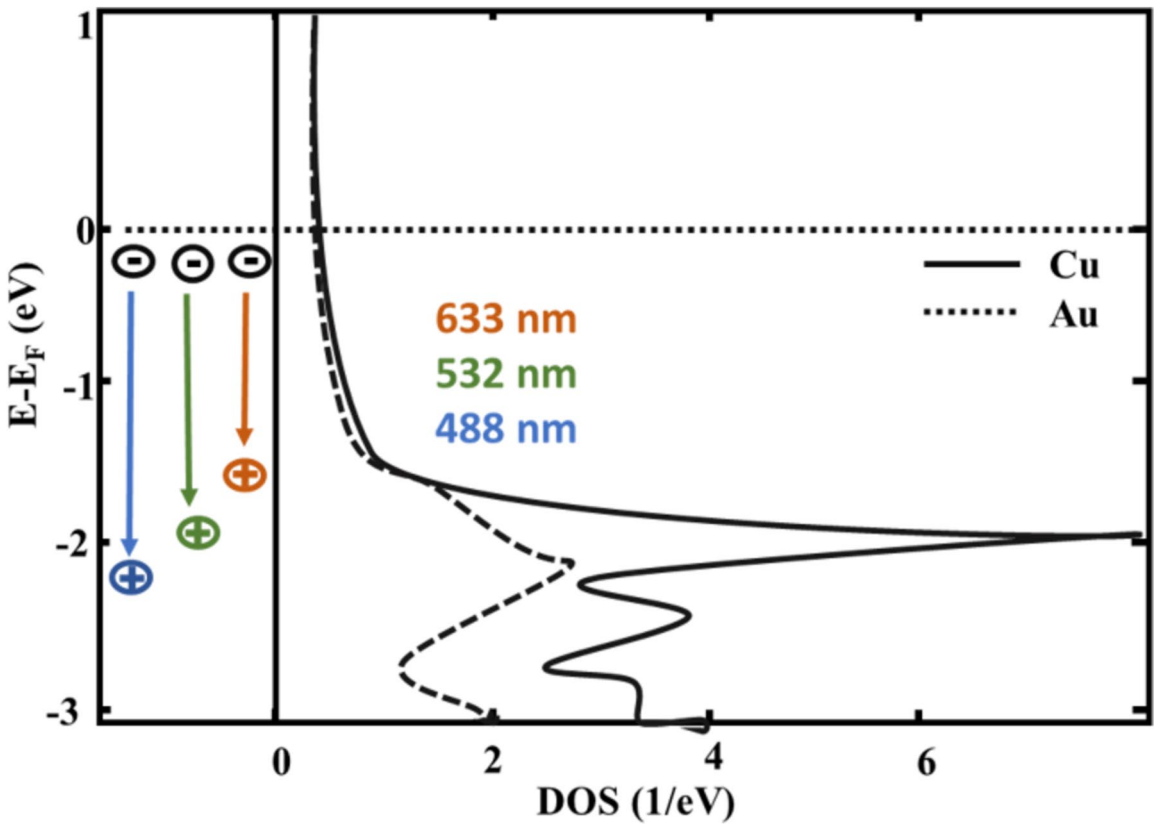

Fig. 15 Schematic diagram of interband emission involving d-holes created by 488, 532, and 633 nm excitations on Au vs Cu

and Ag the main proponents for this field of research, and yet Cu has been studied extensively for its efficacy in catalyzing CO_2 reduction, albeit not very often on the plasmonic angle but through electrochemical reduction catalyzed by it [379]. Meanwhile, a comprehensive and careful summary on plasmonic catalysts in general that exclusively treat CO_2 reduction alone is available [380]. The binding energy of CO on Cu is the critical factor in determining the investigated materials' selectivity and catalytic activity [381] with Cu occupying the middle ground in terms of the binding energy and metals like Ag, Au, and those of Pt, Ni, Ru, and Rh occupying the low and high binding energy regions, respectively. There are studies, however, that have investigated this enhancement in CO_2 reduction using alloys of Au-Cu on TiO_2, yet do not ascribe hot carrier separation-induced reasons for the same [382]. Other reports for example have investigated the synergistic effects of a Cu/Pt/TiO_2 composite as well as an Au-Cu alloyed $SrTiO_3$/TiO_2 composite and report an increase in CO_2 reduction based on the increased photo-generated carriers from TiO_2 [383, 384] and only hold Cu to be responsible for presenting sites for adsorption/desorption with no mention of the plasmonic enhancements from Cu itself. More published research points to the same, wherein the plasmonic contribution by Cu was not investigated (probably due to the nature of the surface Cu species to be oxidized), and its role was as a recombination preventer/adsorption enhancer [385]. A brief mention of the enhanced electromagnetic fields of the Cu plasmons being a contributor to the enhancements was made in this study [386].

The Au-Cu Alloy System

Au being the other poster child of metal photoluminescence has been alloyed with Cu in an extensive array of reports. Careful studies carried out through varying the lattice proportions of Cu, particle sizes, binding ligands, and excitation as well as emission wavelengths revealed that the NIR PL emission from the alloyed NPs arose from transitions within the Au-thiolate (the most often used cap for Au clusters) surface complex. The Kohn–Sham potentials used to reveal the orbitals and the DOS corresponding to this system confirmed this postulation along with excitation spectra, with little variation in the PL position with size. Increasing amounts of Cu resulted in an increasingly redder emission, with atomic percents from 0 to 80% shifting the PL peaks from 947 to 1067 nm [387]. The brightness of these alloyed NPs was also brighter than the best NIR-emitting lanthanide probes, indicating their deployment readiness for various luminescence-based applications.

Furthering such investigations, Au-Cu alloys have been proposed to increase the conversion of nitroaromatics to anilines predominantly through the reason of Cu providing a stronger site for adsorption than Au due to its slightly electropositive nature [388] when present as an alloy. The Au-Cu alloy system has been a strong contender in this field of plasmon-enhanced catalysis due to tunable absorbance and nature of surface sites [389], with studies that report on their uses for example in enhancing rates of conversion of 4-nitrophenol to 4-aminophenol with alloyed triangular prisms [390]. A summary of this system and the reactions studied with the investigation of its plasmonic advantages is provided in Table 4.

The first observation of the interactions between the constituents in a plasmonic alloy is the change in absorption. Among the myriad investigations that often confirm a bathochromic shift with increasing Cu atomic fractions, ordered Au-Cu alloys have also shown a hypsochromic shift, attributed to the ordered creation of the alloys in contrast to a random formation by modifying the synthesis process [407]. Compared to other alloy systems that will be discussed next, computational findings suggest that Au-Cu can be the most favorable composition when looking for a homogeneous mixing of both atoms instead of the atoms becoming segregated. The thermodynamic driving forces calculating the energy of formation predict a decrease in formation energy of Au-Cu compared to Au alone for appropriate proportions of Cu insertion, confirming this conclusion. The close overlap between the Au-5d and the Cu-3d orbitals allowed charge transfer to the more electronegative Au from Cu, and though the simulated clusters consisted only of 100–200 atoms, they exhibited a collective "plasmon-like" electron oscillation due to the close overlap [408].

The presence of Au as a compositing element to Cu rather than an alloying element has also been studied. The resulting coupled plasmon being termed as a charge transfer plasmon (CTP), leads to interesting effects such as a drastically red-shifted resonance position (up to 1200 nm) compared to both Au and Cu. The nature of the contact line between Au and Cu proved to be a deciding factor of the resonance position and width, with adsorption of DNA on the preliminarily synthesized Au seeds also controlling this contact line [409]. Such structures when studied in a more comprehensive manner through multiple investigations can be promising especially in terms of applications concerned with surficial properties, such as sensing and catalysis.

The Cu-Ag Alloy System

Another alloy system of Cu is with its coinage peer of Ag. Interestingly, the Ag-Cu system has been reported to form alloys as well as bimodal compositions, wherein the latter can be present as a core–shell arrangement or as segregated phases of Cu and Ag with separate LSPR peaks for each. Both compositions have been reported with an almost equal occurrence. The bimodal composition being investigated for its plasmonic properties is summarized in Table 5.

Table 4 A summary of Au-Cu alloy system to enhance the plasmonic resonances and the mechanisms of tuning their morphology

S. no.	Configuration	Morphology	Dimension (nm)	LSPR (nm)	Method of tuning LSPR	Ref. no.
1	Silica@Au, Au-Cu Au = 1–15 Wt%	Spheres	Silica-40 Au-2	506	Changing the concentration of Au	[391]
2	Au-Cu @TiO_2 Au = Cu = 1 mol%	Spheres	3.1–3.8	551	Varying the stoichiometric value of Au/Cu	[392]
3	Au-Cu Cu = 12 mol% Au = 1 mol%	Cubes	Edge length = 3–85	530–660	composition varied from $AuCu_3$ to Au_3Cu	[393]
4	Cu-Au Cu = 27% Au = 73%	Spheres	4–7.4	514	Varying the sizes of the Au seeds	[394]
5	Cu-Au Au = 5–43%	Core–shell	Au-1.5 Cu-2.6	–	Varying the stoichiometric value of Au/Cu	[395]
6	Au-Cu and Au-Cu_3	Crystals and wires	Width = 10, height = 11 Dia = 15–25	600	Varying the solvents	[396]
7	Au-Cu alloy Au = 0.6–1.8 Cu = 0.2	Alloy	3–4	527	Absorbance tuning was not a focus of this study	[397]
8	Au-Cu@CdS Au = 0.3–0.5%	Stars	Spike length = 61	640–950	Tuned by the atomic ratio of Cu	[398]
9	Ag@Al_2O_3 Ag = 20 Wt%	Cubes	Edge length = 60	590	Absorbance tuning was not a focus of this study	[399]
10	Cu-Au, Cu-Pt, Cu-Pd Cu = 2–4% Au = 1%	Rods	Aspect ratio = 1–4	600–900	Varying Cu concentration	[400]
11	AuCu Au = 75% Cu = 25%	Spheres	2.2	560	Varying the molar concentration of Au-Cu	[401]
12	Au-Cu Au = 86.2% Cu = 13.8%	Stars	Spike length = 100	450–1500	Varying the precursor molar ratio of Au/Cu	[402]
13	Au-Cu Au = 5%	Spheres	3.2–7.6	530–640	Varying the concentration of Cu	[403]
14	Au-Cu@alumina Cu = 95%	Spheres	6.1	Au:520 Cu:560	Absorbance tuning was not a focus of this study	[404]
15	Au-Cu Au = 6% Cu = 6%	Spheres	3	514	Varying the concentration of Cu	[405]
16	Cu-Au	Tubes	50–70	560	Absorbance tuning was not a focus of this study	[406]

Studies have reported the possibility of controlling the formation of products (azo vs azoxy) through the use of Cu-graphene vs Cu-Ag-ZrO_2. The former resulted in the formation of both azoxybenzene and azobenzene from nitrobenzene, while the latter resulted in the formation of azoxybenzene from nitrobenzene. For the Ag/Cu/ZrO_2 study, multiple investigations were done to rule out/confirm this catalytic activity, ranging from XPS to confirm the metallic state of Cu in the alloy vs when present alone, elemental mapping from TEM to confirm the presence of both Ag and Cu in the lattice, and catalytic activity measurements to confirm that only the alloy enhanced the conversion in an optimal amount compared to its monometallic counterparts, and that only the alloy resulted in a selective conversion to azoxybenzene instead of azobenzene. TEM analyses were concluded to reveal the (111) plane of the alloy's lattice as a governing observation, albeit confirmation through other studies/with calculations could have revealed insights into the DOS distributions for example. The plasmonic peak was observed at approx. 408 nm for the alloy, implying a closer match to that of Ag than Cu. This could be reconciled from the proportions of the Ag: Cu for the alloy, which at values of Cu higher than 4:1 led to a considerably oxidized surface and a loss of catalytic activity. A higher conversion was observed for excitation wavelengths close to 400 nm, implying a plasmon-induced enhancement to the conversion

Table 5 Plasmonic properties of the bimodal composition and the mechanisms of tuning their morphology and the prospective applications

S. no.	Configuration	LSPR (nm)	Prospective applications	Method of tuning LSPR	Novel findings	Ref. no.
1	Ag-Cu-alloy	Ag: 404–430 Cu: 581–588	Sensors	Changing the Molar ratio of Ag and Cu	Smaller aggregate nanostructures with higher fractal dimensions have Ag-rich, while the larger aggregates with low mass fractal dimensions have Cu-rich compositions	[410]
2	Ag-Cu-alloy	Ag: 407 Cu: 585 Ag-Cu: 534	Flip-chip	Varying the reaction time	Silver-copper alloy nanoparticles for the conductive fillers in electrically conductive adhesives	[411]
3	Ag-Cu @Cu core–shell	Ag: 460 Cu: 600	Catalysts, sensors, SERS	Changing Molar ratio and reaction time	Optical property can be controlled by changing the thickness of the Cu shell	[412]
4	Ag-Cu alloy	Ag: 410	–	Changing the Molar ratio of Ag and Cu	The proportion of silver and copper salts varied degrees of solid solubility	[413]

as well as the observation of a lowered activation energy for the irradiated samples confirming this postulation. The study with graphene as a stabilizing support (for Cu in the metallic state) reports the plasmon peak and the associated enhancements to the conversion due to an efficient cleavage of the N–O bond. The conversion efficiency was found to markedly depend on temperature due to the different activation energies and the Bose–Einstein electron distributions [414]. Considering that visible light irradiation has been employed in these studies, it is quite probable that contributions to the effective free carrier densities in the alloys from Cu play an active role to the catalytic rates as well, although the contribution is probably detrimental considering the easy tendency for oxidation of Cu. It is hence a compromise probably that the addition of Cu provides considerable tunability in the LSPR position, while limiting the stability of the pristine metal that it alloys with to a very short period of time (usually days). Reports confirm this observation for the Ag-Cu system as well, wherein tuning from ~ 400 to ~ 600 nm is possible with different mole fractions of Cu albeit with accompanying stability limitations [381, 415]. A novel multi-compositional nanorod comprising of sodium yttrium fluoride ($NaYF_4$), TiO_2, and a Ag-Cu alloy has been investigated for two-photon up conversion-mediated photocatalytic applications with the aim of generating the highest currents on photoexcitation. The specific functions of upconversion in NIR by $NaYF_4$ and injection of the up converted photon into TiO_2 for carrier generation, of TiO_2 for carrier generation, and of the Ag-Cu alloy for preventing carrier recombination and to aid in photocarrier generation due to the overlap of the LSPR with the TiO_2 band-gap were elucidated in this study. The role of Cu however, was attributed only as reducing Ag utilization and hence costs, as substantial amounts of it will shift the LSPR away from the absorption edge of TiO_2 and reduce the photocurrent amplitude [416]. An analogous investigation with the composition of Ag-Cu-decorated SiO_2 on which layers of S-doped carbon nitride (CN) were wrapped on has been reported as an efficient photocatalyst. In this case, however, the generation of hot carriers and their transfer to CN (preventing recombination) which catalyzed the production of H_2 from water was the mechanism of photocatalysis. The molar ratios of 1:3 of Ag: Cu led to the highest H_2 generation rates among the compositions investigated and were optimal to prevent recombination (due to close contact) between the alloy and the CN wrapper. The comparatively lesser reduction in PL intensity for this ratio compared to others confirmed the attribution of this ratio as optimal (due to the absence of hot carrier recombination which would have reduced H_2 production) [417].

Other Plasmonic Cu Composites

The importance of the separation distance between the plasmonic material and the scattering center such as a fluorophore was investigated in a study employing a hierarchical structure of CuNWs and MoS_x dispersed in a Cu foam. Marked differences in PL intensities revealed the differences in recombination rates for the compositions involving MoS_x blended into CuNWs and Cu foam vs those where CuNWs were first blended with MoS_x post which they were dispersed in the foam support, making the former much better for photocatalytic H_2 evolution [418]. Transmetalation of ligands can also be catalyzed by LSPR, and from the one report on this specific reaction, the irradiation wavelength was reported to be crucial. The switch between

homo-coupling to cross-coupling when irradiated with different LSPR active wavelengths (< 500 nm vs > 500 nm) using Cu-Pd particles was attributed to be the reason for the different reaction intermediates that were formed under these conditions. Interestingly, the transmetalation was not observed when using pure Cu or when Cu was combined as a composite with other molecules such as Pt/Al_2O_3. A brief attribution to plasmonically generated hot electrons in Cu was given for the differences in selectivity, and the presence of Pd was critical for better adsorption kinetics, Cu-Pd coupling, or other yet undiscovered factors [419]. Considering the plasmonic metal of Pt, an interesting investigation wherein hybrid propagating modes that arise due to coupling between a specific periodic arrangement of nanostructures and the plasmon modes has been reported in the bimetallic system of Pt-Cu. Galvanic displacement of lithographically patterned Cu squares by Pt led to this bimetallic configuration, and the absorption signatures were dominated by Cu (interband transitions at 510 nm, dipolar plasmon at 675 nm) and a hybrid surface lattice resonance (HSLR) at 865 nm which was invoked due to the coupling. The photocatalytic enhancements were not found to be influenced by the Pt plasmon. Among the different experimental conditions tested to quantify the catalytic activity such as in dark conditions, with and without Pt, and with different shell thicknesses of Pt and size/spacing of Cu, the strongest enhancements arose in the presence of the HSLR, attributed to the intense electromagnetic fields at the boundary between the Cu/Pt nanoparticle and the ITO substrate [383].

The higher energies of plasmonically generated hot electrons compared to those generated by decay of interband transitioning ones have been predicted and confirmed, making the latter process more efficient than the direct inter-band excitation [420]. This stems from the fact that LSPR being confined close to the surface, only electrons near the Fermi level will be influenced by LSPR energy transfer, leading to a higher energy as they transition to the excited state compared with the electrons that are excited from lower energies below the Fermi level. Hence, exploiting plasmons for creating hot carriers is more advantageous than generating them through inter-band transitions. Towards further investigations of this plasmonic angle presented by Cu, *p*-NiO has been used to effectively accept hot holes, thereby segregating the hot electrons in the Cu. It is important to have a semiconductor that is transparent in the range of plasmon absorption (example: a band-gap of 3.7 eV for NiO) such that the semiconductor's valence band (example: − 5.4 eV in vacuum for NiO) lies below that of the metal (− 4.5 eV in vacuum for Cu) for hole extraction. The enhanced rates of production of both CO and formate ($HCOO^-$) on visible light irradiation confirmed the role of LSPR-generated hot electrons in Cu, thought to form these products from the creation of the anion radical first. Importantly, the competing mechanism of H_2 evolution which always occurs along with CO_2 reduction was suppressed. The hypothesis that this is the case because of the increased dissociation of H_2 that does evolve on the Cu surface but dissociates through the DIET (desorption-induced electron transitions) mechanism has been put forward to explain the reason for this selectivity [421]. The DIET mechanism has also been proposed to be a reason for the reduced activation barrier for desorption of reaction products in the reaction of NH_3 to produce H_2 on a Ru-Cu alloy. The reductions in the activation barriers of all the reaction steps beginning with the scission of the first N–H bond to the final desorption of the products were predicted to be influenced by the charge transfer of hot electrons to the adsorbate orbitals, with enhancements to the reaction rates ranging from ~ 20 to ~ 177 compared to when only Cu or only Ru was present [422]. In another research studying epoxidation of alkenes including styrene, trans-stilbene, cis-stilbene, and norbornene, the required energy for the reaction was achievable only at energies higher than 500 nm and hence excluded plasmons from playing any role, except for cis-stilbene where the epoxidation was observed for the excitation wavelengths matching the LSPR absorption of the Cu-TiN composite nanomaterial [423].

Hot electrons, being of obvious interest in a myriad of applications involving reaction enhancements and facilitation, have been reported to be generated through the mechanism of plasmon relaxation even in sub-3 nm Cu nanoparticles. This is probably a controversial work reviewed here, with the ascribing of the inter-band absorptions observed (centered at 395 nm) to an LSPR absorption which is intraband. The authors clearly ascribe the higher energy of this absorption due to band discretization but still attribute the same to LSPR. Regardless, a novel approach of controlling the distance between the sub-3 nm CuNPs and the support materials of TiO_2 to distances of approx. 0.42 nm was followed (with the help of multiple linker molecules), so that only hot electrons with the required energy (to cross the resulting Schottky barrier height of 0.88 eV) can transfer into the semiconductor and aid in the eventual evolution of H_2 [424].

A side note on the LSPR of small (< 3 nm) CuNPs is apt to be had here. Multiple studies such as this attribute a "shift" in LSPR to energies up to 6.2 eV (200 Nm) [65, 425] for the particle sizes observed, while the studies cited for these reports only mention a vanishing of LSPR at these sizes with no mention of such a marked shift in the LSPR energy, and clearly describe the impossibility of a continuous DOS (and hence an LSPR) at these sizes nearing 1 nm [426]. There are studies that report an absorbance peak analogous to plasmonic absorption for particles from 2 nm down to nearly 0.6 nm, with a marked decrease in contribution towards this absorbance by free carrier absorption (LSPR) as compared to bound carrier absorption

(inter-band transitions). It stands then for Cu that for sizes less than 10 nm (the mean free path for Cu), the plasmon is highly damped, and that the LSPR contribution to absorption is substantially negligible at sizes less than 2 nm where energy band discretization into discrete energy levels occurs [427]. With all the investigations on plasmon-enhanced catalysis, commercialization presents fresh challenges in terms of cost, efficiency, precision, etc. Towards addressing these issues, amine-capped CuNWs were through a facile process of drop-casting dispersed on a fabric, enhancing porosity and dispersion simultaneously. Plasmon-enhanced PT temperatures of up to 250 °C were achieved, resulting in this configuration being a viable proposition for the catalytic azide-alkyne cycloaddition reaction. Furthering this investigation to include the reproducibility and optimization and affirmation of the role of morphology (as no distinct plasmonic peak was reported and yet was attribute to as a reason for the high absorption of incident energy), for example, can make such ligand-stabilized nanostructures marketable [428].

A survey of research reveals that PT therapy (PTT) is more effective when employing composites or alloys instead of pristine materials. This is primarily (from a plasmonic point of view) because of the ease of tailoring the dielectric constants (which determine the proportions of irradiated energy that is scattered vs that which is absorbed) and the ease of tuning the absorption energies. Both of these abilities are vital, when considering for example that the breadth of absorption energies of only the pristine materials has limitations. Cu has been investigated for PTT with this reasoning primarily as sulfides and selenides as discussed in this review. However, novel compositions have been attempted, with promising results. As an example, Cu-Ag_2S has been synthesized as an alloy with both Cu and Ag in the + 1 oxidation states, indicating a reduction in free electron density. This reduction made possible the peaking of the LSPR of this alloy in the infrared, making it apt for PTT. The reported PT conversion efficiencies (58.2%) were better than the CuS class (27.1%) when the same loadings were used. Careful measurements of the reasons for this, such as the dispersion, retention times, and the effective dielectric constants, can reveal the complete understanding of the material functioning [429]. Another example of an alloy composition with Cu is with Pd, with the Cu component being added for the sole purpose of aiding in autophagy [430] of the tumor cells. The LSPR properties of the composition were not investigated in detail apart from a brief mentioning of the sharp tips of the formed plasmonic tetrapod causing a temperature increase of up to 71 °C on irradiation with an 808 nm laser. Justification of the shape being the major causal factor for the improved PT heating was done by comparing the heating efficiency with spherical nanostructures wherein the latter resulted in much lower temperatures (approx. 45°) realized due to the less intense field accumulations [431]. Investigations of modifications to the lattice of this system can lead to more aspects of plasmonic manifestation such as the phase modifications, stabilities against chemical and thermal environments, causes of the observed morphologies, and the extinction cross-sections, as both these elements have explicit benefits in applications such as H_2 sensing and storage and thermal energy storage and transfer. Indeed, such an investigation has been done for the more common Au-Cu alloy system, wherein the five-fold twinned edges of the initially formed seeds were found to be the growth planes, leading eventually to a starfish-shaped nanostructure. The differences in particle sizes (ranging from 70 to 200 nm) were hypothesized as the reason for the observed plasmonic absorbances in the visible to the infrared. Notably, the atomic percent of only one particle size was quantified. We believe that compositional studies of each size could have revealed differences in atomic percent between Au and Cu, which could have added an additional variable that caused the observed LSPR characteristics. The 70 nm particles were deemed more suitable despite the poorer temperature rises achieved (due to less overlap between the 808 nm excitation and the NIR LSPR for this particle) as they could be retained for a longer duration in vivo post coating with a bio-compatible layer of PEG [402].

Optoelectronic materials, concerned with tuning the band gap for use as light emitters, are often explored with the CZTS/Se (Cu, Zn, Sn, S/Se) class of materials. The plasmonic behavior of these materials has been extensively reported including in the discussion in this review. One study projects their suitability for solution-processed photovoltaic devices due to their easy reversible gelation ability [432]. The LSPR peak was centered at 1326 nm, with variations in position as well as intensity achieved by varying the Cu concentrations. An interesting study that observed the intermediate phases that led to the final composition of Cu_2ZnSnS_4 through SERS reported the formation of the plasmonic $Cu_{2-x}S$ phase in the beginning stages, which gradually disappeared as the final composition materialized [433]. In the prevalent optoelectronic application of solar cell fabrication and improvement, CuNPs were found to increase the efficiency of a PEDOT: PSS-based perovskite solar cell by 115% due to the LSPR property. Specifically, time-resolved photoluminescence experiments revealed the shortening of the radiative recombination of photo-generated carriers due to the strong coupling of the plasmon to the host material as the reason for the efficiency enhancement. A contradiction in their conclusion must be noted here that the least average lifetime of emission was observed for a particular concentration (2 mg of Cu per ml of the composite solution), and yet this concentration had a higher lifetime for the plasmonic component and a lower lifetime for other less influential components governed by traps/defects, leading to

the contradicting but inevitable postulation that the reduction in average lifetime does not always imply an enhancement to scattering. It can be understood from the results of the PL emission experiments [434] that the significantly increased intensity of PL for the 2 mg Cu sample could be the reason for the observation of the best efficiencies. Similar cursory conclusions of the enhancements to photocurrents being due to LSPR in solar cells based on Cu-PEDOT:PSS and Cu-TiO_2 have been made in other studies, with necessary investigations into the other aspects such as the influence of the interface/particle diameter and shape, coverage, and durability towards oxidation unaddressed [435–437]. An illustration of the reflectance of Cu as a function of wavelength overlapped with the solar spectrum shown in Fig. 16 [438] has been given to visualize the benefit of utilizing Cu for enhancing solar absorption for various applications including solar cell efficiency improvement. The selection, therefore, of the wavelength of absorption is crucial, wherein studies have reported enhanced magnitudes of photocurrent even in the proximity of Cu due to a plasmonic nanoantenna effect [439]. This effect, simply put, is the complete concentration of the incident energy into plasmon excitation, which led to a higher photocurrent due to more efficient carrier generation from plasmon-TCPP coupling. The promise of nanotechnology especially for plasmonics is the possibility of manipulation of a wave plasmon vs localized plasmon vs hybrid plasmons by a facile manipulation of morphology and/or the excitation configuration. Such manipulation has also been cursorily investigated for solar cell applications, specifically on the use of Cu nanowires for inducing a wave plasmon. Through the well-researched combination of Cu-TiO_2, the nanowire morphology was found to enhance the incident photon to electron (IPCE) conversion efficiency by 7.5% compared to devices with only CuNWs and by 24% compared to when only a dye was used for photocurrent generation without any CuNWs on visible light illumination. Combinatorial factors of the proximity of dye molecules to the TiO_2 and Cu, the Cu plasmon for generating hot carriers that entered the conduction channel in TiO_2, and an unsubstantiated "waveguide" property of a propagating SPP in the nanowire were attributed to be the reasons for the same [440].

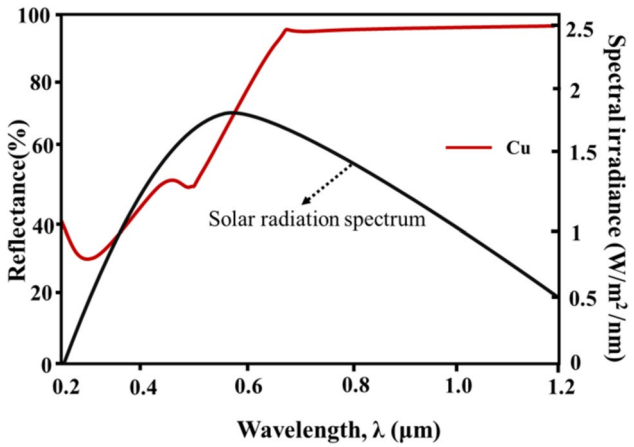

Fig. 16 Reflectance of Cu as a function of wavelength compared with the solar spectral irradiance

Other Compounds of Cu Yet Unexplored/ Emerging for Plasmonic Applications

Interesting chemistries of Cu have been synthesized, such as a mixed metal compound consisting of an antimony/Cu complex ($(((Sb_2(Ncy)_4)_2Cu_4)$ [441], $CsCuTeS_3$ [442], and $CuIn_{1-x}Ga_xS_2$ [443] for which explicit treatments of the plasmonic behavior can be done. More examples exist, such as the mixed chalcogenide-based $Cu_yFe_4Sn_{12}X_{32}$ (X = S, Se) [444] and the CZTS/Se family of materials containing both S and Se such as $Cu_2ZnSn(S_{1-x}Se_x)_4$ [445–448] all of which were scrutinized for their band-gap values primarily, along with carrier masses and mobilities aimed at optoelectronic applications. Similar to the prospect of finding an intermediate/lattice component that is plasmonic in such materials like the Cu_{2-x} phase as discussed in this review, a plasmonic $Cu_{2-x}Se_yS_{1-y}$ phase was formed as an intermediate in research that reported the formation of $Cu_2ZnSn(S, Se)_4$, wherein the plasmonic component was largely quenched while transitioning towards the final phase [432]. Other Janus-type nanoparticle compositions with distinct surficial properties have been synthesized, such as the composition of Cu-Cu_3P [449] whose LSPR aspects can be very unique once revealed through future investigations.

The property of LSPR hybridization with other propagating optical modes such as SPP has been explored for use as a directional glazing material, composed of periodically patterned Cu on a continuous film. By changing the position of the deposited substrate from one that has a continuous film of Cu on one side to one where the nanopatterned Cu is present, energy could either be reflected or be absorbed and converted into heat, making the substrate an ideal conformation as a coating for building windows to maintain indoor temperatures. Such metasurfaces can provide versatility in tuning the light extinction by controlling predominantly the spacing between the patterned features, leading to hybridized [450] modes with broadband plasmonic absorption.

Metal–metal alloy/composites comprised of Pt and Cu have been reported to be effective for PTT. However, the high absorbances in the NIR region had no signatures of typical LSPR absorption. Assessments of the lattice structure, LDOS calculations, and incident field enhancements of the dendritic structures of Pt/Cu achieved here could lead to these materials being extremely tunable agents for

applications concerning light-to-heat conversion [451]. A highly multi-elemental composition of $[Au_{12}Cu_{13}(Ph_3P)_{10}I_7](SbF_6)_2$ is among a common class of possibly plasmonic nanocomposites. The base configuration of such compositions is M_nL_m where n and m are the number of metal atoms and the protective surficial ligands [452]. Despite the effectiveness of these composites being proven for various applications such as non-degassed phosphorescence (i.e., in luminescence applications that require no de-gassing which typically causes PL quenching) and photocatalysis, the plasmonic aspects have, to the best of our knowledge, not been paid due investigations and hence merit analysis. The LSPR property cannot be completely reconciled in such clusters unless the particle diameter exceeds ~ 2 nm, corresponding to an atomic number of ~ 300 atoms for Cu. Yet, these intricate structures [452] with single atom level manipulations can likely exhibit LSPR characteristics by tailoring the number of atoms [453] and hence the free electron density to such appropriate levels, enabling their access to a myriad of applications concerning LSPR such as the capability to serve as hot carrier injectors and PT manipulators. Among the multiple bimodal/bimetallic alloy systems of Cu, the Cu-Ni system is a rarely reported candidate. With analogous observations of a red-shifted resonance with Cu content and particle size, this tuning of the effective dielectric constant can be of use similar to the other systems. Also, the fabrication procedure of the Cu-Ni bimetallic alloy through de-wetting of films from different substrates and the resulting differences in the particle diameter, distribution, and the diameter: height ratios can be a beneficial route for intricate exploitation of the plasmonic properties, extendable to other alloy systems as well [454].

Similar to chalcogenides, phosphides of Cu have been reported to be both plasmonic and semiconducting. To tune the LSPR in the mid-IR for these materials the nucleation controlling agent of Trioctylphosphine (TOP) was used, which showed a trend of inducing lesser Cu vacancies and hence a more-red shifted LSPR with its increase. This material too has promise due to the ability of tuning LSPR by tuning multiple parameters such as the concentrations of TOP, the surrounding material, and the shape and size of the achieved structure, although the latter was found to play a much lesser role in this investigation [455]. The plasmonic nature of this compound is being confirmed by observation of refractive index tuning as well as the inherent negative energy of formation of Cu vacancies, and additional confirmations came in from the observation of the *p*-type nature of the materials indicating a hole-based LSPR. A solid step towards comprehending the fundamental nature of the LSPR in this composition has been done through pump-probe spectroscopy which resulted in a non-linear and instantaneously bleached signal at approx. 1100 nm, indicative of LSPR nature [456]. The promise of these materials, however, has room for exploration, as their potential has only been mentioned in passing for applications such as photovoltaics and synthesis of cation-exchanged novel compositions. For photovoltaic applications aspects such as the illumination power and wavelength, play a critical role as confirmed by a study employing composited graphene/$Cu_{3-x}P$ nanomaterials. The investigation revealed an increase in photocurrent when illuminated at the LSPR wavelength, but mechanisms causing this increase were not addressed although the generic cause of hot carrier generation and transfer can be intuited to have an influence [457]. Studies revealing the mechanisms for resonance and the locations of the Cu vacancies from EELS and atomic contrast STEM imaging revealed that the vacancies arise from the absence of Cu at lattice sites of type Cu1 and Cu2 rather than of types Cu3 and Cu4 [458], and that two modes of plasmonic oscillation are present. The first one corresponds to the dipolar mode while the second one to a non-polar breathing mode (also termed as a dark plasmonic mode as it cannot couple to light [459]) with radial oscillations that can be excited only with an electron beam. Such studies reveal the carrier concentrations, origins, and localizations of collective plasmons and hence are critical in establishing the potential of emerging materials such as phosphides for applications such as Q-switching and NLO [460].

With regards to other materials for which the LSPR has not been given credit but where it is probably a contributing factor to the observed improvements to properties, one composition is of CuNPs embedded in a CNT/pCN composite which was investigated for its improved photocatalytic CO_2 reduction [461]. A more detailed analysis of the plasmonic aspect of these materials is expected to unambiguously contribute to a variety of fields in ways which have been discussed here.

A very interesting proposition of LSPR is on generating low-frequency plasmons, specifically those that exist in the microwave frequencies. Although the plasma frequency of Cu lies in the visible, studies reviewed here have shown the dramatic changes possible in the peaking frequencies. As per Eq. (12), SPR occurs when the permittivity of the dielectric is negative compared to that of the metal. Remarkably, distribution of CuNPs on a three-dimensional matrix so that a threshold of percolation (usually a vol% of Cu, dictated by the particle size and the matrix's morphology and composition) is exceeded led to this negative permittivity at microwave frequencies, with the induction of a delocalized electron oscillation. The creation of metallic networks was proposed to create this delocalized electron cloud of the individual NPs resulting in the collective excitation. Further studies on achieving/confirming/tuning of this low-frequency plasmon should reveal new opportunities for these materials such as in attenuating devices [462]. Such

Table 6 A summary of the different materials that have been used with Cu as over layers to enhance SSA

S. no.	Material deposited on Cu	Absorbance wavelength (nm)	Absorptance (%)	Ref. no.
1	Cr, Fe, Mo, Ni, Ta, and W	Reflectance = 300–1500	85–90	[467]
2	Ti	Reflectance = 100–1500	94	[468]
3	Fe, Cr, and Ni	300–2500	94	[469]
4	Cr, Mo, and SS	300–2500	90	[470]
5	Cr, Fe, Mo, Ti, Ta, SS, and W	300–2500	75–80	[471]
6	Fe, Cr, SS, and Ni	200–800	80	[472]
7	Cr-Cr_2O_3 and Mo-Al_2O_3	Reflectance = 600–2000	75–95	[473]
8	Ti-TiN_yO_x and Cr-Cr_xO_y	Reflectance = 300–2000	91 and 94	[474]
9	Ag-Al_2O_3	500–1200	93	[475]
10	CrN-Cr_xO_y	Reflectance = 600–2000	93	[476]

oscillations have been observed for multiple combinations of Cu, such as Cu/$BaTiO_3$ [463, 464], Cu/YIG, Cu/Ni-Zn ferrite [465, 466], and Cu/polyphenylene sulfide.

Studies on employing Cu as an enhancer of SSA which can tailor make the Cu architecture to be solely absorbing instead of absorbing and scattering is an example of research that can immensely benefit this area which is highly driven towards large-scale production. A summary of the different materials that have been used with Cu as deposited over layers for the purpose of enhancing SSA is presented in Table 6. Investigations of the interfaces in such architectures on various aspects such as the influences of Cu morphology, deposited film parameters, and other interfacial properties are essential to discover the relevancy of such compositions for plasmonic purposes.

A wide array of materials has been investigated as partners of Cu for the specific purpose of enhancing absorption of solar energy. In all these studies, strictly cursorial treatments of the absorbances are present, with multiple questions on the plasmonic aspects unaddressed.

Finally, plasmons in non-stoichiometric and layered CuO have been found to be plausibly responsible for high-temperature superconductivity. The likelihood of the plasmons pairing with electrons for superconductivity was found to be high if the lattice was in a layered fashion, as the localized plasmon DOS of such a structure was found to be conducive for plasmon excitation and coupling with superconducting electron motion. It was, thus, concluded that along with other excitations such as phonons, excitons, and spin-fluctuations, plasmons also facilitated attractive electron–electron interactions and hence superconductivity [477].

Conclusions and Outlook on the Future of Cu Plasmonics

The multiple directions pursued in the research on plasmonic Cu have been attempted to be methodically covered in this review. Plasmonic Cu has come a long way since its discovery and ostracization soon after for plasmonic applications. The maturation of synthesis technologies according to the authors is an important and probably a spearheading reason for the continued expansion of Cu plasmonics, keeping in mind the changes to the concentrated field distributions that can be manipulated seemingly at will due to this maturation. Indeed, the coupling between far-fields of the LSPR of CuNPs with other excitations such as inter-band as well as hybrid excitations which has been discussed in this review underlines the possibilities in terms of material design [478]. The possibility of experimenting with combinations that are increasingly novel while standing on the shoulders of the foundational materials and technologies can be understood from the discussions on the various topics of this review. The control over morphology, composition, oxidation, dispersion in the case of nanoparticles, and analogous aspects of roughness, precision, uniformity, and purity while pondering over films have been enablers for this burgeoning of investigations. However, much space exists in terms of locking down plasmonic Cu as a material for which a complete understanding/application of its optical properties has been achieved.

To mention a few areas where improvements are possible, separating the contributions to enhanced catalytic performance due to plasmonic contributions can be better elucidated, as with eccentric but precise techniques such as scanning tunneling microscopy and EELS. Revealing these details can help in better exploiting and designing materials aimed at harvesting of unutilized energy (such as solar energy and waste heat), as well as designing better materials that can prevent carrier recombination and improve reaction rates. The authors opine for example, that the myriad of studies that report Cu (such as in the Au-Cu system) only to enhance the adsorption of reactant molecules with no part to play in plasmonic hot carrier generation (attributed to the Au component of the compound) though illuminated with visible light can be furthered to study the likely plasmonic contribution of Cu. Metal-enhanced fluorescence is one of the fascinating areas of research that can benefit by a margin

from mechanistic insights into the phenomenon. With the importance of the proximity of the fluorophore to PC, their location within a material plays a critical role in determining the near vs far-field enhancements/quenching to MEF [479]. Studies such as pump-probe spectroscopy combined with simulations can be of use in this regard, as they have in the past in terms of revealing the sequence of events that probably lead to the enhancements. Bettering the illumination method to achieve a total irradiance of CuNPs and their conjugated fluoromers is another aspect of bettering fluorescence and scattering performance in general. NLO is a field that can actively employ plasmonic materials, from the few reports reviewed here on the possibilities and unaddressed features of this research area.

The phenomenon of oxidation has in this review been revealed to be beneficial as pertinent to the application. The prevention (through passivation), control (through passivation/utilizing designs that self-limit oxidation), and reversal (through chemicals/fabrication processes) can go a long way in opening up possible uses of Cu especially in terms of improving their durability and even the plasmonic virtues such as the intensity and reach of the near and far fields [480]. Intense investigations of multiple configurations and morphologies of Cu as discussed in the respective sections illuminate the road ahead in terms of realizing CuNPs with a short shackle for oxygen.

Copper compounds have immense potential and have already been explored for example for unconventional applications such as plasmonic batteries [481, 482] and plasmonic electrical switches in the form of phase and composition-controlled chalcogenides for example. All of these emerging fields of PC applications can benefit from the UV, visible, and near infrared photon harvesting from the ambient solar spectrum, catalyzing and controlling the electrochemistry of these energy storage devices [483]. Such unconventional applications indeed seem to be restricted only by contemplations of appropriate design/methods of study. Cu alloys are another class of highly nascent materials, wherein only preliminary reports of the observations of differing plasmonic properties with regard to different material parameters have been done. Investigations of the electronic structure of these alloys are hardly if ever dealt with, which is crucial to gain insights on the mechanisms of plasmonic manifestation. This aspect need not be complex, as simpler tools can reveal elemental presence post which simulation tools can take over the electronic structure calculations in many cases. Considering the inaccessibility of sophisticated imaging technologies for looking at the atomic level structures of Cu-based plasmonic alloys and compounds, computational tools need to be sought. These tools have their own shortcomings from the aspect of having available accurate material constants for novel material combinations, although approximations can help considerably. It is admitted, however, that multiple metal combinations have been explored as alloying elements with Cu already.

A general observation is that reports of plasmon-enhanced properties cannot be compared in most cases and yet they are, with the resulting materials being touted as better performers. A prevalent example of this is in PT energy conversion, wherein apparent differences in irradiation powers are still compared with another published research and reported to be better. This is intuitively a roadblock to achieve materials that are benchmarked globally to be evolving candidates for such applications. A similar application that suffers from the same drawback is theranostics, wherein the parameters of irradiation intensity for therapy vary and yet are compared against one another. Consistent comparisons or parameters hence need to be established, which when quantified for the different materials for a particular purpose nullify differences, thereby serving as a universal metric for establishing the best materials. One such parameter is the refractive index sensitivity, which carries the same definition across studies. Another parameter is the Keldysh constant, which allows confirmation of the plasmonic contributions from a material. Such variables are invariably needed especially in the fields of theranostic and PT energy storage, as the comparability between investigations can only be correct if done through them. With the promise held by Cu in plasmonics and its increasing participation as a frontrunner in this field, it stands that multiple avenues of research and commercialization will see Cu as a very good option in the realms of the ultra-violet to the near infrared, with even extensions to the microwave regime [484].

Author Contribution Indhu conceptualized and wrote the manuscript. Dharanya C was involved in the preparation of the figures and the graphical abstract. Gnanaprakash Dharmalingam and all authors reviewed the manuscript.

Funding The authors gratefully acknowledge the funding received from PSG Sons' and Charities for supporting this publication.

Availability of Data and Materials All the data required for this publication have been included in the manuscript.

Declarations

Competing Interests The authors declare no competing interests.

References

1. Homola J, Yee SS, Gauglitz G (1999) Surface plasmon resonance sensors: review. Sens Actuators B Chem 54:3–15. https://doi.org/10.1016/S0925-4005(98)00321-9
2. Baishya K, Idrobo JC, Öğüt S, Yang M, Jackson KA, Jellinek J (2011) First-principles absorption spectra of Cun (n=2–20) clusters. Phys Rev B Condens Matter Mater Phys 83:245402. https://doi.org/10.1103/PhysRevB.83.245402

3. Aslam U, Rao VG, Chavez S, Linic S (2018) Catalytic conversion of solar to chemical energy on plasmonic metal nanostructures. Nat Catal 1:656–665. https://doi.org/10.1038/s41929-018-0138-x
4. Fort E (2013) Plasmonics. Optics in instruments: applications in biology and medicine. Wiley, pp 179–216. https://doi.org/10.1002/9781118574386.ch5
5. Zayats AV, Smolyaninov II, Maradudin AA (2005) Nano-optics of surface plasmon polaritons. Phys Rep 408:131–314. https://doi.org/10.1016/j.physrep.2004.11.001
6. Wang ZL (2017) On Maxwell' s displacement current for energy and sensors: the origin of nanogenerators. Biochem Pharmacol 00:1–9. https://doi.org/10.1016/j.mattod.2016.12.001
7. Riffe DM (2018) Canonical models of dielectric response. 4415. http://arxiv.org/abs/1806.05158
8. Hong Y, Huh YM, YoonDS Yang J (2012) Nanobiosensors based on localized surface plasmon resonance for biomarker detection. J Nanomater 2012:759830. https://doi.org/10.1155/2012/759830
9. Keerthana L, Ahmad Dar M, Dharmalingam G (2021) Plasmonic Au-metal oxide nanocomposites for high-temperature and harsh environment sensing applications. Chem An Asian J 16:3558–3584. https://doi.org/10.1002/asia.202100885
10. Bansal A, Verma SS (2014) Searching for alternative plasmonic materials for specific applications. Indian J Mater Sci 2014:1–10. https://doi.org/10.1155/2014/897125
11. Grigorchuk NI (2012) Radiative damping of surface plasmon resonance in spheroidal metallic nanoparticle embedded in a dielectric medium. J Opt Soc Am B 29:3404. https://doi.org/10.1364/josab.29.003404
12. Yeshchenko OA, Bondarchuk IS, Gurin VS, Dmitruk IM, Kotko AV (2013) Temperature dependence of the surface plasmon resonance in gold nanoparticles. Surf Sci 608:275–281. https://doi.org/10.1016/j.susc.2012.10.019
13. Ziashahabi A, Ghodselahi T, Heidari M (2013) Localized surface plasmon resonance properties of copper nano-clusters : a theoretical study of size dependence. J Phys Chem Solids 74:929–933. https://doi.org/10.1016/j.jpcs.2013.02.009
14. Zhang X, Cheng X, Yin H, Yuan J, Xu C (2008) Preparation of needle shaped nano-copper by microwave-assisted water system and study on its application of enhanced epoxy resin coating electrical conductivity. Appl Surf Sci 254:5757–5759. https://doi.org/10.1016/j.apsusc.2008.03.078
15. Jain S, Jain A, Kachhawah P, Devra V (2015) Synthesis and size control of copper nanoparticles and their catalytic application. Trans Nonferrous Met Soc China 25:3995–4000. https://doi.org/10.1016/S1003-6326(15)64048-1
16. Markina NE, Pozharov MV, Markin AV (2016) Synthesis of copper(I) oxide particles with variable color: demonstrating size-dependent optical properties for high school students. J Chem Educ 93:704–707. https://doi.org/10.1021/acs.jchemed.5b00563
17. Dang CM, Trinh CD, Dang DMT, Fribourg-Blanc E (2013) Characteristics of colloidal copper particles prepared by using polyvinyl pyrrolidone and polyethylene glycol in chemical reduction method. Int J Nanotechnol 10:296–303. https://doi.org/10.1504/IJNT.2013.053143
18. Toh HS, Jurkschat K, Compton RG (2015) The influence of the capping agent on the oxidation of silver nanoparticles: nano-impacts versus stripping voltammetry. Chem A Eur J 21:2998–3004. https://doi.org/10.1002/chem.201406278
19. Lisiecki I, Billoudet F, Pileni MP (1996) Control of the shape and the size of copper metallic particles. J Phys Chem 100:4160–4166. https://doi.org/10.1021/jp9523837
20. Markin AV, Markina NE (2019) Experimenting with plasmonic copper nanoparticles to demonstrate color changes and reactivity at the nanoscale. J Chem Educ. https://doi.org/10.1021/acs.jchemed.8b01050
21. Parveen F, Sannakki B, Mandke MV, Pathan HM (2016) Solar energy materials & solar cells copper nanoparticles : synthesis methods and its light harvesting performance. Sol Energy Mater Sol Cells 144:371–382. https://doi.org/10.1016/j.solmat.2015.08.033
22. Wu C, Mosher BP, Zeng T (2006) One-step green route to narrowly dispersed copper nanocrystals. J Nanoparticle Res 8:965–969. https://doi.org/10.1007/s11051-005-9065-2
23. Yu W, Xie H, Chen L, Li Y, Zhang C (2009) Synthesis and characterization of monodispersed copper colloids in polar solvents. Nanoscale Res Lett 4:465–470. https://doi.org/10.1007/s11671-009-9264-3
24. Salavati-Niasari M, Davar F (2009) Synthesis of copper and copper(I) oxide nanoparticles by thermal decomposition of a new precursor. Mater Lett 63:441–443. https://doi.org/10.1016/j.matlet.2008.11.023
25. Salavati-niasari M, Fereshteh Z, Davar F (2009) Synthesis of oleylamine capped copper nanocrystals via thermal reduction of a new precursor. Polyhedron 28:126–130. https://doi.org/10.1016/j.poly.2008.09.027
26. Mallick K, Witcomb MJ, Scurrell MS (2006) In situ synthesis of copper nanoparticles and poly(o-toluidine): a metal-polymer composite material. Eur Polym J 42:670–675. https://doi.org/10.1016/j.eurpolymj.2005.09.020
27. Hu M, Zhou K, Wang C, Xu R (2008) Cl- induced synthesis of submicron cubic copper particles in solution. J Univ Sci Technol Beijing Miner Metall Mater 15:659–664. https://doi.org/10.1016/S1005-8850(08)60123-1
28. Wang H, Tam F, Grady NK, Halas NJ (2005) Cu nanoshells: effects of interband transitions on the nanoparticle plasmon resonance. J Phys Chem B 109:18218–18222. https://doi.org/10.1021/jp053863t
29. Athawale AA, Katre PP, Kumar M, Majumdar MB (2005) Synthesis of CTAB-IPA reduced copper nanoparticles. Mater Chem Phys 91:507–512. https://doi.org/10.1016/j.matchemphys.2004.12.017
30. Pastoriza-Santos I, Sánchez-Iglesias A, Rodríguez-González B, Liz-Marzán LM (2009) Aerobic synthesis of Cu nanoplates with intense plasmon resonances. Small 5:440–443. https://doi.org/10.1002/smll.200801088
31. Guo H, Chen Y, Cortie MB, Liu X, Xie Q, Wang X, Peng DL (2014) Shape-selective formation of monodisperse copper nanospheres and nanocubes via disproportionation reaction route and their optical properties. J Phys Chem C 118:9801–9808. https://doi.org/10.1021/jp5014187
32. Crane CC, Wang F, Li J, Tao J, Zhu Y, Chen J (2017) Synthesis of copper-silica core-shell nanostructures with sharp and stable localized surface plasmon resonance. J Phys Chem C 121:5684–5692. https://doi.org/10.1021/acs.jpcc.6b11891
33. Zheng P, Tang H, Liu B, Kasani S, Huang L, Wu N (2019) Origin of strong and narrow localized surface plasmon resonance of copper nanocubes. Nano Res 12:63–68. https://doi.org/10.1007/s12274-018-2178-6
34. Jin M, He G, Zhang H, Zeng J, Xie Z, Xia Y (2011) Shape-controlled synthesis of copper nanocrystals in an aqueous solution with glucose as a reducing agent and hexadecylamine as a capping agent. Angew Chemie Int Ed 50:10560–10564. https://doi.org/10.1002/anie.201105539
35. Mott D, Galkowski J, Wang L, Luo J, Zhong CJ (2007) Synthesis of size-controlled and shaped copper nanoparticles. Langmuir 23:5740–5745. https://doi.org/10.1021/la0635092
36. Songping W, Shuyuan M (2006) Preparation of micron size copper powder with chemical reduction method. Mater Lett 60:2438–2442. https://doi.org/10.1016/j.matlet.2004.08.051
37. Saikova SV, Vorob'Ev SA, Nikolaeva RB, Mikhlin YL (2010) Conditions for the formation of copper nanoparticles by

reduction of copper(II) ions with hydrazine hydrate solutions. Russ J Gen Chem 80:1122–1127. https://doi.org/10.1134/S1070363210060149
38. Paquin F, Rivnay J, Salleo A, Stingelin N, Silva C (2015) Multi-phase semicrystalline microstructures drive exciton dissociation in neat plastic semiconductors. J Mater Chem C 3:10715–10722. https://doi.org/10.1039/b000000x
39. Ye S, Rathmell AR, Stewart IE, Ha YC, Wilson AR, Chen Z, Wiley BJ (2014) A rapid synthesis of high aspect ratio copper nanowires for high-performance transparent conducting films. Chem Commun 50:2562–2564. https://doi.org/10.1039/c3cc48561g
40. Wu S (2007) Preparation of fine copper powder using ascorbic acid as reducing agent and its application in MLCC. Mater Lett 61:1125–1129. https://doi.org/10.1016/j.matlet.2006.06.068
41. Wu SH, Chen DH (2004) Synthesis of high-concentration Cu nanoparticles in aqueous CTAB solutions. J Colloid Interface Sci 273:165–169. https://doi.org/10.1016/j.jcis.2004.01.071
42. Xiong J, Wang Y, Xue Q, Wu X (2011) Synthesis of highly stable dispersions of nanosized copper particles using L-ascorbic acid. Green Chem 13:900–904. https://doi.org/10.1039/c0gc00772b
43. Chang Y, Lye ML, Zeng HC (2005) Large-scale synthesis of high-quality ultralong copper nanowires. Langmuir 21:3746–3748. https://doi.org/10.1021/la050220w
44. Wang Y, Biradar AV, Wang G, Sharma KK, Duncan CT, Rangan S, Asefa T (2010) Controlled synthesis of water-dispersible faceted crystalline copper nanoparticles and their catalytic properties. Chem A Eur J 16:10735–10743. https://doi.org/10.1002/chem.201000354
45. Wang Y, Chen P, Liu M (2006) Synthesis of well-defined copper nanocubes by a one-pot solution process. Nanotechnology 17:6000–6006. https://doi.org/10.1088/0957-4484/17/24/016
46. Wei W, Lu Y, Chen W, Chen S (2011) One-pot synthesis, photoluminescence, and electrocatalytic properties of subnanometer-sized copper clusters. J Am Chem Soc 133:2060–2063. https://doi.org/10.1021/ja109303z
47. Luo M, Ruditskiy A, Peng HC, Tao J, Figueroa-Cosme L, He Z, Xia Y (2016) Penta-twinned copper nanorods: facile synthesis via seed-mediated growth and their tunable plasmonic properties. Adv Funct Mater 26(8):1209–1216. https://doi.org/10.1002/adfm.201504217
48. Jeong S, Liu Y, Zhong Y, Zhan X, Li Y, Wang Y, Cha PM, Chen J, Ye X (2020) Heterometallic seed-mediated growth of monodisperse colloidal copper nanorods with widely tunable plasmonic resonances. Nano Lett 20:7263–7271. https://doi.org/10.1021/acs.nanolett.0c02648
49. Salzemann C, Brioude A, Pileni MP (2006) Tuning of copper nanocrystals optical properties with their shapes. J Phys Chem B 110:7208–7212. https://doi.org/10.1021/jp0601567
50. Kidwai M, Bansal V, Saxena A, Aerry S, Mozumdar S (2006) Cu-Nanoparticles: efficient catalysts for the oxidative cyclization of Schiffs' bases. Tetrahedron Lett 47:8049–8053. https://doi.org/10.1016/j.tetlet.2006.09.066
51. Lisiecki I, Pileni MP (1993) Synthesis of copper metallic clusters using reverse micelles as microreactors. J Am Chem Soc 115:3887–3896. https://doi.org/10.1021/ja00063a006
52. Woo K, Kim D, Kim JS, Lim S, Moon J (2009) Ink-jet printing of Cu-Ag-based highly conductive tracks on a transparent substrate. Langmuir 25:429–433. https://doi.org/10.1021/la802182y
53. Park BK, Kim D, Jeong S, Moon J, Kim JS (2007) Direct writing of copper conductive patterns by ink-jet printing. Thin Solid Films 515:7706–7711. https://doi.org/10.1016/j.tsf.2006.11.142
54. Tilaki RM, Zad AI, Mahdavi SM (2007) Size, composition and optical properties of copper nanoparticles prepared by laser ablation in liquids. Appl Phys A Mater Sci Process 88:415–419. https://doi.org/10.1007/s00339-007-4000-2
55. Liu P, Wang H, Li X, Rui M, Zeng H (2015) Localized surface plasmon resonance of Cu nanoparticles by laser ablation in liquid media. RSC Adv 5:79738–79745. https://doi.org/10.1039/c5ra14933a
56. Zhou R, Wu X, Hao X, Zhou F, Li H, Rao W (2008) Influences of surfactants on the preparation of copper nanoparticles by electron beam irradiation. Nucl Instrum Methods Phys Res Sect B Beam Interact Mater Atoms 266:599–603. https://doi.org/10.1016/j.nimb.2007.11.040
57. Chan GH, Zhao J, Hicks EM, Schatz GC, Van Duyne RP (2007) Plasmonic properties of copper nanoparticles fabricated by nanosphere lithography. Nano Lett 7:1947–1952. https://doi.org/10.1021/nl070648a
58. Yang HJ, He SY, Chen HL, Tuan HY (2014) Monodisperse copper nanocubes: synthesis, self-assembly, and large-area dense-packed films. Chem Mater 26:1785–1793. https://doi.org/10.1021/cm403098d
59. Moghimi-Rad J, Zabihi F, Hadi I, Ebrahimi S, Isfahani TD, Sabbaghzadeh J (2010) Effect of ultrasound radiation on the size and size distribution of synthesized copper particles. J Mater Sci 45:3804–3811. https://doi.org/10.1007/s10853-010-4435-2
60. Harsojo H, Puspita LA, Mardiansyah D, Roto R, Triyana K (2017) The roles of hydrazine and ethylenediamine in wet synthesis of Cu Nanowire. Indones J Chem 17:43–48. https://doi.org/10.22146/ijc.23618
61. Jing JJ, Xie JM, Chen GY, Li WH, Zhang MM (2013) Synthesis of copper nanohexagons and microflowers via a surfactant-assisted hydrothermal process. Adv Mater Res 785–786:420–423. https://doi.org/10.4028/www.scientific.net/AMR.785-786.420
62. Liu Y, Chu Y, Zhuo Y, Dong L, Li L, Li M (2007) Controlled synthesis of various hollow Cu nano/microstructures via a novel reduction route. Adv Funct Mater 17:933–938. https://doi.org/10.1002/adfm.200600333
63. Zhu HT, Zhang CY, Yin YS (2004) Rapid synthesis of copper nanoparticles by sodium hypophosphite reduction in ethylene glycol under microwave irradiation. J Cryst Growth 270:722–728. https://doi.org/10.1016/j.jcrysgro.2004.07.008
64. Raspolli Galletti AM, Antonetti C, Marracci M, Piccinelli F, Tellini B (2013) Novel microwave-synthesis of Cu nanoparticles in the absence of any stabilizing agent and their antibacterial and antistatic applications. Appl Surf Sci 280:610–618. https://doi.org/10.1016/j.apsusc.2013.05.035
65. Tseng PH, Wang YZ, Hsieh TH, Ho KS, Tsai CH, Chen KT (2018) Preparation of sub 3 nm copper nanoparticles by microwave irradiation in the presence of triethylene tetramin. Nanotechnology 29:085603. https://doi.org/10.1088/1361-6528/aaa35e
66. Kawasaki H, Kosaka Y, Myoujin Y, Narushima T, Yonezawa T, Arakawa R (2011) Microwave-assisted polyol synthesis of copper nanocrystals without using additional protective agents. Chem Commun 47:7740–7742. https://doi.org/10.1039/c1cc12346g
67. Vázquez-Vázquez C, Bañobre-López M, Mitra A, López-Quintela MA, Rivas J (2009) Synthesis of small atomic copper clusters in microemulsions. Langmuir 25:8208–8216. https://doi.org/10.1021/la900100w
68. Qi L, Ma J, Shen J (1997) Synthesis of copper nanoparticles in nonionic water-in-oil microemulsions. J Colloid Interface Sci 186:498–500. https://doi.org/10.1006/jcis.1996.4647
69. Park YS, Chae HK (2010) Geometric control and intense plasmon resonances of colloidal truncated triangular copper nanoplates in nonionic microemulsions containing tetrabutylammonium hydroxide. Chem Mater 22:6280–6290. https://doi.org/10.1021/cm101961g
70. Solanki JN, Sengupta R, Murthy ZVP (2010) Synthesis of copper sulphide and copper nanoparticles with microemulsion

method. Solid State Sci 12:1560–1566. https://doi.org/10.1016/j.solidstatesciences.2010.06.021
71. Simon HJ, Mitchell DE, Watson JG (1974) Optical second-harmonic generation with surface plasmons in silver films. Phys Rev Lett 33:1531–1534. https://doi.org/10.1103/PhysRevLett.33.1531
72. Kinkhabwala A, Yu Z, Fan S, Avlasevich Y, Müllen K, Moerner WE (2009) Large single-molecule fluorescence enhancements produced by a bowtie nanoantenna. Nat Photonics 3:654–657. https://doi.org/10.1038/nphoton.2009.187
73. Wang X, Huang SC, Hu S, Yan S, Ren B (2020) Fundamental understanding and applications of plasmon-enhanced Raman spectroscopy. Nat Rev Phys 2:253–271. https://doi.org/10.1038/s42254-020-0171-y
74. Genevet P, Tetienne JP, Gatzogiannis E, Blanchard R, Kats MA, Scully MO, Capasso F (2010) Large enhancement of nonlinear optical phenomena by plasmonic nanocavity gratings. Nano Lett 10:4880–4883. https://doi.org/10.1021/nl102747v
75. Li RK, To H, Andonian G, Feng J, Polyakov A, Scoby CM, Thompson K, Wan W, Padmore HA, Musumeci P (2013) Surface-plasmon resonance-enhanced multiphoton emission of high-brightness electron beams from a nanostructured copper cathode. Phys Rev Lett 110:10–15. https://doi.org/10.1103/PhysRevLett.110.074801
76. Wu Z, Wang J, Liu Y, Hou S, Liu X, Zhang Q, Cao F (2021) A review of spectral controlling for renewable energy harvesting and conserving. Mater Today Phys 18:100388. https://doi.org/10.1016/j.mtphys.2021.100388
77. Zhang Y, He S, Guo W, Hu Y, Huang J, Mulcahy JR, Wei WD (2018) Surface-plasmon-driven hot electron photochemistry. Chem Rev 118:2927–2954. https://doi.org/10.1021/acs.chemrev.7b00430
78. Eesley GL (1986) Generation of nonequilibrium electron and lattice temperatures in copper by picosecond laser pulses. Phys Rev B 33:2144–2151. https://doi.org/10.1103/PhysRevB.33.2144
79. Yamaguchi T, Kazuma E, Sakai N, Tatsuma T (2012) Photoelectrochemical responses from polymer-coated plasmonic copper nanoparticles on TiO 2. Chem Lett 41:1340–1342. https://doi.org/10.1246/cl.2012.1340
80. Janczarek M, Kowalska E (2017) On the origin of enhanced photocatalytic activity of copper-modified titania in the oxidative reaction systems. Catalysts 7:317. https://doi.org/10.3390/catal7110317
81. Brown AM, Sundararaman R, Narang P, Goddard WA, Atwater HA (2016) Nonradiative plasmon decay and hot carrier dynamics: effects of phonons, surfaces, and geometry. ACS Nano 10:957–966. https://doi.org/10.1021/acsnano.5b06199
82. Lee C, Park Y, Park JY (2019) Hot electrons generated by intraband and interband transition detected using a plasmonic Cu/TiO2 nanodiode. RSC Adv 9:18371–18376. https://doi.org/10.1039/c9ra02601k
83. Sun QC, Ding Y, Goodman SM, Funke HH, Nagpal P (2014) Copper plasmonics and catalysis: Role of electron-phonon interactions in dephasing localized surface plasmons. Nanoscale 6:12450–12457. https://doi.org/10.1039/c4nr04719b
84. Bigot JY, Merle JY, Cregut O, Daunois A (1995) Electron dynamics in copper metallic nanoparticles probed with femtosecond optical pulses. Phys Rev Lett 75:4702–4705. https://doi.org/10.1103/PhysRevLett.75.4702
85. Nisoli M, Stagira S, De Silvestri S, Stella A, Tognini P, Cheyssac P, Kofman R (1997) Ultrafast electronic dynamics in solid and liquid gallium nanoparticles. Phys Rev Lett 78:3575–3578. https://doi.org/10.1103/PhysRevLett.78.3575
86. Hodak JH, Henglein A, Hartland GV (2000) Electron-phonon coupling dynamics in very small (between 2 and 8 nm diameter) Au nanoparticles. J Chem Phys 112:5942–5947. https://doi.org/10.1063/1.481167
87. Darugar Q, Qian W, El-Sayed MA, Pileni MP (2006) Size-dependent ultrafast electronic energy relaxation and enhanced fluorescence of copper nanoparticles. J Phys Chem B 110:143–149. https://doi.org/10.1021/jp0545445
88. Messinger BJ, Von Raben KU, Chang RK, Barber PW (1981) Local fields at the surface of noble-metal microspheres. Phys Rev B 24:649–657. https://doi.org/10.1103/PhysRevB.24.649
89. Chen J, Feng J, Yang F, Aleisa R, Zhang Q, Yin Y (2019) Space-confined seeded growth of Cu nanorods with strong surface plasmon resonance for photothermal actuation. Angew Chemie Int Ed 58:9275–9281. https://doi.org/10.1002/anie.201904828
90. Fan P, Wu H, Zhong M, Zhang H, Bai B, Jin G (2016) Large-scale cauliflower-shaped hierarchical copper nanostructures for efficient photothermal conversion. Nanoscale 8:14617–14624. https://doi.org/10.1039/c6nr03662g
91. Lin Y, Chen Z, Fang L, Meng M, Liu Z, Di Y, Cai W, Huang S, Gan Z (2018) Copper nanoparticles with near-unity, omnidirectional, and broadband optical absorption for highly efficient solar steam generation. Nanotechnology 30:015402. https://doi.org/10.1088/1361-6528/aae678
92. Mandal J, Wang D, Overvig AC, Shi NN, Paley D, Zangiabadi A, Cheng Q, Barmak K, Yu N, Yang Y (2017) Scalable, "dip-and-dry" fabrication of a wide-angle plasmonic selective absorber for high-efficiency solar–thermal energy conversion. Adv Mater 29:1–9. https://doi.org/10.1002/adma.201702156
93. Wang J, Zhao X, Tang F, Li Y, Yan Y, Li L (2021) Synthesis of copper nanoparticles with controllable crystallinity and their photothermal property. Colloids Surf A Physicochem Eng Asp 626:126970. https://doi.org/10.1016/j.colsurfa.2021.126970
94. Yeshchenko OA, Dmitruk IM, Alexeenko AA, Dmytruk AM (2007) Size-dependent melting of spherical copper nanoparticles embedded in a silica matrix. Phys Rev B Condens Matter Mater Phys 75:1–6. https://doi.org/10.1103/PhysRevB.75.085434
95. Karabacak T, Deluca JS, Wang PI, Ten Eyck GA, Ye D, Wang GC, Lu TM (2006) Low temperature melting of copper nanorod arrays. J Appl Phys 99:064304. https://doi.org/10.1063/1.2180437
96. Zhou M, Tian M, Li C (2016) Copper-based nanomaterials for cancer imaging and therapy. Bioconjug Chem 27:1188–1199. https://doi.org/10.1021/acs.bioconjchem.6b00156
97. Li KC, Chu HC, Lin Y, Tuan HY, Hu YC (2016) PEGylated copper nanowires as a novel photothermal therapy agent. ACS Appl Mater Interfaces 8:12082–12090. https://doi.org/10.1021/acsami.6b04579
98. Tao B, Lin C, Deng Y, Yuan Z, Shen X, Chen M, He Y, Peng Z, Hu Y, Cai K (2019) Copper-nanoparticle-embedded hydrogel for killing bacteria and promoting wound healing with photothermal therapy. J Mater Chem B 7:2534–2548. https://doi.org/10.1039/C8TB03272F
99. Chen S, Tang F, Tang L, Li L (2017) Synthesis of Cu-nanoparticle hydrogel with self-healing and photothermal properties. ACS Appl Mater Interfaces 9:20895–20903. https://doi.org/10.1021/acsami.7b04956
100. Kale MJ, Avanesian T, Christopher P (2014) Direct photocatalysis by plasmonic nanostructures. ACS Catal 4:116–128. https://doi.org/10.1021/cs400993w
101. Wang M, Tang Y, Jin Y (2019) Modulating catalytic performance of metal-organic framework composites by localized surface plasmon resonance. ACS Catal 9:11502–11514. https://doi.org/10.1021/acscatal.9b03971
102. Brooks JL, Warkentin CL, Saha D, Keller EL, Frontiera RR (2018) Toward a mechanistic understanding of plasmon-mediated photocatalysis. Nanophotonics 7:1697–1724. https://doi.org/10.1515/nanoph-2018-0073
103. Marimuthu A, Zhang J, Linic S (2013) Tuning selectivity in propylene epoxidation by plasmon mediated photo-switching of Cu

oxidation state. Science 340(80):1590–1593. https://doi.org/10.1126/science.1231631
104. Huang S, Liu J, He Q, Chen H, Cui J, Xu S, Zhao Y, Chen C, Wang L (2015) Smart Cu1.75S nanocapsules with high and stable photothermal efficiency for NIR photo-triggered drug release. Nano Res 8:4038–4047. https://doi.org/10.1007/s12274-015-0905-9
105. Yu Y, Sundaresan V, Willets KA (2018) Hot carriers versus thermal effects: resolving the enhancement mechanisms for plasmon-mediated photoelectrochemical reactions. J Phys Chem C 122:5040–5048. https://doi.org/10.1021/acs.jpcc.7b12080
106. Anderson SR, Mohammadtaheri M, Kumar D, O'Mullane AP, Field MR, Ramanathan R, Bansal V (2016) Robust nanostructured silver and copper fabrics with localized surface plasmon resonance property for effective visible light induced reductive catalysis. Adv Mater Interfaces 3:1–8. https://doi.org/10.1002/admi.201500632
107. Ying ZC, Ho W (1990) Photodissociation of adsorbed Mo(CO)6 induced by direct photoexcitation and hot electron attachment. I. Surface chemistry. J Chem Phys 93:9077–9088. https://doi.org/10.1063/1.459706
108. Lindstrom CD, Zhu XY (2006) Photoinduced electron transfer at molecule - metal interfaces. Chem Rev 106:4281–4300. https://doi.org/10.1021/cr0501689
109. Kazuma E, Jung J, Ueba H, Trenary M, Kim Y (2018) Supplementary materials for reaction of a single molecule 526:521–526
110. Petek H, Ogawa S (1997) Femtosecond time-resolved two-photon photoemission studies of electron dynamics in metals. Prog Surf Sci 56:239–310. https://doi.org/10.1016/S0079-6816(98)00002-1
111. Echenique PM, Berndt R, Chulkov EV, Fauster T, Goldmann A, Höfer U (2004) Decay of electronic excitations at metal surfaces. Surf Sci Rep 52:219–317. https://doi.org/10.1016/j.surfrep.2004.02.002
112. Frischorn C, Wolf M (2006) Femtochemistry at metal surfaces: nonadiabatic reaction dynamics. Chem Rev 106:4207–4233. https://doi.org/10.1021/cr050161r
113. Bao JL, Carter EA (2019) Surface-plasmon-induced ammonia decomposition on copper: excited-state reaction pathways revealed by embedded correlated wavefunction theory. ACS Nano 13:9944–9957. https://doi.org/10.1021/acsnano.9b05030
114. Guselnikova O, Kalachyova Y, Elashnikov R, Cieslar M, Kolska Z, Sajdl P, Postnikov P, Svorcik V, Lyutakov O (2020) Taking the power of plasmon-assisted chemistry on copper NPs: preparation and application of COFs nanostructures for CO2 sensing in water. Microporous Mesoporous Mater 309:110577. https://doi.org/10.1016/j.micromeso.2020.110577
115. Aslan K, Lakowicz JR, Geddes CD (2005) Rapid deposition of triangular silver nanoplates on planar surfaces: application to metal-enhanced fluorescence. J Phys Chem B 109:6247–6251. https://doi.org/10.1021/jp044235z
116. Geddes CD, Cao H, Gryczynski I, Gryczynski Z, Fang J, Lakowicz JR (2003) Metal-enhanced fluorescence (MEF) due to silver colloids on a planar surface: potential applications of indocyanine green to in vivo imaging. J Phys Chem A 107:3443–3449. https://doi.org/10.1021/jp022040q
117. Zhang Y, Aslan K, Previte MJR, Malyn SN, Geddes CD (2006) Metal-enhanced phosphorescence: interpretation in terms of triplet-coupled radiating plasmons. J Phys Chem B 110:25108–25114. https://doi.org/10.1021/jp065261v
118. Chowdhury MH, Aslan K, Malyn SN, Lakowicz JR, Geddes CD (2006) Metal-enhanced chemiluminescence: radiating plasmons generated from chemically induced electronic excited states. Appl Phys Lett 88:4–7. https://doi.org/10.1063/1.2195776
119. Yeshchenko OA, Dmitruk IM, Dmytruk AM, Alexeenko AA (2007) Influence of annealing conditions on size and optical properties of copper nanoparticles embedded in silica matrix. Mater Sci Eng B Solid-State Mater Adv Technol 137:247–254. https://doi.org/10.1016/j.mseb.2006.11.030
120. Boyd GT, Yu ZH, Shen YR (1986) Photoinduced luminescence from the noble metals and its enhancement on roughened surfaces. Phys Rev B 33:7923–7936. https://doi.org/10.1103/PhysRevB.33.7923
121. Geddes CD, Parfenov A, Roll D, Fang J, Lakowicz JR (2003) Electrochemical and laser deposition of silver for use in metal-enhanced fluorescence. Langmuir 19:6236–6241. https://doi.org/10.1021/la020930r
122. Aslan K, Badugu R, Lakowicz JR, Geddes CD (2005) Metal-enhanced fluorescence from plastic substrates. J Fluoresc 15:99–104. https://doi.org/10.1007/s10895-005-2515-5
123. Aslan K, Malyn SN, Geddes CD (2007) Metal-enhanced fluorescence from gold surfaces: angular dependent emission. J Fluoresc 17:7–13. https://doi.org/10.1007/s10895-006-0149-x
124. Malta OL, Couto dos Santos MA (1990) Theoretical analysis of the fluorescence yield of rare earth ions in glasses containing small metallic particles. Chem Phys Lett 174:13–18. https://doi.org/10.1016/0009-2614(90)85319-8
125. Zhang Y, Aslan K, Previte MJR, Geddes CD (2007) Metal-enhanced fluorescence from copper substrates. Appl Phys Lett 90:17–20. https://doi.org/10.1063/1.2732185
126. Maliwal BP, Gryczynski Z, Lakowicz JR (2001) Long-wavelength long-lifetime luminophores. Anal Chem 73:4277–4285. https://doi.org/10.1021/ac0101050
127. Lakowicz JR (2005) Radiative decay engineering 5: Metal-enhanced fluorescence and plasmon emission. Anal Biochem 337:171–194. https://doi.org/10.1016/j.ab.2004.11.026
128. Robusto PF, Braunstein R (1981) Optical measurements of the surface plasmon of copper. Phys Status Solidi 107:443–449. https://doi.org/10.1002/pssb.2221070207
129. Chowdhury S, Bhethanabotla VR, Sen R (2011) Quenching of fluorescence from CdSe/ZnS nanocrystal QDs near copper nanoparticles in aqueous solution. Plasmonics 6:735–740. https://doi.org/10.1007/s11468-011-9257-9
130. Yeshchenko OA, Bondarchuk IS, Losytskyy MY (2014) Surface plasmon enhanced photoluminescence from copper nanoparticles: influence of temperature. J Appl Phys 116:054309. https://doi.org/10.1063/1.4892432
131. Reisfeld R, Grinberg M, Levchenko V, Kukliński B, Mahlik S, Magdassi S, Grouchko M (2014) Sol-gel glasses with enhanced luminescence of laser dye rhodamine B due to plasmonic coupling by copper nanoparticles. Opt Mater (Amst) 36:1611–1615. https://doi.org/10.1016/j.optmat.2013.11.011
132. Sugawa K, Tamura T, Tahara H, Yamaguchi D, Akiyama T, Otsuki J, Kusaka Y, Fukuda N, Ushijima H (2013) Metal-enhanced fluorescence platforms based on plasmonic ordered copper arrays: wavelength dependence of quenching and enhancement effects. ACS Nano 7:9997–10010. https://doi.org/10.1021/nn403925d
133. Anger P, Bharadwaj P, Novotny L (2006) Enhancement and quenching of single-molecule fluorescence. Phys Rev Lett 96:3–6. https://doi.org/10.1103/PhysRevLett.96.113002
134. Ruppin R (1982) Decay of an excited molecule near a small metal sphere. J Chem Phys 76:1681–1684. https://doi.org/10.1063/1.443196
135. Gersten J, Nitzan A (1981) Spectroscopic properties of molecules interacting with small dielectric particles. J Chem Phys 75:1139–1152. https://doi.org/10.1063/1.442161
136. Mertens H, Polman A (2009) Strong luminescence quantum-efficiency enhancement near prolate metal nanoparticles: dipolar versus higher-order modes. J Appl Phys 105:044302. https://doi.org/10.1063/1.3078108
137. Volpati D, Spada ER, Cid CCP, Sartorelli ML, Aroca RF, Constantino CJL (2015) Exploring copper nanostructures as highly uniform and reproducible substrates for plasmon-enhanced

fluorescence. Analyst 140:476–482. https://doi.org/10.1039/c4an00889h
138. Hartland GV, Besteiro L, Johns P, Govorov AO (2017) Subscriber access provided by UNIV OF ARIZONA What's so hot about electrons in metal nanoparticles? ACS Energy Lett 2:1641–1653. http://pubs.acs.org
139. Koenderink AF (2010) On the use of Purcell factors for plasmon antennas. Opt Lett 35(24):4208–4210. https://doi.org/10.1364/OL.35.004208
140. King FW, Schatz GC (1979) Theory of Raman scattering by molecules adsorbed at electrode surfaces. Model calculations for resonance Raman scattering by an adsorbed diatomic. Chem Phys 38(2):245–256. https://doi.org/10.1016/0301-0104(79)85068-5
141. Efrima S, Metiu H (1978) Classical theory of light scattering by a molecule located near a solid surface. Chem Phys Lett 60(1):59–64. https://doi.org/10.1016/0009-2614(78)85710-8
142. Efrima S, Metiu H (1980) Surface induced resonance Raman scattering (SIRRS). Surf Sci 92:417–432. https://doi.org/10.1016/0039-6028(80)90214-9
143. Dreyfus S, Dreyfus H (1980) A five-stage model of the mental activities involved in directed skill acquisition. http://stinet.dtic.mil/cgi-bin/GetTRDoc?AD=ADA084551&Location=U2&doc=GetTRDoc.pdf
144. Maniv T, Metiu H (1980) Electron gas effects in the spectroscopy of molecules chemisorbed at a metal surface. I. Theory. J Chem Phys 72:1996–2006. https://doi.org/10.1063/1.439348
145. Hilton PR, Oxtoby DW (1979) Surface enhanced Raman spectra: a critical review of the image dipole description. J Chem Phys 72:6346–6348. https://doi.org/10.1063/1.439158
146. Feibelman PJ (1980) Local field at an irradiated adatom on jellium—exact microscopic results. Phys Rev B 22(8):3654. https://doi.org/10.1103/PhysRevB.22.3654
147. Zeman EJ, Schatz GC (1987) An accurate electromagnetic theory study of surface enhancement factors for Ag, Au, Cu, Li, Na, Al, Ga, In, Zn, and Cd. J Phys Chem 91:634–643. https://doi.org/10.1021/j100287a028
148. Wenning U, Pettinger B, Wetzel H (1980) Anguler-resolved raman spectroscopy of pyridine on copper and gold electrodes. Chem Phys Lett 70:49–54. https://doi.org/10.1016/0009-2614(80)80058-3
149. Allen CS, Schatz GC, Van Duyne RP (1980) Tunable laser excitation profile of surface enhanced raman scattering from pyridine adsorbed on a copper electrode surface. Chem Phys Lett 75:201–205. https://doi.org/10.1016/0009-2614(80)80496-9
150. Shin KS, Lee HS, Joo SW, Kim K (2007) Surface-induced photoreduction of 4-nitrobenzenethiol on Cu revealed by surface-enhanced Raman scattering spectroscopy. J Phys Chem C 111:15223–15227. https://doi.org/10.1021/jp073053c
151. Dong B, Fang Y, Chen X, Xu H, Sun M (2011) Substrate-, wavelength-, and time-dependent plasmon-assisted surface catalysis reaction of 4-nitrobenzenethiol dimerizing to p, p′- dimercaptoazobenzene on Au, Ag, and Cu films. Langmuir 27:10677–10682. https://doi.org/10.1021/la2018538
152. Lust M, Pucci A, Akemann W, Otto A (2008) SERS of CO2 on cold-deposited Cu: an electronic effect at a minority of surface sites. J Phys Chem C 112:11075–11077. https://doi.org/10.1021/jp8032403
153. Otto A, Lust M, Pucci A, Meyer G (2007) SERS active sites, facts, and open questions. Can J Anal Sci Spectrosc 52:150–171
154. Zöphel S, Repp J, Meyer G, Rieder KH (1999) Determination of binding sites in ordered phases of CO/Cu(211) employing molecular level manipulation. Chem Phys Lett 310:145–149. https://doi.org/10.1016/S0009-2614(99)00757-5
155. Chen Y, Duan X, Matuschek M, Zhou Y, Neubrech F, Duan H, Liu N (2017) Dynamic color displays using stepwise cavity resonators. Nano Lett 17:5555–5560. https://doi.org/10.1021/acs.nanolett.7b02336
156. Böhme A, Sterl F, Kath E, Ubl M, Manninen V, Giessen H (2019) Electrochemistry on inverse copper nanoantennas: active plasmonic devices with extraordinarily large resonance shift. ACS Photonics 6:1863–1868. https://doi.org/10.1021/acsphotonics.9b00716
157. Mevik B-H, Wehrens R (2007) PDF hosted at the Radboud Repository of the Radboud University Nijmegen article information. J Stat Softw 18:3–6
158. Huang HH, Yan FQ, Kek YM et al (1997) Synthesis, characterization, and nonlinear optical properties of copper nanoparticles. Langmuir 13:172–175. https://doi.org/10.1021/la9605495
159. Kim DK, Yoo SM, Park TJ, Yoshikawa H, Tamiya E, Park JY, Lee SY (2011) Plasmonic properties of the multispot copper-capped nanoparticle array chip and its application to optical biosensors for pathogen detection of multiplex dnas. Anal Chem 83:6215–6222. https://doi.org/10.1021/ac2007762
160. Yao LH, Zhang JP, Dai HW, Wang MS, Zhang LM, Wang X, Han JB (2018) Plasmon-enhanced versatile optical nonlinearities in a Au-Ag-Au multi-segmental hybrid structure. Nanoscale 10:12695–12703. https://doi.org/10.1039/c8nr02938e
161. Wang CY, Chen HY, Sun L, Chen WL, Chang YM, Ahn H, Li X, Gwo S (2015) Giant colloidal silver crystals for low-loss linear and nonlinear plasmonics. Nat Commun 6:1–7. https://doi.org/10.1038/ncomms8734
162. Dikkumbura AS, Hamal P, Chen M, Babayode DA, Ranasinghe JC, Lopata K, Haber LH (2021) Growth dynamics of colloidal silver-gold core-shell nanoparticles studied by in situ second harmonic generation and extinction spectroscopy. J Phys Chem C 125:25615–25623. https://doi.org/10.1021/acs.jpcc.1c06094
163. Boroviks S, Kiselev A, Achouri K, Martin OJF (2023) Demonstration of a plasmonic nonlinear pseudodiode. Nano Lett. https://doi.org/10.1021/acs.nanolett.3c00367
164. Valev VK, Silhanek AV, Jeyaram Y, Denkova D, De Clercq B, Petkov V, Zheng X, Volskiy V, Gillijns W, Vandenbosch GAE, Aktsipetrov OA, Ameloot M, Moshchalkov VV, Verbiest T (2011) Hotspot decorations map plasmonic patterns with the resolution of scanning probe techniques. Phys Rev Lett 106:1–4. https://doi.org/10.1103/PhysRevLett.106.226803
165. Ding Y, Wei C, Su H, Sun S, Tang Z, Wang Z, Li G, Liu D, Gwo S, Dai J, Shi J (2021) Second harmonic generation covering the entire visible range from a 2D material–plasmon hybrid metasurface. Adv Opt Mater 9:2100625. https://doi.org/10.1002/adom.202100625
166. Hatamie A, Zargar B, Jalali A (2014) Copper nanoparticles: a new colorimetric probe for quick, naked-eye detection of sulfide ions in water samples. Talanta 121:234–238. https://doi.org/10.1016/j.talanta.2014.01.008
167. Stebunov YV, Yakubovsky DI, Fedyanin DY, Arsenin AV, Volkov VS (2018) Superior sensitivity of copper-based plasmonic biosensors. Langmuir 34:4681–4687. https://doi.org/10.1021/acs.langmuir.8b00276
168. Science A, Division D, House W, Road P (1990) Langmuir -Blodgett 2:265–269
169. Kravets VG, Jalil R, Kim YJ, Ansell D, Aznakayeva DE, Thackray B, Britnell L, Belle BD, Withers F, Radko IP, Han Z, Bozhevolnyi SI, Novoselov KS, Geim AK, Grigorenko AN (2014) Graphene-protected copper and silver plasmonics. Sci Rep 4:1–8. https://doi.org/10.1038/srep05517
170. Rifat AA, Mahdiraji GA, Ahmed R, Chow DM, Sua YM, Shee YG, Adikan FRM (2016) Copper-graphene-based photonic crystal fiber plasmonic biosensor. IEEE Photonics J 8:1–8. https://doi.org/10.1109/JPHOT.2015.2510632
171. Mohanty G, Sahoo BK (2016) III-V nitrides and performance of graphene on copper plasmonic biosensor. Superlattices

Microstruct 93:226–233. https://doi.org/10.1016/j.spmi.2016.03.040
172. Barchiesi D, Gharbi T, Cakir D, Anglaret E, Fréty N, Kessentini S, Maâlej R (2022) Performance of surface plasmon resonance sensors using copper/copper oxide films: influence of thicknesses and optical properties. Photonics 9:104. https://doi.org/10.3390/photonics9020104
173. Rodrigues EP, Oliveira LC, Silva MLF, Moreira CS, Lima AMN (2020) Surface plasmon resonance sensing characteristics of thin copper and gold films in aqueous and gaseous interfaces. IEEE Sens J 20:7701–7710. https://doi.org/10.1109/JSEN.2020.2980388
174. Rodrigues EP, Lima AMN, Oliveira LC, De Sousa TAT, Neff H (2018) Surface plasmon resonance features of corrugated gold films: wavelength interrogation mode for exhaled gas detection. J Phys Conf Ser 1044:1–6. https://doi.org/10.1088/1742-6596/1044/1/012062
175. Susman MD, Feldman Y, Vaskevich A, Rubinstein I (2012) Chemical deposition and stabilization of plasmonic copper nanoparticle films on transparent substrates. Chem Mater 24:2501–2508. https://doi.org/10.1021/cm300699f
176. Wang S, Liu N, Cheng Q, Pang B, Lv J (2021) Surface plasmon resonance on the antimonene–Fe2O3–copper layer for optical attenuated total reflection spectroscopic application. Plasmonics 16:559–566. https://doi.org/10.1007/s11468-020-01309-1
177. Lee HS, Awada C, Boutami S, Charra F, Douillard L, de Lamaestre RE (2012) Loss mechanisms of surface plasmon polaritons propagating on a smooth polycrystalline Cu surface. Opt Express 20:8974. https://doi.org/10.1364/oe.20.008974
178. Krasavin AV, Zayats AV (2010) Silicon-based plasmonic waveguides. Opt Express 18:11791. https://doi.org/10.1364/oe.18.011791
179. Fedyanin DY, Yakubovsky DI, Kirtaev RV, Volkov VS (2016) Ultralow-loss CMOS copper plasmonic waveguides. Nano Lett 16:362–366. https://doi.org/10.1021/acs.nanolett.5b03942
180. Alam MZ, Aitchison JS, Mojahedi M (2014) A marriage of convenience: hybridization of surface plasmon and dielectric waveguide modes. Laser Photonics Rev 8:394–408. https://doi.org/10.1002/lpor.201300168
181. Oulton RF, Sorger VJ, Genov DA, Pile DFP, Zhang X (2008) A hybrid plasmonic waveguide for subwavelength confinement and long-range propagation. Nat Photonics 2:496–500. https://doi.org/10.1038/nphoton.2008.131
182. Chu H-S, Zhu S, Png CE (2016) On-chip high performance plasmonic-CMOS components based on horizontal hybrid Cu-SiO2-Si platform. Conf. Lasers Electro-Optics, OSA, Washington, D.C., p STh4E.7. https://doi.org/10.1364/CLEO_SI.2016.STh4E.7
183. Zhu S, Chee JY, Lo GQ, Bai P, Kwong DL (2012) Horizontal Cu/SiO2/Si/SiO2/Cu plasmonic waveguide components integrated in silicon photonic circuits. Opt. Fiber Commun. Conf., OSA, Washington, D.C., p OW1E.2. https://doi.org/10.1364/OFC.2012.OW1E.2
184. Delacour C, Blaize S, Grosse P, Fedeli JM, Bruyant A, Salas-Montiel R, Lerondel G, Chelnokov A (2010) Efficient directional coupling between silicon and copper plasmonic nanoslot waveguides: toward metal-oxide-silicon nanophotonics. Nano Lett 10:2922–2926. https://doi.org/10.1021/nl101065q
185. Chee J, Zhu S, Lo GQ, Barwicz T, Watts MR, Popovic MA, Rakich PT, Socci L, Kartner FX, Ippen EP, Smith HI, Hosseini A, Rahimi S, Xu X, Kwong D, Covey J, Chen RT (2007) CMOS compatible polarization splitter using hybrid plasmonic waveguide references and links "polarization-transparent microphotonic devices in the strong confinement limit. Nat Photonics 1:57–60. http://www.lumerical.com
186. Ye L, Xiao Y, Liu Y, Zhang L, Cai G, Liu QH (2016) Strongly confined spoof surface plasmon polaritons waveguiding enabled by planar staggered plasmonic waveguides. Sci Rep 6:1–8. https://doi.org/10.1038/srep38528
187. Zhu S, Lo GQ, Xie J, Kwong DL (2013) Towards athermal nanoplasmonic resonators based on Cu-TiO2-Si hybrid plasmonic waveguide. Opt. Fiber Commun. Conf. Fiber Opt. Eng. Conf. 2013, OSA, Washington, D.C., p OW3F.1. https://doi.org/10.1364/OFC.2013.OW3F.1
188. Kesarwani R, Khare A (2018) Surface plasmon resonance and nonlinear optical behavior of pulsed laser-deposited semitransparent nanostructured copper thin films. Appl Phys B Lasers Opt 124:116. https://doi.org/10.1007/s00340-018-6986-x
189. Mohapatra S, Mishra YK, Warrier AM, Philip R, Sahoo S, Arora AK, Avasthi DK (2012) Plasmonic, low-frequency Raman, and nonlinear optical-limiting studies in copper-silica nanocomposites. Plasmonics 7:25–31. https://doi.org/10.1007/s11468-011-9271-y
190. Karthikeyan B, Anija M, Suchand Sandeep CS, Muhammad Nadeer TM, Philip R (2008) Optical and nonlinear optical properties of copper nanocomposite glasses annealed near the glass softening temperature. Opt Commun 281:2933–2937. https://doi.org/10.1016/j.optcom.2008.01.032
191. Takeda Y, Lu J, Plaksin OA, Amekura H, Kono K, Kishimoto N (2004) Optical properties of dense Cu nanoparticle composites fabricated by negative ion implantation. Nucl Instrum Methods Phys Res Sect B Beam Interact Mater Atoms 219–220:737–741. https://doi.org/10.1016/j.nimb.2004.01.153
192. Uemura T, Furumoto M, Nakano T, Akai-Kasaya M, Saito A, Aono M, Kuwahara Y (2007) Local-plasmon-enhanced upconversion fluorescence from copper phthalocyanine. Chem Phys Lett 448:232–236. https://doi.org/10.1016/j.cplett.2007.09.084
193. Li RK, To H, Andonian G, Feng J, Polyakov A, Scoby CM, Thompson K, Wan W, Padmore HA, Musumeci P (2013) Surface-plasmon resonance-enhanced multiphoton emission of high-brightness electron beams from a nanostructured copper cathode. Phys Rev Lett 110:1–5. https://doi.org/10.1103/PhysRevLett.110.074801
194. Futamata M (1997) Application of attenuated total reflection surface-plasmon-polariton Raman spectroscopy to gold and copper. Appl Opt 36:364. https://doi.org/10.1364/ao.36.000364
195. Aslan K, McDonald K, Previte MJR, Zhang Y, Geddes CD (2008) Silver island nanodeposits to enhance surface plasmon coupled fluorescence from copper thin films. Chem Phys Lett 464:216–219. https://doi.org/10.1016/j.cplett.2008.09.041
196. Previte MJR, Zhang Y, Aslan K, Geddes CD (2007) Surface plasmon coupled fluorescence from copper substrates. Appl Phys Lett 91:89–92. https://doi.org/10.1063/1.2794761
197. Sun M, Huang Y, Xia L, Chen X, Xu H (2011) The pH-Controlled Plasmon-Assisted Surface Photocatalysis Reaction of 4-Aminothiophenol to p, p′-Dimercaptoazobenzene on Au, Ag, and Cu colloids. J Phys Chem C 115(19):9629–9636. https://doi.org/10.1021/jp201002v
198. Li R, Zhao Y, Li R, Liu H, Ge Y, Xu Z (2021) Plasmonic optical trapping of nanoparticles using T-shaped copper nanoantennas. Opt Express 29(7):9826–9835. https://doi.org/10.1364/OE.420651
199. Atkinson A (1985) Transport processes during the growth of oxide films at elevated temperature. Rev Mod Phys 57:437–470. https://doi.org/10.1103/RevModPhys.57.437
200. Fu Q, Wagner T (2007) Interaction of nanostructured metal overlayers with oxide surfaces. Surf Sci Rep 62:431–498. https://doi.org/10.1016/j.surfrep.2007.07.001
201. Lagrow AP, Ward MR, Lloyd DC, Gai PL, Boyes ED (2017) Visualizing the Cu/Cu2O interface transition in nanoparticles with environmental scanning transmission electron microscopy. J Am Chem Soc 139:179–185. https://doi.org/10.1021/jacs.6b08842
202. Schey JA (ed) (1970) Metal deformation processes: friction and lubrication (No. 1). M. Dekker

203. Drury RC (1989) Advances in materials science and changes in the metal industry. Nat Resour Forum 13(4):322–324. https://doi.org/10.1111/j.1477-8947.1989.tb00356.x
204. Yanase A, Komiyama H (1991) In situ observation of oxidation and reduction of small supported copper particles using optical absorption and X-ray diffraction. Surf Sci 248:11–19. https://doi.org/10.1016/0039-6028(91)90056-X
205. Kim JH, Ehrman SH, Germer TA (2004) Influence of particle oxide coating on light scattering by submicron metal particles on silicon wafers. Appl Phys Lett 84:1278–1280. https://doi.org/10.1063/1.1650555
206. Pedersen DB, Wang S, Liang SH (2008) Charge-transfer-driven diffusion processes in Cu@Cu-oxide core-shell nanoparticles: oxidation of 3.0 ± 0.3 nm diameter copper nanoparticles. J Phys Chem C 112:8819–8826. https://doi.org/10.1021/jp710619r
207. Ramsey JA, Garlick GFJ, Roberts JK (n.d.) Theory of the oxidation of metals Some interactions of gases with metals and crystalline solids. Rep Prog Phys 12:163. http://iopscience.iop.org/0034-4885/12/1/308
208. Yang JC, Kolasa B, Gibson JM, Yeadon M (1998) Self-limiting oxidation of copper. Appl Phys Lett 73:2841–2843. https://doi.org/10.1063/1.122608
209. Barr TL (1978) An ESCA study of the termination of the passivation of elemental metals. J Phys Chem 82:1801–1810. https://doi.org/10.1021/j100505a006
210. Chen CH, Yamaguchi T, Sugawara KI, Koga K (2005) Role of stress in the self-limiting oxidation of copper nanoparticles. J Phys Chem B 109:20669–20672. https://doi.org/10.1021/jp0546498
211. Ghodselahi T, Vesaghi MA, Shafiekhani A, Baghizadeh A, Lameii M (2008) XPS study of the Cu@Cu 2 O core-shell nanoparticles. Appl Surf Sci 255:2730–2734. https://doi.org/10.1016/j.apsusc.2008.08.110
212. Cudennec Y, Lecerf A, Gerault Y (2020) Synthesis of C (OH) 2 and CuO by soft chemistry. 32:1013–1022. HAL Id: hal-02865530
213. Cudennec Y, Lecerf A, Riou A, Gerault Y, Cudennec Y, Lecerf A, Riou AYG (2020) Synthesis and study of sodium hydroxicuprate: Na 2 Cu(OH) 4 and copper hydroxide: Cu(OH) 2. HAL Id: hal-02888335
214. Cudennec Y, Lecerf A, Cudennec Y, Lecerf A, State S (2003) The transformation of Cu (OH) 2 into CuO, revisited.5:1471–1474. HAL Id: hal-02503180
215. Azarian A, Zad AI, Dolati A, Ghorbani M (2007) Time dependence of the surface plasmon resonance of copper nanorods. J Phys Condens Matter 19:446007. https://doi.org/10.1088/0953-8984/19/44/446007
216. Qin LX, Jing C, Li Y, Li DW, Long YT (2012) Real-time monitoring of the aging of single plasmonic copper nanoparticles. Chem Commun 48:1511–1513. https://doi.org/10.1039/c1cc14326c
217. Chavez KL, Hess DW (2001) A novel method of etching copper oxide using acetic acid. J Electrochem Soc 148:G640. https://doi.org/10.1149/1.1409400
218. Lim YF, Chu CS, Lee CJJ, Chi D (2014) Sol–gel deposited Cu2O and CuO thin films for photocatalytic water splitting. Phys Chem Chem Phys 16:25928–25934. https://doi.org/10.1039/C4CP03241A
219. Popok VN, Novikov SM, Lebedinskij YY, Markeev AM, Andreev AA, Trunkin IN, Arsenin AV, Volkov VS (2021) Gas-aggregated copper nanoparticles with long-term plasmon resonance stability. Plasmonics 16:333–340. https://doi.org/10.1007/s11468-020-01287-4
220. Kanninen P, Johans C, Merta J, Kontturi K (2008) Influence of ligand structure on the stability and oxidation of copper nanoparticles. J Colloid Interface Sci 318:88–95. https://doi.org/10.1016/j.jcis.2007.09.069
221. Tadmor R, Rosensweig RE, Frey J, Klein J (2000) Resolving the puzzle of ferrofluid dispersants. Langmuir 16:9117–9120. https://doi.org/10.1021/la0009137
222. Laibinis PE, Whitesides GM (1992) Self-assembled monolayers of n-alkanethiolates on copper are barrier films that protect the metal against oxidation by air. J Am Chem Soc 114:9022–9028. https://doi.org/10.1021/ja00049a038
223. Laibinis PE, Whitesides GM, Aliara DL, Tao YT, Parikh AN, Nuzzo RG (1991) Comparison of the structures and wetting properties of self-assembled monolayers of n-alkanethiols on the coinage metal surfaces, Cu, Ag, Au. J Am Chem Soc 113:7152–7167. https://doi.org/10.1021/ja00019a011
224. Blackman LCF, Dewar MJS, Hampson H (2007) An investigation of compounds promoting the dropwise condensation of steam. J Appl Chem 7:160–171. https://doi.org/10.1002/jctb.5010070403
225. Hutt DA, Liu C (2005) Oxidation protection of copper surfaces using self-assembled monolayers of octadecanethiol. Appl Surf Sci 252:400–411. https://doi.org/10.1016/j.apsusc.2005.01.019
226. Bekhit M, Sobhy A, Ali ZI, Gafar SM (2019) Efficient monitoring of dosimetric behaviour for copper nanoparticles through studying its optical properties. Radiochim Acta 107:523–529. https://doi.org/10.1515/ract-2018-3010
227. Tang L, Zhu L, Tang F, Yao C, Wang J, Li L (2018) Mild synthesis of copper nanoparticles with enhanced oxidative stability and their application in antibacterial films. Langmuir 34:14570–14576. https://doi.org/10.1021/acs.langmuir.8b02470
228. Kim I, Kim Y, Woo K, Ryu EH, Yon KY, Cao G, Moon J (2013) Synthesis of oxidation-resistant core-shell copper nanoparticles. RSC Adv 3:15169–15177. https://doi.org/10.1039/c3ra41480a
229. Stepanov AL, Popok VN, Hole DE, Khaibullin IB (2002) Ion synthesis and laser annealing of Cu nanoparticles in Al2O3. Appl Phys A Mater Sci Process 74:441–446. https://doi.org/10.1007/s003390101076
230. Jiménez JA (2019) Thermal effects on the surface plasmon resonance of Cu nanoparticles in phosphate glass: Impact on Cu+ luminescence. Nanoscale Adv 1:1826–1832. https://doi.org/10.1039/c8na00385h
231. Popok VN, Nuzhdin VI, Valeev VF, Stepanov AL (2015) Copper nanoparticles synthesized in polymers by ion implantation: surface morphology and optical properties of the nanocomposites. J Mater Res 30:86–92. https://doi.org/10.1557/jmr.2014.324
232. Preston AS, Hughes RA, Demille TB, Neretina S (2020) Plasmonics under attack: protecting copper nanostructures from harsh environments. Chem Mater 32:6788–6799. https://doi.org/10.1021/acs.chemmater.0c02715
233. Albrecht G, Ubl M, Kaiser S, Giessen H, Hentschel M (2018) Comprehensive study of plasmonic materials in the visible and near-infrared: linear, refractory, and nonlinear optical properties. ACS Photonics 5:1058–1067. https://doi.org/10.1021/acsphotonics.7b01346
234. Gonzalez-Posada F, Sellappan R, Vanpoucke B, Chakarov D (2014) Oxidation of copper nanoparticles in water monitored in situ by localized surface plasmon resonance spectroscopy. RSC Adv 4:20659–20664. https://doi.org/10.1039/c3ra47473a
235. Desario PA, Pietron JJ, Brintlinger TH, McEntee M, Parker JF, Baturina O, Stroud RM, Rolison DR (2017) Oxidation-stable plasmonic copper nanoparticles in photocatalytic TiO2 nanoarchitectures. Nanoscale 9:11720–11729. https://doi.org/10.1039/c7nr04805j
236. Zhang S, Peng B, Yang S, Wang H, Yu H, Fang Y, Peng F (2015) Non-noble metal copper nanoparticles-decorated TiO2 nanotube arrays with plasmon-enhanced photocatalytic hydrogen evolution under visible light. Int J Hydrogen Energy 40:303–310. https://doi.org/10.1016/j.ijhydene.2014.10.122

237. Jiang B, Friis J, Holmestad R, Zuo JM, O'Keeffe M, Spence JCH (2004) Electron density and implication for bonding in Cu. Phys Rev B Condens Matter Mater Phys 69:1–6. https://doi.org/10.1103/PhysRevB.69.245110
238. Rice KP, Walker EJ, Stoykovich MP, Saunders AE (2011) Solvent-dependent surface plasmon response and oxidation of copper nanocrystals. J Phys Chem C 115:1793–1799. https://doi.org/10.1021/jp110483z
239. Sarmah K, Roy UK, Maji TK, Pratihar S (2018) Role of metal exchange toward the morphology and photocatalytic activity of Cu/Ag/Au-Doped ZnO: a study with a zinc-sodium acetate complex as the precursor. ACS Appl Nano Mater 1:2049–2056. https://doi.org/10.1021/acsanm.8b00436
240. Dai B, Zhao W, Huang H, Li S, Yang G, Wu H, Sun C, Leung DYC (2022) Constructing an ohmic junction of copper@ cuprous oxide nanocomposite with plasmonic enhancement for photocatalysis. J Colloid Interface Sci 616:163–176. https://doi.org/10.1016/j.jcis.2022.02.056
241. Alvarez MM, Khoury JT, Schaaff TG, Shafigullin MN, Vezmar I, Whetten RL (1997) Optical absorption spectra of nanocrystal gold molecules. J Phys Chem B 101:3706–3712. https://doi.org/10.1021/jp962922n
242. Putnis A (1976) The transformation behaviour of cuprous sulphides and its application to the efficiency of CuxS-CdS solar cells. Philos Mag 34:1083–1086. https://doi.org/10.1080/00318087608227730
243. Agrawal A, Johns RW, Milliron DJ (2017) Control of localized surface plasmon resonances in metal oxide nanocrystals. Annu Rev Mater Res 47:1–31. https://doi.org/10.1146/annurev-matsci-070616-124259
244. Jiang R, Li B, Fang C, Wang J (2014) Metal/semiconductor hybrid nanostructures for plasmon-enhanced applications. Adv Mater 26:5274–5309. https://doi.org/10.1002/adma.201400203
245. Liu X, Swihart MT (2014) Heavily-doped colloidal semiconductor and metal oxide nanocrystals: an emerging new class of plasmonic nanomaterials. Chem Soc Rev 43:3908–3920. https://doi.org/10.1039/c3cs60417a
246. Xu W, Liu H, Zhou D, Chen X, Ding N, Song H, Ågren H (2020) Localized surface plasmon resonances in self-doped copper chalcogenide binary nanocrystals and their emerging applications. Nano Today 33:100892. https://doi.org/10.1016/j.nantod.2020.100892
247. Kriegel I, Scotognella F, Manna L (2017) Plasmonic doped semiconductor nanocrystals: properties, fabrication, applications and perspectives. Phys Rep 674:1–52. https://doi.org/10.1016/j.physrep.2017.01.003
248. Agrawal A, Cho SH, Zandi O, Ghosh S, Johns RW, Milliron DJ (2018) Localized surface plasmon resonance in semiconductor nanocrystals. Chem Rev 118:3121–3207. https://doi.org/10.1021/acs.chemrev.7b00613
249. Goel S, Chen F, Cai W (2014) Synthesis and biomedical applications of copper sulfide nanoparticles: from sensors to theranostics. Small 10:631–645. https://doi.org/10.1002/smll.201301174
250. Mattox TM, Ye X, Manthiram K, Schuck PJ, Alivisatos AP, Urban JJ (2015) Chemical control of plasmons in metal chalcogenide and metal oxide nanostructures. Adv Mater 27:5830–5837. https://doi.org/10.1002/adma.201502218
251. Liu Y, Liu M, Swihart MT (2017) Plasmonic copper sulfide-based materials: a brief introduction to their synthesis, doping, alloying, and applications. J Phys Chem C 121:13435–13447. https://doi.org/10.1021/acs.jpcc.7b00894
252. Nair PK, Nair MTS, Fernandez A, Ocampo M (1989) Prospects of chemically deposited metal chalcogenide thin films for solar control applications. J Phys D Appl Phys 22:829–836. https://doi.org/10.1088/0022-3727/22/6/021
253. Gadave KM, Lokhande CD (1993) Formation of Cux S films through a chemical bath deposition process. Thin Solid Films 229:1–4. https://doi.org/10.1016/0040-6090(93)90397-8
254. Pramanik P, Akhter MA, Basu PK (1987) Modified chemical method for the deposition of Cu1.8S thin film. J Mater Sci Lett 6:1277–1279. https://doi.org/10.1007/BF01794588
255. Partain LD, McLeod PS, Duisman JA, Peterson TM, Sawyer DE, Dean CS (1983) Degradation of a CuxS/CdS solar cell in hot, moist air and recovery in hydrogen and air. J Appl Phys 54:6708–6720. https://doi.org/10.1063/1.331858
256. Kuzuya T, Itoh K, Sumiyama K (2008) Low polydispersed copper-sulfide nanocrystals derived from various Cu-alkyl amine complexes. J Colloid Interface Sci 319:565–571. https://doi.org/10.1016/j.jcis.2007.11.053
257. Klimov V, Haring Bolivar P, Kurz H, Karavanskii V, Krasovskii V, Korkishko Y (1995) Linear and nonlinear transmission of Cux S quantum dots. Appl Phys Lett 67:653. https://doi.org/10.1063/1.115192
258. Zhao Y, Pan H, Lou Y, Qiu X, Zhu J, Burda C (2009) Plasmonic Cu 2-xS nanocrystals: optical and structural properties of copper-deficient copper(I) sulfides. J Am Chem Soc 131:4253–4261. https://doi.org/10.1021/ja805655b
259. Zhao Y, Burda C (2012) Development of plasmonic semiconductor nanomaterials with copper chalcogenides for a future with sustainable energy materials. Energy Environ Sci 5:5564–5576. https://doi.org/10.1039/c1ee02734d
260. Wu Y, Wadia C, Ma W, Sadtler B, Alivisatos AP (2008) Synthesis and photovoltaic application of copper(1) sulfide nanocrystals. Nano Lett 8:2345–2350. https://doi.org/10.1021/nl801817d
261. Ku G, Zhou M, Song S, Huang Q, Hazle J, Li C (2012) Copper sulfide nanoparticles as a new class of photoacoustic contrast agent for deep tissue imaging at 1064 nm. ACS Nano 6:7489–7496. https://doi.org/10.1021/nn302782y
262. Li Y, Lu W, Huang Q, Li C, Chen W (2010) Copper sulfide nanoparticles for photothermal ablation of tumor cells. Nanomedicine 5:1161–1171. https://doi.org/10.2217/nnm.10.85
263. Tian Q, Tang M, Sun Y, Zou R, Chen Z, Zhu M, Yang S, Wang J, Wang J, Hu J (2011) Hydrophilic flower-like cus superstructures as an efficient 980 nm laser-driven photothermal agent for ablation of cancer cells. Adv Mater 23:3542–3547. https://doi.org/10.1002/adma.201101295
264. Dong K, Liu Z, Li Z, Ren J, Qu X (2013) Hydrophobic anticancer drug delivery by a 980 nm laser-driven photothermal vehicle for efficient synergistic therapy of cancer cells in vivo. Adv Mater 25:4452–4458. https://doi.org/10.1002/adma.201301232
265. Hsu SW, On K, Tao AR (2011) Localized surface plasmon resonances of anisotropic semiconductor nanocrystals. J Am Chem Soc 133:19072–19075. https://doi.org/10.1021/ja2089876
266. Dorfs D, Härtling T, Miszta K, Bigall NC, Kim MR, Genovese A, Falqui A, Povia M, Manna L (2011) Reversible tunability of the near-infrared valence band plasmon resonance in Cu2- xSe nanocrystals. J Am Chem Soc 133:11175–11180. https://doi.org/10.1021/ja2016284
267. Garcia G, Buonsanti R, Runnerstrom EL, Mendelsberg RJ, Llordes A, Anders A, Richardson TJ, Milliron DJ (2011) Dynamically modulating the surface plasmon resonance of doped semiconductor nanocrystals. Nano Lett 11:4415–4420. https://doi.org/10.1021/nl202597n
268. De Nanoparticles T, Saldanha PL, Brescia R, Prato M, Li H, Povia M, Manna L, Lesnyak V (2014) Generalized one-pot synthesis of copper sul fi de, selenide-sul fi de, and telluride-sul fi de nanoparticles. Chem Mater 26:1442–1449
269. Luther JM, Jain PK, Ewers T, Alivisatos AP (2011) Localized surface plasmon resonances arising from free carriers in doped quantum dots. Nat Mater 10:361–366. https://doi.org/10.1038/nmat3004

270. Hsu SW, Ngo C, Tao AR (2014) Tunable and directional plasmonic coupling within semiconductor nanodisk assemblies. Nano Lett 14:2372–2380. https://doi.org/10.1021/nl404777h
271. Lukashev P, Lambrecht WRL, Kotani T, Van Schilfgaarde M (2007) Electronic and crystal structure of Cu2-x S: full-potential electronic structure calculations. Phys Rev B Condens Matter Mater Phys 76:1–14. https://doi.org/10.1103/PhysRevB.76.195202
272. Mazin II (2012) Structural and electronic properties of the two-dimensional superconductor CuS with 113-valent copper. Phys Rev B Condens Matter Mater Phys 85:1–5. https://doi.org/10.1103/PhysRevB.85.115133
273. Xie Y, Carbone L, Nobile C, Grillo V, D'Agostino S, Della Sala F, Giannini C, Altamura D, Oelsner C, Kryschi C, Cozzoli PD (2013) Metallic-like stoichiometric copper sulfide nanocrystals: phase- and shape-selective synthesis, near-infrared surface plasmon resonance properties, and their modeling. ACS Nano 7:7352–7369. https://doi.org/10.1021/nn403035s
274. Xie Y, Riedinger A, Prato M, Casu A, Genovese A, Guardia P, Sottini S, Sangregorio C, Miszta K, Ghosh S, Pellegrino T, Manna L (2013) Copper sulfide nanocrystals with tunable composition by reduction of covellite nanocrystals with Cu+ ions. J Am Chem Soc 135:17630–17637. https://doi.org/10.1021/ja409754v
275. Hartstein KH, Brozek CK, Hinterding SOM, Gamelin DR (2018) Copper-coupled electron transfer in colloidal plasmonic copper-sulfide nanocrystals probed by in situ spectroelectrochemistry. J Am Chem Soc 140:3434–3442. https://doi.org/10.1021/jacs.8b00174
276. Jain PK, Manthiram K, Engel JH, White SL, Faucheaux JA, Alivisatos AP (2013) Doped nanocrystals as plasmonic probes of redox chemistry. Angew Chemie - Int Ed 52:13671–13675. https://doi.org/10.1002/anie.201303707
277. Knauth P, Tuller HL (2002) Solid-state ionics: roots, status, and future prospects. J Am Ceram Soc 85:1654–1680. https://doi.org/10.1111/j.1151-2916.2002.tb00334.x
278. Wang F, Huang Y, Chai Z, Zeng M, Li Q, Wang Y, Xu D (2016) Photothermal-enhanced catalysis in core-shell plasmonic hierarchical Cu7S4 microsphere@zeolitic imidazole framework-8. Chem Sci 7:6887–6893. https://doi.org/10.1039/c6sc03239g
279. Cui J, Li Y, Liu L, Chen L, Xu J, Ma J, Fang G, Zhu E, Wu H, Zhao L, Wang L, Huang Y (2015) Near-infrared plasmonic-enhanced solar energy harvest for highly efficient photocatalytic reactions. Nano Lett 15:6295–6301. https://doi.org/10.1021/acs.nanolett.5b00950
280. Sundararaman R, Narang P, Jermyn AS, Goddard WA, Atwater HA (2014) Theoretical predictions for hot-carrier generation from surface plasmon decay. Nat Commun 5:1–8. https://doi.org/10.1038/ncomms6788
281. Wang R, Liu H, Wang X, Li X, Gu X, Zheng Z (2020) Plasmon-enhanced furfural hydrogenation catalyzed by stable carbon-coated copper nanoparticles driven from metal-organic frameworks. Catal. Sci Technol 10:6483–6494. https://doi.org/10.1039/d0cy01162b
282. Ren K, Yin P, Zhou Y, Cao X, Dong C, Cui L, Liu H, Du X (2017) Localized defects on copper sulfide surface for enhanced plasmon resonance and water splitting. Small 13:1–7. https://doi.org/10.1002/smll.201700867
283. Tian Q, Jiang F, Zou R, Liu Q, Chen Z, Zhu M, Yang S, Wang J, Wang J, Hu J (2011) Hydrophilic Cu 9S 5 nanocrystals: a photothermal agent with a 25.7% heat conversion efficiency for photothermal ablation of cancer cells in vivo. ACS Nano 5:9761–9771. https://doi.org/10.1021/nn203293t
284. Tian Q, Hu J, Zhu Y, Zou R, Chen Z, Yang S, Li R, Su Q, Han Y, Liu X (2013) Sub-10 nm Fe3O4@Cu2–xS core–shell nanoparticles for dual-modal imaging and photothermal therapy. J Am Chem Soc 135(23):8571–8577. https://doi.org/10.1021/ja4013497
285. Wu ZC, Li WP, Luo CH, Su CH, Yeh CS (2015) Rattle-type Fe3O4@CuS developed to conduct magnetically guided photoinduced hyperthermia at first and second NIR biological windows. Adv Funct Mater 25:6527–6537. https://doi.org/10.1002/adfm.201503015
286. Lakshmanan SB, Zou X, Hossu M, Ma L, Yang C, Chen W (2012) Local field enhanced Au/CuS nanocomposites as efficient photothermal transducer agents for cancer treatment. J Biomed Nanotechnol 8:883–890. https://doi.org/10.1166/jbn.2012.1486
287. Rand BP, Peumans P, Forrest SR (2004) Long-range absorption enhancement in organic tandem thin-film solar cells containing silver nanoclusters. J Appl Phys 96:7519–7526. https://doi.org/10.1063/1.1812589
288. Zhou M, Li J, Liang S, Sood AK, Liang D, Li C (2015) CuS Nanodots with ultrahigh efficient renal clearance for positron emission tomography imaging and image-guided photothermal therapy. ACS Nano 9:7085–7096. https://doi.org/10.1021/acsnano.5b02635
289. Yi X, Yang K, Liang C, Zhong X, Ning P, Song G, Wang D, Ge C, Chen C, Chai Z, Liu Z (2015) Imaging-guided combined photothermal and radiotherapy to treat subcutaneous and metastatic tumors using iodine-131-doped copper sulfide nanoparticles. Adv Funct Mater 25:4689–4699. https://doi.org/10.1002/adfm.201502003
290. Gabka G, Bujak P, Ostrowski A, Tomaszewski W, Lisowski W, Sobczak JW, Pron A (2016) Cu-Fe-S nanocrystals exhibiting tunable localized surface plasmon resonance in the visible to NIR spectral ranges. Inorg Chem 55(13):6660–6669. https://doi.org/10.1021/acs.inorgchem.6b00912 (Epub 2016 Jun 14)
291. Comin A, Manna L (2014) New materials for tunable plasmonic colloidal nanocrystals. Chem Soc Rev 43:3957–3975. https://doi.org/10.1039/c3cs60265f
292. Kays JC, Conti CR, Margaronis A, Kuszynski JE, Strouse GF, Dennis AM (2021) Controlled synthesis and exploration of CuxFeS4bornite nanocrystals. Chem Mater 33:7408–7416. https://doi.org/10.1021/acs.chemmater.1c02029
293. Niezgoda JS, Harrison MA, Mcbride JR, Rosenthal SJ (2012) Novel synthesis of chalcopyrite CuxInyS2 quantum dots with tunable localized surface plasmon resonances. Chem Mater 24:3294–3298. https://doi.org/10.1021/cm3021462
294. Jiang SJ, Wan SM, Luo W et al (2020) J Materials chemistry C. J Mater Chem 1:3777. http://ncesr.unl.edu/wordpress/wp-content/uploads/2010/07/Synthesis-of-high-quality-inverse-opals-J-Mater-Chem-C-article.pdf
295. Van Der Stam W, Gudjonsdottir S, Evers WH, Houtepen AJ (2017) Switching between plasmonic and fluorescent copper sulfide nanocrystals. J Am Chem Soc 139:13208–13217. https://doi.org/10.1021/jacs.7b07788
296. Xie Y, Chen W, Bertoni G, Kriegel I, Xiong M, Li N, Prato M, Riedinger A, Sathya A, Manna L (2017) Tuning and locking the localized surface plasmon resonances of CuS (covellite) nanocrystals by an amorphous CuPdxS shell. Chem Mater 29:1716–1723. https://doi.org/10.1021/acs.chemmater.6b05184
297. Gurin VS, Prokopenko VB, Alexeenko AA, Wang S, Yumashev KV, Prokoshin PV (2001) Sol-gel silica glasses with nanoparticles of copper selenide: synthesis, optics and structure. Int J Inorg Mater 3:493–496. https://doi.org/10.1016/S1466-6049(01)00061-7
298. Deka S, Genovese A, Zhang Y, Miszta K, Bertoni G, Krahne R, Giannini C, Manna L (2010) Phosphine-free synthesis of p-type copper(I) selenide nanocrystals in hot coordinating solvents. J Am Chem Soc 132:8912–8914. https://doi.org/10.1021/ja103223x
299. Mansour BA, Demian SE, Zayed HA (1992) Determination of the effective mass for highly degenerate copper selenide from reflectivity measurements. J Mater Sci Mater Electron 3:249–252. https://doi.org/10.1007/BF00703036

300. Liu X, Wang X, Zhou B, Law WC, Cartwright AN, Swihart MT (2013) Size-controlled synthesis of Cu2-xE (E = S, Se) nanocrystals with strong tunable near-infrared localized surface plasmon resonance and high conductivity in thin films. Adv Funct Mater 23:1256–1264. https://doi.org/10.1002/adfm.201202061
301. Balitskii OA, Sytnyk M, Stangl J, Primetzhofer D, Groiss H, Heiss W (2014) Tuning the localized surface plasmon resonance in Cu2-xSe nanocrystals by postsynthetic ligand exchange. ACS Appl Mater Interfaces 6:17770–17775. https://doi.org/10.1021/am504296y
302. Li W, Zamani R, Ibáñez M, Cadavid D, Shavel A, Morante JR, Arbiol J, Cabot A (2013) Metal ions to control the morphology of semiconductor nanoparticles: copper selenide nanocubes. J Am Chem Soc 135:4664–4667. https://doi.org/10.1021/ja400472m
303. Riha SC, Johnson DC, Prieto AL (2011) Cu2Se nanoparticles with tunable electronic properties due to a controlled solid-state phase transition driven by copper oxidation and cationic conduction. J Am Chem Soc 133:1383–1390. https://doi.org/10.1021/ja106254h
304. Wu XJ, Huang X, Liu J, Li H, Yang J, Li B, Huang W, Zhang H (2014) Two-dimensional cuse nanosheets with microscale lateral size: synthesis and template-assisted phase transformation. Angew Chemie Int Ed 53:5083–5087. https://doi.org/10.1002/anie.201311309
305. Scotognella F, Della Valle G, Srimath Kandada AR, Dorfs D, Zavelani-Rossi M, Conforti M, Miszta K, Comin A, Korobchevskaya K, Lanzani G, Manna L, Tassone F (2011) Plasmon dynamics in colloidal Cu2-xSe nanocrystals. Nano Lett 11:4711–4717. https://doi.org/10.1021/nl202390s
306. Marbella LE, Gan XY, Kaseman DC, Millstone JE (2017) Correlating carrier density and emergent plasmonic features in Cu2-xSe nanoparticles. Nano Lett 17:2414–2419. https://doi.org/10.1021/acs.nanolett.6b05420
307. White SL, Banerjee P, Jain PK (2017) Liquid-like cationic sublattice in copper selenide clusters. Nat Commun 8:1–11. https://doi.org/10.1038/ncomms14514
308. Hu C, Zhang Z, Liu S, Liu X, Pang M (2019) Monodispersed CuSe sensitized covalent organic framework photosensitizer with an enhanced photodynamic and photothermal effect for cancer therapy. ACS Appl Mater Interfaces 11:23072–23082. https://doi.org/10.1021/acsami.9b08394
309. Gan XY, Keller EL, Warkentin CL, Crawford SE, Frontiera RR, Millstone JE (2019) Plasmon-enhanced chemical conversion using copper selenide nanoparticles. Nano Lett 19:2384–2388. https://doi.org/10.1021/acs.nanolett.8b05088
310. Liu Z, Wang J, Qiu K, Liao X, Rees TW, Ji L, Chao H (2019) Fabrication of red blood cell membrane-camouflaged Cu2-: XSe nanoparticles for phototherapy in the second near-infrared window. Chem Commun 55:6523–6526. https://doi.org/10.1039/c9cc03148k
311. Zhao Z, Jia G, Liu Y, Zhang Q, Wang N (2019) Microwave-assisted synthesis and photothermal conversion of Cu 2–x Se hollow structure. J Nanoparticle Res 21:47. https://doi.org/10.1007/s11051-019-4489-2
312. Llorente VB, Dzhagan VM, Gaponik N, Iglesias RA, Zahn DRT, Lesnyak V (2017) Electrochemical tuning of localized surface plasmon resonance in copper chalcogenide nanocrystals. J Phys Chem C 121:18244–18253. https://doi.org/10.1021/acs.jpcc.7b05334
313. Hessel CM, Pattani VP, Rasch M, Panthani MG, Koo B, Tunnell JW, Korgel BA (2011) Copper selenide nanocrystals for photothermal therapy. Nano Lett 11:2560–2566. https://doi.org/10.1021/nl201400z
314. Zhang S, Sun C, Zeng J, Sun Q, Wang G, Wang Y, Wu Y, Dou S, Gao M, Li Z (2016) Ambient aqueous synthesis of ultrasmall PEGylated Cu2−xSe nanoparticles as a multifunctional theranostic agent for multimodal imaging guided photothermal therapy of cancer. Adv Mater 28:8927–8936. https://doi.org/10.1002/adma.201602193
315. Liu X, Law WC, Jeon M, Wang X, Liu M, Kim C, Prasad PN, Swihart MT (2013) Cu2-xSe Nanocrystals with localized surface plasmon resonance as sensitive contrast agents for in vivo photoacoustic imaging: demonstration of sentinel lymph node mapping. Adv Healthc Mater 2:952–957. https://doi.org/10.1002/adhm.201200388
316. Liu X, Wang Q, Li C, Zou R, Li B, Song G, Xu K, Zheng Y, Hu J (2014) Cu2-xSe@mSiO2-PEG core-shell nanoparticles: A low-toxic and efficient difunctional nanoplatform for chemo-photothermal therapy under near infrared light radiation with a safe power density. Nanoscale 6:4361–4370. https://doi.org/10.1039/c3nr06160d
317. Liu X, Lee C, Law WC, Zhu D, Liu M, Jeon M, Kim J, Prasad PN, Kim C, Swihart MT (2013) Au–Cu2–xSe heterodimer nanoparticles with broad localized surface plasmon resonance as contrast agents for deep tissue imaging. Nano Lett 13(9):4333–4339. https://doi.org/10.1021/nl402124h
318. Marin BC, Hsu SW, Chen L, Lo A, Zwissler DW, Liu Z, Tao AR (2016) Plasmon-enhanced two-photon absorption in photoluminescent semiconductor nanocrystals. ACS Photonics 3:526–531. https://doi.org/10.1021/acsphotonics.6b00037
319. Wang X, Liu X, Yin D, Ke Y, Swihart MT (2015) Size-, shape-, and composition-controlled synthesis and localized surface plasmon resonance of copper tin selenide nanocrystals. Chem Mater 27:3378–3388. https://doi.org/10.1021/acs.chemmater.5b00618
320. Dilena E, Dorfs D, George C, Miszta K, Povia M, Genovese A, Casu A, Prato M, Manna L (2012) Colloidal Cu2-x(SySe1-y) alloy nanocrystals with controllable crystal phase: synthesis, plasmonic properties, cation exchange and electrochemical lithiation. J Mater Chem 22:13023–13031. https://doi.org/10.1039/c2jm30788j
321. Xu J, Tang YB, Chen X, Luan CY, Zhang WF, Zapien JA, Zhang WJ, Kwong HL, Meng XM, Lee ST, Lee CS (2010) Synthesis of homogeneously alloyed Cu2-x(SySe 1-y) nanowire bundles with tunable compositions and bandgaps. Adv Funct Mater 20:4190–4195. https://doi.org/10.1002/adfm.201000771
322. Wang JJ, Xue DJ, Guo YG, Hu JS, Wan LJ (2011) Bandgap engineering of monodispersed $Cu_{2-x}S_ySe_{1-y}$ nanocrystals through chalcogen ratio and crystal structure. J Am Chem Soc 133(46):18558–18561. https://doi.org/10.1021/ja208043g
323. Liu X, Wang X, Swihart MT (2013) $Cu_{2-x}S_{1-y}Se_y$ alloy nanocrystals with broadly tunable near-infrared localized surface plasmon resonance. Chem Mater 25(21):4402–4408. https://doi.org/10.1021/cm402848k
324. Zeng Y, Joo PH, Yang K, Tao AR (2021) Computation-motivated design of ternary plasmonic copper chalcogenide nanocrystals. Chem Mater 33:117–125. https://doi.org/10.1021/acs.chemmater.0c02951
325. Li W, Zamani R, Rivera Gil P, Pelaz B, Ibáñez M, Cadavid D, Shavel A, Alvarez-Puebla RA, Parak WJ, Arbiol J, Cabot A (2013) CuTe nanocrystals: shape and size control, plasmonic properties, and use as SERS probes and photothermal agents. J Am Chem Soc 135:7098–7101. https://doi.org/10.1021/ja401428e
326. Kriegel I, Jiang C, Rodríguez-Fernández J, Schaller RD, Talapin DV, Da Como E, Feldmann J (2012) Tuning the excitonic and plasmonic properties of copper chalcogenide nanocrystals. J Am Chem Soc 134:1583–1590. https://doi.org/10.1021/ja207798q
327. Jiang Y, Xie B, Wu J, Yuan S, Wu Y, Huang H, Qian Y (2002) Room-temperature synthesis of copper and silver, nanocrystalline chalcogenides in mixed solvents. J Solid State Chem 167:28–33. https://doi.org/10.1006/jssc.2002.9610
328. Dmitruk I, Blonskiy I, Pavlov I, Yeshchenko O, Alexeenko A, Dmytruk A, Korenyuk P, Kadan V (2009) Surface plasmon as a probe of local field enhancement. Plasmonics 4:115–119. https://doi.org/10.1007/s11468-009-9081-7

329. Mugnaioli E, Gemmi M, Tu R, David J, Bertoni G, Gaspari R, De Trizio L, Manna L (2018) Ab initio structure determination of Cu2- xTe plasmonic nanocrystals by precession-assisted electron diffraction tomography and HAADF-STEM imaging. Inorg Chem 57:10241–10248. https://doi.org/10.1021/acs.inorgchem.8b01445
330. Kriegel I, Rodríguez-Fernández J, Wisnet A, Zhang H, Waurisch C, Eychmüller A, Dubavik A, Govorov AO, Feldmann J (2013) Shedding light on vacancy-doped copper chalcogenides: shape-controlled synthesis, optical properties, and modeling of copper telluride nanocrystals with near-infrared plasmon resonances. ACS Nano 7:4367–4377. https://doi.org/10.1021/nn400894d
331. Kriegel I, Wisnet A, Srimath Kandada AR, Scotognella F, Tassone F, Scheu C, Zhang H, Govorov AO, Rodríguez-Fernández J, Feldmann J (2014) Cation exchange synthesis and optoelectronic properties of type II CdTe-Cu_{2-x}Te nano-heterostructures. J Mater Chem C 2:3189–3198. https://doi.org/10.1039/c3tc32049a
332. Zhang J, Tang Y, Lee K, Ouyang M (2010) Tailoring light-matter-spin interactions in colloidal hetero-nanostructures. Nature 466:91–95. https://doi.org/10.1038/nature09150
333. Hsu SW, Bryks W, Tao AR (2012) Effects of carrier density and shape on the localized surface plasmon resonances of Cu 2-xS Nanodisks. Chem Mater 24:3765–3771. https://doi.org/10.1021/cm302363x
334. Mou J, Li P, Liu C, Xu H, Song L, Wang J, Zhang K, Chen Y, Shi J, Chen H (2015) Ultrasmall Cu2-xS nanodots for highly efficient photoacoustic imaging-guided photothermal therapy. Small 11:2275–2283. https://doi.org/10.1002/smll.201403249
335. Mou J, Liu C, Li P, Chen Y, Xu H, Wei C, Song L, Shi J, Chen H (2015) Biomaterials A facile synthesis of versatile Cu 2 À x S nanoprobe for enhanced MRI and infrared thermal / photoacoustic multimodal imaging. Biomaterials 57:12–21. https://doi.org/10.1016/j.biomaterials.2015.04.020
336. Li W, Shavel A, Guzman R, Rubio-Garcia J, Flox C, Fan J, Cadavid D, Ibáñez M, Arbiol J, Morante JR, Cabot A (2011) Morphology evolution of Cu2-xS nanoparticles: from spheres to dodecahedrons. Chem Commun 47:10332–10334. https://doi.org/10.1039/c1cc13803k
337. Alam R, Labine M, Karwacki CJ, Kamat PV (2016) Modulation of Cu2-xS nanocrystal plasmon resonance through reversible photoinduced electron transfer. ACS Nano 10:2880–2886. https://doi.org/10.1021/acsnano.5b08066
338. Liu Z, Liu X, Du Y, Ren J, Qu X (2015) Using plasmonic copper sulfide nanocrystals as smart light-driven sterilants. ACS Nano 9:10335–10346. https://doi.org/10.1021/acsnano.5b04380
339. Zhou M, Zhang R, Huang M, Lu W, Song S, Melancon MP, Tian M, Liang D, Li C (2010) A chelator-free multifunctional [64Cu]CuS nanoparticle platform for simultaneous micro-PET/CT imaging and photothermal ablation therapy. J Am Chem Soc 132:15351–15358. https://doi.org/10.1021/ja106855m
340. Ding K, Zeng J, Jing L, Qiao R, Liu C, Jiao M, Li Z, Gao M (2015) Aqueous synthesis of PEGylated copper sulfide nanoparticles for photoacoustic imaging of tumors. Nanoscale 7:11075–11081. https://doi.org/10.1039/c5nr02180d
341. Liu L, Zhong H, Bai Z, Zhang T, Fu W, Shi L, Xie H, Deng L, Zou B (2013) Controllable transformation from rhombohedral Cu1.8S nanocrystals to hexagonal CuS clusters: phase- and composition-dependent plasmonic properties. Chem Mater 25:4828–4834. https://doi.org/10.1021/cm403420u
342. Li B, Wang Q, Zou R, Liu X, Xu K, Li W, Hu J (2014) Cu7.2S4 nanocrystals: a novel photothermal agent with a 56.7% photothermal conversion efficiency for photothermal therapy of cancer cells. Nanoscale 6:3274–3282. https://doi.org/10.1039/c3nr06242b
343. Xie Y, Bertoni G, Riedinger A, Sathya A, Prato M, Marras S, Tu R, Pellegrino T, Manna L (2015) Nanoscale transformations in covellite (CuS) nanocrystals in the presence of divalent metal cations in a mild reducing environment. Chem Mater 27:7531–7537. https://doi.org/10.1021/acs.chemmater.5b03892
344. Manzi A, Simon T, Sonnleitner C, Döblinger M, Wyrwich R, Stern O, Stolarczyk JK, Feldmann J (2015) Light-induced cation exchange for copper sulfide based CO2 reduction. J Am Chem Soc 137:14007–14010. https://doi.org/10.1021/jacs.5b06778
345. Luther JM, Zheng H, Sadtler B, Alivisatos AP (2009) Synthesis of PbS nanorods and other ionic nanocrystals of complex morphology by sequential cation exchange reactions. J Am Chem Soc 131:16851–16857. https://doi.org/10.1021/ja906503w
346. Hsu SW, Ngo C, Bryks W, Tao AR (2015) Shape focusing during the anisotropic growth of CuS triangular nanoprisms. Chem Mater 27:4957–4963. https://doi.org/10.1021/acs.chemmater.5b01223
347. Turo MJ, Macdonald JE (2014) Crystal-bound vs surface-bound thiols on nanocrystals. ACS Nano 8:10205–10213. https://doi.org/10.1021/nn5032164
348. Chen L, Sakamoto M, Haruta M, Nemoto T, Sato R, Kurata H, Teranishi T (2016) Tin ion directed morphology evolution of copper sulfide nanoparticles and tuning of their plasmonic properties via phase conversion. Langmuir 32:7582–7587. https://doi.org/10.1021/acs.langmuir.6b02035
349. Thimsen E, Kortshagen UR, Aydil ES (2014) Plasma synthesis of stoichiometric Cu2S nanocrystals stabilized by oleylamine. Chem Commun 50:8346–8349. https://doi.org/10.1039/c4cc00998c
350. Kwon YT, Lim GD, Kim S, Ryu SH, Lim HR, Choa YH (2019) Effect of localized surface plasmon resonance on dispersion stability of copper sulfide nanoparticles. Appl Surf Sci 477:204–210. https://doi.org/10.1016/j.apsusc.2017.11.006
351. Lesyuk R, Klein E, Yaremchuk I, Klinke C (2018) Copper sulfide nanosheets with shape-tunable plasmonic properties in the NIR region. Nanoscale 10:20640–20651. https://doi.org/10.1039/c8nr06738d
352. Rabkin A, Friedman O, Golan Y (2015) Surface plasmon resonance in surfactant coated copper sulfide nanoparticles: role of the structure of the capping agent. J Colloid Interface Sci 457:43–51. https://doi.org/10.1016/j.jcis.2015.06.044
353. Serhan M, Sprowls M, Jackemeyer D, Long M, Perez ID, Maret W, Tao N, Forzani E (2019) Total iron measurement in human serum with a smartphone. AIChE Annu Meet Conf Proc 2019-Novem. https://doi.org/10.1109/JTEHM.2020.3005308
354. Yang G, Lv R, He F, Qu F, Gai S, Du S, Wei Z, Yang P (2015) A core/shell/satellite anticancer platform for 808 NIR light-driven multimodal imaging and combined chemo-/photothermal therapy. Nanoscale 7(32):13747–13758. https://doi.org/10.1039/C5NR03085D
355. Liu X, Ren Q, Fu F, Zou R, Wang Q, Xin G, Xiao Z, Huang X, Liu Q, Hu J (2015) CuS@mSiO2-PEG core-shell nanoparticles as a NIR light responsive drug delivery nanoplatform for efficient chemo-photothermal therapy. Dalt Trans 44:10343–10351. https://doi.org/10.1039/c5dt00198f
356. Cao Y, Li S, Chen C, Wang D, Wu T, Dong H, Zhang X (2018) Rattle-type Au@Cu2−xS hollow mesoporous nanocrystals with enhanced photothermal efficiency for intracellular oncogenic microRNA detection and chemo-photothermal therapy. Biomaterials 158:23–33. https://doi.org/10.1016/j.biomaterials.2017.12.009
357. Ding X, Liow CH, Zhang M, Huang R, Li C, Shen H, Liu M, Zou Y, Gao N, Zhang Z, Li Y, Wang Q, Li S, Jiang J (2014) Surface plasmon resonance enhanced light absorption and photothermal therapy in the second near-infrared window. J Am Chem Soc 136:15684–15693. https://doi.org/10.1021/ja508641z
358. Regulacio MD, Ye C, Lim SH, Bosman M, Polavarapu L, Koh WL, Zhang J, Xu QH, Han MY (2011) One-pot synthesis of Cu1.94S-CdS and Cu1.94S-Zn xCd1-xS nanodisk heterostructures. J Am Chem Soc 133:2052–2055. https://doi.org/10.1021/ja1090589

359. Han SK, Gong M, Bin Yao H, Wang ZM, Yu SH (2012) One-pot controlled synthesis of hexagonal-prismatic Cu 1.94S-ZnS, Cu 1.94S-ZnS-Cu 1.94S, and Cu 1.94S-ZnS-Cu 1.94S-ZnS-Cu 1.94S heteronanostructures. Angew Chemie Int Ed 51:6365–6368. https://doi.org/10.1002/anie.201202128
360. Gao Y, Wang L, Tian G, Zang S, Wang H, Niu J, Li LS (2020) Morphology controlled synthesis of composition related plasmonic CuCdS alloy nanocrystals. Front Chem 8:1–8. https://doi.org/10.3389/fchem.2020.628536
361. Sun Z, Yang Z, Zhou J, Yeung MH, Ni W, Wu H, Wang J (2009) A general approach to the synthesis of gold-metal sulfide core-shell and heterostructures. Angew Chemie Int Ed 48:2881–2885. https://doi.org/10.1002/anie.200806082
362. Li Y, Pan G, Liu Q, Ma L, Xie Y, Zhou L, Hao Z, Wang Q (2018) Coupling resonances of surface plasmon in gold nanorod/copper chalcogenide core−shell nanostructures and their enhanced photothermal effect. ChemPhysChem 19:1852–1858. https://doi.org/10.1002/cphc.201701338
363. Dong L, Zhang P, Xu X, Lei P, Du K, Zhang M, Wang D, Feng J, Li W, Zhang H (2018) Simple construction of Cu2-: XS: Pt nanoparticles as nanotheranostic agent for imaging-guided chemo-photothermal synergistic therapy of cancer. Nanoscale 10:10945–10951. https://doi.org/10.1039/c8nr02692k
364. Ha DH, Caldwell AH, Ward MJ, Honrao S, Mathew K, Hovden R, Koker MKA, Muller DA, Hennig RG, Robinson RD (2014) Solid-solid phase transformations induced through cation exchange and strain in 2D heterostructured copper sulfide nanocrystals. Nano Lett 14:7090–7099. https://doi.org/10.1021/nl5035607
365. Willhammar T, Sentosun K, Mourdikoudis S, Goris B, Kurttepeli M, Bercx M, Lamoen D, Partoens B, Pastoriza-Santos I, Pérez-Juste J, Liz-Marzán LM, Bals S, Van Tendeloo G (2017) Structure and vacancy distribution in copper telluride nanoparticles influence plasmonic activity in the near-infrared. Nat Commun 8:1–7. https://doi.org/10.1038/ncomms14925
366. Yang HJ, Chen CY, Yuan FW, Tuan HY (2013) Designed synthesis of solid and hollow Cu2- xTe nanocrystals with tunable near-infrared localized surface plasmon resonance. J Phys Chem C 117:21955–21964. https://doi.org/10.1021/jp407559b
367. Ivanchenko M, Nooshnab V, Myers AF, Large N, Evangelista AJ, Jing H (2022) Enhanced dual plasmonic photocatalysis through plasmonic coupling in eccentric noble metal-nonstoichiometric copper chalcogenide hetero-nanostructures. Nano Res 15:1579–1586. https://doi.org/10.1007/s12274-021-3705-4
368. Zhu H, Wang Y, Chen C, Ma M, Zeng J, Li S, Xia Y, Gao M (2017) Monodisperse dual plasmonic Au@Cu2-xE (E= S, Se) core@shell supraparticles: aqueous fabrication, multimodal imaging, and tumor therapy at in vivo level. ACS Nano 11:8273–8281. https://doi.org/10.1021/acsnano.7b03369
369. Wang F, Li Q, Lin L, Peng H, Liu Z, Xu D (2015) Monodisperse copper chalcogenide nanocrystals: controllable synthesis and the pinning of plasmonic resonance absorption. J Am Chem Soc 137:12006–12012. https://doi.org/10.1021/jacs.5b05591
370. Chowdhury S, Bhethanabotla VR, Sen R (2009) Effect of Ag-Cu alloy nanoparticle composition on luminescence enhancement/quenching. J Phys Chem C 113:13016–13022. https://doi.org/10.1021/jp900294z
371. Li YF, Dong FX, Chen Y, Zhang XL, Wang L, Bi YG, Tian ZN, Liu YF, Feng J, Sun HB (2016) As-grown graphene/copper nanoparticles hybrid nanostructures for enhanced intensity and stability of surface plasmon resonance. Sci Rep 6:1–8. https://doi.org/10.1038/srep37190
372. Li YF, Feng J, Dong FX, Ding R, Zhang ZY, Zhang XL, Chen Y, Bi YG, Sun HB (2017) Surface plasmon-enhanced amplified spontaneous emission from organic single crystals by integrating graphene/copper nanoparticle hybrid nanostructures. Nanoscale 9:19353–19359. https://doi.org/10.1039/c7nr06750j
373. Huang T, Xu Z, Zeng G, Zhang P, Song T, Wang Y, Wang T, Huang S, Wang T, Zeng H (2019) Selective deposition of plasmonic copper on few layers graphene with specific defects for efficiently synchronous photocatalytic hydrogen production. Carbon N Y 143:257–267. https://doi.org/10.1016/j.carbon.2018.11.029
374. Du Y, Wang S, Chen B (2020) A review of biomimetic nanoparticle drug delivery systems based on cell membranes. Drug Des Devel Ther 14:5495–5503. https://doi.org/10.2147/DDDT.S282368
375. Duchene JS, Sweeny BC, Johnston-Peck AC, Su D, Stach EA, Wei WD (2014) Prolonged hot electron dynamics in plasmonic-metal/semiconductor heterostructures with implications for solar photocatalysis. Angew Chem Int Ed 53:7887–7891. https://doi.org/10.1002/anie.201404259
376. Cai Y, Collins SSE, Gallagher MJ, Bhattacharjee U, Zhang R, Chow TH, Ahmadivand A, Ostovar B, Al-zubeidi A, Wang J, Nordlander P, Landes CF, Link S (2019) Single-particle emission spectroscopy resolves d-hole relaxation in copper nanocubes. ACS Energy Lett 4:2458–2465. https://doi.org/10.1021/acsenergylett.9b01747
377. Campillo I, Rubio A, Pitarke JM, Goldmann A, Echenique PM (2000) Hole dynamics in noble metals. Phys Rev Lett 85(15):3241–3244. https://doi.org/10.1103/PhysRevLett.85.3241
378. Knoesel E, Hotzel A, Wolf M (1998) Ultrafast dynamics of hot electrons and holes in copper: excitation, energy relaxation, and transport effects. Phys Rev B 57:812–824. https://doi.org/10.1103/PhysRevB.57.12812
379. Nitopi S, Bertheussen E, Scott SB, Liu X, Engstfeld AK, Horch S, Seger B, Stephens IEL, Chan K, Hahn C, Nørskov JK, Jaramillo TF, Chorkendor I (2019) Progress and perspectives of electrochemical CO 2 reduction on copper in aqueous electrolyte. Chem Rev 119:7610–7672. https://doi.org/10.1021/acs.chemrev.8b00705
380. Seah K, Kuan T, Cheong Y (2013) Advances of Ag, Cu, and Ag – Cu alloy nanoparticles synthesized via chemical reduction route. J Nanopart Res 15:1–29. https://doi.org/10.1007/s11051-013-1537-1
381. Yu S, Wilson AJ, Kumari G, Zhang X, Jain PK (2017). Opportunities and challenges of solar-energy- driven carbon dioxide to fuel conversion with plasmonic catalysts. https://doi.org/10.1021/acsenergylett.7b00640
382. Peterson AA, Abild-Pedersen F, Studt F, Rossmeisl J, Nørskov JK (2010) How copper catalyzes the electroreduction of carbon dioxide into hydrocarbon fuels. Energy Environ Sci 3:1311–1315. https://doi.org/10.1039/c0ee00071j
383. Deng S, Zhang B, Choo P, Smeets PJM, Odom TW (2021) Plasmonic photoelectrocatalysis in copper-platinum core-shell nanoparticle lattices. Nano Lett 21(3):1523–1529. https://doi.org/10.1021/acs.nanolett.0c05029 (Epub 2021 Jan 28)
384. Neatu S, Macia-agullo JA, Concepción P, Garcia H, Neațu Ș, Maciá-Agulló JA, Concepción P, Garcia H (2014) Gold-copper nanoalloys supported on TiO 2 as photocatalysts for CO 2 reduction by water. J Am Chem Soc 136:15969–15976. https://doi.org/10.1021/ja506433k
385. Janczarek M, Wei Z, Endo M, Ohtani B, Kowalska E (2016) Silver- and copper-modified decahedral anatase titania particles as visible light-responsive plasmonic photocatalyst. J Photonics Energy 7:012008. https://doi.org/10.1117/1.jpe.7.012008
386. Zhai Q, Xie S, Fan W, Zhang Q, Wang Y, Deng W, Wang Y (2013) Angewandte Photocatalytic conversion of carbon dioxide with water into methane: platinum and copper (I) oxide co-catalysts with a core – shell structure. Ang Chem Int Ed 52:5776–5779. https://doi.org/10.1002/anie.201301473
387. Andolina CM, Dewar AC, Smith AM, Marbella LE, Hartmann MJ, Millstone JE (2013) Photoluminescent gold-copper nanoparticle alloys with composition-tunable near-infrared emission. J Am Chem Soc 135:5266–5269. https://doi.org/10.1021/ja400569u

388. Kang Q, Wang T, Li P, Liu L, Chang K, Li M, Ye J (2015) Photocatalytic reduction of carbon dioxide by hydrous hydrazine over Au–Cu alloy nanoparticles supported on SrTiO3/TiO2 coaxial nanotube arrays. Ang Chem 127(3):855–859. https://doi.org/10.1002/anie.201409183
389. Tan JZY, Fernández Y, Liu D, Maroto-valer M, Bian J, Zhang X (2012) Photoreduction of CO 2 using copper-decorated TiO 2 nanorod films with localized surface plasmon behavior. Chem Phys Lett 531:149–154. https://doi.org/10.1016/j.cplett.2012.02.016
390. Hajfathalian M, Gilroy KD, Yaghoubzade A, Tan T, Hughes RA, Neretina S (2015) Photocatalytic enhancements to the reduction of 4- nitrophenol by resonantly excited triangular gold-copper nanostructures. J Physi Chem C 119:17308–17315. https://doi.org/10.1021/acs.jpcc.5b04618
391. Schünemann S, Dodekatos G, Tüysüz H (2015) Mesoporous silica supported Au and AuCu nanoparticles for surface plasmon driven glycerol oxidation. Chem Mater 27:7743–7750. https://doi.org/10.1021/acs.chemmater.5b03520
392. Sugano Y, Shiraishi Y, Tsukamoto D, Ichikawa S, Tanaka S, Hirai T (2013) Supported Au-Cu bimetallic alloy nanoparticles: an aerobic oxidation catalyst with regenerable activity by visible-light irradiation. Angew Chemie Int Ed 52:5295–5299. https://doi.org/10.1002/anie.201301669
393. Liu Y, Walker ARH (2010) Monodisperse gold-copper bimetallic nanocubes: facile one-step synthesis with controllable size and composition. Angew. Chemie 122:6933–6937. https://doi.org/10.1002/ange.201001931
394. Chen W, Yu R, Li L, Wang A, Peng Q, Li Y (2010) A seed-based diffusion route to monodisperse intermetallic CuAu nanocrystals. Angew Chemie Int Ed 49:2917–2921. https://doi.org/10.1002/anie.200906835
395. Yin F, Wang ZW, Palmer RE (2011) Controlled formation of mass-selected Cu-Au core-shell cluster beams. J Am Chem Soc 133:10325–10327. https://doi.org/10.1021/ja201218n
396. Sra AK, Ewers TD, Schaak RE (2005) Direct solution synthesis of intermetallic AuCu and AuCu3 nanocrystals and nanowire networks. ChemInform 36:758–766. https://doi.org/10.1002/chin.200519238
397. Wang X, Wang R, Wang J, Fan C, Zheng Z (2020) The synergistic role of the support surface and Au-Cu alloys in a plasmonic Au-Cu@LDH photocatalyst for the oxidative esterification of benzyl alcohol with methanol. Phys Chem Chem Phys 22:1655–1664. https://doi.org/10.1039/c9cp05992j
398. Liu QY, Zhong Y, Jiang ZZ, Chen K, Ma S, Wang PF, Wang W, Zhou L, Luoshan MD, Wang QQ (2020) A controlled growth of triangular AuCu alloy nanostars and high photocatalytic activities of AuCu@CdS heterostars. J Mater Chem C 8:4869–4875. https://doi.org/10.1039/d0tc00098a
399. Christopher P, Xin H, Linic S (2011) Visible-light-enhanced catalytic oxidation reactions on plasmonic silver nanostructures. Nat Chem 3:467–472. https://doi.org/10.1038/nchem.1032
400. Chen S, Jenkins SV, Tao J, Zhu Y, Chen J (2013) Anisotropic seeded growth of Cu-M (M = Au, Pt, or Pd) bimetallic nanorods with tunable optical and catalytic properties. J Phys Chem C 117:8924–8932. https://doi.org/10.1021/jp4013653
401. Yin J, Shan S, Yang L, Mott D, Malis O, Petkov V, Cai F, Shan Ng M, Luo J, Chen BH, Engelhard M, Zhong CJ (2012) Gold-copper nanoparticles: nanostructural evolution and bifunctional catalytic sites. Chem Mater 24:4662–4674. https://doi.org/10.1021/cm302097c
402. He R, Wang YC, Wang X, Wang Z, Liu G, Zhou W, Wen L, Li Q, Wan X, Chen X, Zeng J, Hou JG (2014) Facile synthesis of pentacle gold-copper alloy nanocrystals and their plasmonic and catalytic properties. Nat Commun 5:4327. https://doi.org/10.1038/ncomms5327
403. Yin A, Wen C, Dai WL, Fan K (2011) Nanocasting of CuAu alloy nanoparticles for methyl glycolate synthesis. J Mater Chem 21:8997–8999. https://doi.org/10.1039/c1jm10646e
404. Najafishirtari S, Brescia R, Guardia P, Marras S, Manna L, Colombo M (2015) Nanoscale transformations of alumina-supported AuCu ordered phase nanocrystals and their activity in CO oxidation. ACS Catal 5:2154–2163. https://doi.org/10.1021/cs501923x
405. Liu X, Wang A, Wang X, Mou CY, Zhang T (2008) Au-Cu Alloy nanoparticles confined in SBA-15 as a highly efficient catalyst for CO oxidation. Chem Commun 27:3187–3189. https://doi.org/10.1039/b804362k
406. Jiang Z, Zhang Q, Zong C, Liu BJ, Ren B, Xie Z, Zheng L (2012) Cu-Au alloy nanotubes with five-fold twinned structure and their application in surface-enhanced Raman scattering. J Mater Chem 22:18192–18197. https://doi.org/10.1039/c2jm33863g
407. Oh H, Kim M, Park Y, Ryu S, Song H (2021) Abnormal hypsochromic shifts of surface plasmon scattering by atomic ordering in gold-copper intermetallic nanoparticles. J Phys Chem C. https://doi.org/10.1021/acs.jpcc.1c06555
408. Malola S, Hartmann NJ, Hakkinen H (2015) Copper induces a core plasmon in intermetallic Au(144,145)−xCux(SR)60 nanoclusters. J Phys Chem Lett 6(3):515–20. https://doi.org/10.1021/jz502637b (Epub 2015 Jan 26)
409. Zhu Q, Song X, Deng Z (2020) Tunable charge transfer plasmon at gold/copper heterointerface. Acta Chim Sin 78:675–679. https://doi.org/10.6023/A20050145
410. Singh M, Sinha I, Singh AK, Mandal RK (2011) LSPR and SAXS studies of starch stabilized Ag-Cu alloy nanoparticles. Colloids Surfaces A Physicochem Eng Asp 384:668–674. https://doi.org/10.1016/j.colsurfa.2011.05.037
411. Jiang H, Moon KS, Wong CP (2005) Synthesis of Ag-Cu alloy nanoparticles for lead-free interconnect materials. Proc Int Symp Exhib Adv Packag Mater Process Prop Interfaces 2005:173–177. https://doi.org/10.1109/ISAPM.2005.1432072
412. Tsuji M, Hikino S, Tanabe R, Matsunaga M, Sano Y (2010) Syntheses of Ag/Cu alloy and Ag/Cu alloy core Cu shell nanoparticles using a polyol method. CrystEngComm 12:3900–3908. https://doi.org/10.1039/c0ce00064g
413. Singh M, Sinha I, Mandal RK (2009) Synthesis of nanostructured Ag-Cu alloy ultra-fine particles. Mater Lett 63:2243–2245. https://doi.org/10.1016/j.matlet.2009.07.043
414. Guo X, Hao C, Jin G, Zhu H, Guo X (2014) Copper nanoparticles on graphene support: an efficient photocatalyst for coupling of nitroaromatics in visible light. Angew Chem Int Ed 53:1973–1977. https://doi.org/10.1002/anie.201309482
415. Tan KS, Cheong KY (2013) Advances of Ag, Cu, and Ag-Cu alloy nanoparticles synthesized via chemical reduction route. J Nanoparticle Res 15:1537. https://doi.org/10.1007/s11051-013-1537-1
416. Shi J (2018) Novel Ag-Cu bimetallic alloy decorated near-infrared responsive architectures for efficient photocatalytic water purification Affiliations: Corresponding author. J Colloid Interface Sci. https://doi.org/10.1016/j.jcis.2018.02.005
417. Babu P, Dash SR, Behera A, Vijayaraghavan T, Ashok A, Parida K (2022) Nanoscale advances prominence of Cu in a plasmonic Cu–Ag alloy. Nanoscale Adv 4:150–162. https://doi.org/10.1039/d1na00633a
418. Tian Y, Song Y, Liu J, Ji J, Wang F (2020) MoSx Coated copper nanowire on copper foam as a highly stable photo- electrode for enhanced photoelectrocatalytic hydrogen evolution reaction. Chem Eng J 398:125554. https://doi.org/10.1016/j.cej.2020.125554
419. Liu X, Shi Y, Jin Y, Tana T, Peiris E, Zhang X, Xu F, Waclawik ER, Bottle SE, Zhu H, Sarina S (2022) Surface-plasmon-enhanced transmetalation between copper and palladium nanoparticle

catalyst. Angew Chem Int Ed Engl 61(24):e202203158. https://doi.org/10.1002/anie.202203158 (Epub 2022 Apr 20)
420. Zheng BY, Zhao H, Manjavacas A, Mcclain M, Nordlander P, Halas NJ (2015) Distinguishing between plasmon-induced and photoexcited carriers in a device geometry. Nat Commun 6:7797. https://doi.org/10.1038/ncomms8797
421. Duchene JS, Tagliabue G, Welch AJ, Li X, Cheng WH, Atwater HA (2020) Optical excitation of a nanoparticle Cu/p-NiO photocathode improves reaction selectivity for CO2 reduction in aqueous electrolytes. Nano Lett 20:2348–2358. https://doi.org/10.1021/acs.nanolett.9b04895
422. Zhou L, Swearer DF, Zhang C, Robatjazi H, Zhao H, Henderson L, Dong L, Christopher P, Carter EA, Nordlander P, Halas NJ (2018) Quantifying hot carrier and thermal contributions in plasmonic photocatalysis. Science 362:69–72. https://doi.org/10.1126/science.aat6967
423. Huang Y, Liu Z, Gao G, Xiao G, Bottle SE, Sarina S, Zhu H, Huang Y, Liu Z, Gao G, Xiao G, Du A, Bottle S, Sarina S (2017) Stable copper nanoparticle photocatalysts for selective epoxidation of alkenes with visible light. ACS Catal 7:4975–4985
424. Hattori Y, Messing ME, Pavliuk MV, Gutie S, Czapla-maszta J, Szlachetko J, Silva JL, Araujo CM, Fernandes DLA, Lu L, Kiely CJ, Abdellah M (2019) Hydrated electron generation by excitation of copper localized surface plasmon resonance. J Phys Chem Lett 10:1743–1749. https://doi.org/10.1021/acs.jpclett.9b00792
425. Xiao L, Zhang Q, Chen P, Chen L, Ding F, Tang J, Li YJ, Au CT, Yin SF (2019) Copper-mediated metal-organic framework as efficient photocatalyst for the partial oxidation of aromatic alcohols under visible-light irradiation: synergism of plasmonic effect and schottky junction. Appl Catal B Environ 248:380–387. https://doi.org/10.1016/j.apcatb.2019.02.012
426. Vilar-Vidal N, Blanco MC, López-Quintela MA, Rivas J, Serra C (2010) Electrochemical synthesis of very stable photoluminescent copper clusters. J Phys Chem C 114:15924–15930. https://doi.org/10.1021/jp911380s
427. De Investigaciones C, Conicet O, Videla F (2013) Plasmon spectroscopy for subnanometric Copper particles: dielectric function and core–shell sizing. Plasmonics 8:341–348. https://doi.org/10.1007/s11468-012-9395-8
428. Chuang CC, Chu HC, Huang SB, Chang WS, Tuan HY (2020) Laser-induced plasmonic heating in copper nanowire fabric as a photothermal catalytic reactor. Chem Eng J 379:122285. https://doi.org/10.1016/j.cej.2019.122285
429. Dong L, Ji G, Liu Y, Xu X, Lei P, Du K, Song S, Feng J, Zhang H (2018) Multifunctional Cu-Ag2S nanoparticles with high photothermal conversion efficiency for photoacoustic imaging-guided photothermal therapy: in vivo. Nanoscale 10:825–831. https://doi.org/10.1039/c7nr07263e
430. Zhong W, Zhu H, Sheng F, Tian Y, Zhou J, Chen Y, Li S, Lin J (2014) Activation of the MAPK11/12/13/14 (p38MAPK) pathway regulates the transcription of autophagy genes in response to oxidative stress induced by a novel copper complex in HeLa cells. Autophagy 14:1285–1300. https://doi.org/10.4161/auto.28789
431. Zhang Y, Sha R, Zhang L, Zhang W, Jin P, Xu W, Ding J, Lin J, Qian J, Yao G, Zhang R, Luo F, Zeng J, Cao J, Wen LP (2018) Harnessing copper-palladium alloy tetrapod nanoparticle-induced pro-survival autophagy for optimized photothermal therapy of drug-resistant cancer. Nat Commun 9:4236. https://doi.org/10.1038/s41467-018-06529-y
432. Ayyappan S, Scarpellini A, Manna L (2014) Alloyed copper chalcogenide nanoplatelets via partial cation exchange reactions. ACS Nano 8:8407–8418. https://doi.org/10.1021/nn502906z
433. Tan JMR, Lee YH, Pedireddy S, Baikie T, Ling XY, Wong LH (2014) Understanding the synthetic pathway of a single-phase quarternary semiconductor using surface-enhanced Raman scattering: a case of wurtzite Cu2ZnSnS4 nanoparticles. J Am Chem Soc 136:6684–6692. https://doi.org/10.1021/ja501786s (Epub 2014 Apr 24)
434. Jhuang LS, Kumar G, Chen FC (2021) Localized surface plasmon resonance of copper nanoparticles improves the performance of quasi-two-dimensional perovskite light-emitting diodes. Dye Pigment 188:109204. https://doi.org/10.1016/j.dyepig.2021.109204
435. Liu Z, Lee SY, Lee E, Liu Z, Lee SY, Lee E (2014) Copper nanoparticle incorporated plasmonic organic bulk-heterojunction solar cells. Appl Phys Lett 105:223306. https://doi.org/10.1063/1.4903749
436. Huang CL, Kumar G, Sharma GD, Chen FC (2020) Plasmonic effects of copper nanoparticles in polymer photovoltaic devices for outdoor and indoor applications. Appl Phys Lett 116:253302. https://doi.org/10.1063/5.0010427
437. Parveen F, Sannakki B, Jagtap CV (2017) Electrodeposited copper nanoparticles: plasmon enhanced performance of TiO2 for dye sensitized solar cell. J Mater Sci Mater Electron 28:5082–5087. https://doi.org/10.1007/s10854-016-6149-y
438. Ezugwu SC (2012) Synthesis and characterization of copper nanoparticles and copper-polymer nanocomposites for plasmonic photovoltaic applications, i–133. Electronic Thesis and Dissertation Repository. 1025
439. Sugawa K, Yamaguchi D, Tsunenari N, Uchida K, Tahara H, Takeda H, Tokuda K, Jin S, Kusaka Y, Fukuda N, Ushijima H, Akiyama T, Watanuki Y, Nishimiya N, Otsuki J, Yamada S (2017) Efficient photocurrent enhancement from porphyrin molecules on plasmonic copper arrays: beneficial utilization of copper nanoanntenae on plasmonic photoelectric conversion systems. ACS Appl Mater Interfaces 9:750–762. https://doi.org/10.1021/acsami.6b13147
440. Zhang Y, Zhou N, Zhang K, Yan F (2017) Plasmonic copper nanowire@TiO2nanostructures for improving the performance of dye-sensitized solar cells. J Power Sources 342:292–300. https://doi.org/10.1016/j.jpowsour.2016.12.068
441. Barr D, Edwards AJ, Paver MA, Raithby PR, Rennie M, Russell CA, Wright DS (1994) [{$Sb_2(Ncy)_4$}$_2Cu_4$]: a mixed-metal antimony(III)/copper(I) complex containing a Cu4 square plane. Angew Chem Int Ed 33:1875–1876. https://doi.org/10.1002/anie.199418751
442. Zhang X, Kanatzidis MG (1994) AMTeS3 (A = K, Rb, Cs; M = Cu, Ag): a new class of compounds based on a new polychalcogenide anion, TeS32-. J Am Chem Soc 116:1890–1898. https://doi.org/10.1021/ja00084a032
443. Singh A, Coughlan C, Laffir F, Ryan KM (2012) Assembly of CuIn1-xGaxS2 nanorods into highly ordered 2D and 3D superstructures. ACS Nano 6:6977–6983. https://doi.org/10.1021/nn301999b
444. Cuyfesnx XS, Suekuni K, Tsuruta K, Ariga T, Koyano M, Suekuni K, Tsuruta K, Ariga T, Koyano M (2017) Variable-range-hopping conduction and low thermal conductivity in chalcogenide spinel $Cu_yFe_4Sn_{12}X_{32}$ (X = S, Se). J Appl Phys 109:083709. https://doi.org/10.1063/1.3569624
445. Riha SC, Parkinson BA, Prieto AL (2011) Compositionally tunable Cu2ZnSn(S(1–x)Se(x))4 nanocrystals: probing the effect of Se-inclusion in mixed chalcogenide thin films. J Am Chem Soc 133(39):15272–15275. https://doi.org/10.1021/ja2058692 (Epub 2011 Sep 13)
446. Wang J, Hu J, Guo Y, Wan L (2012) Wurtzite Cu 2 ZnSnSe 4 nanocrystals for high-performance organic – inorganic hybrid photodetectors. NPG Asia Mater 4:e2. https://doi.org/10.1038/am.2012.2
447. Singh A, Geaney H, Laffir F, Ryan KM (2012) Colloidal synthesis of wurtzite Cu 2 ZnSnS 4 nanorods and their perpendicular assembly. J Am Chem Soc 134:2910–2913
448. Mechanism F (2012) Colloidal nanocrystals of wurtzite-type Cu 2 ZnSnS 4: facile noninjection synthesis and formation

mechanism. Chem Eur J 18:3127–3131. https://doi.org/10.1002/chem.201103635
449. De Trizio L, Figuerola A, Manna L, Genovese A, George C, Brescia R, Saghi Z, Simonutti R, Van Huis M, Falqui A (2012) Size-tunable, hexagonal plate-like Cu 3P and Janus-like Cu-Cu 3P nanocrystals. ACS Nano 6:32–41. https://doi.org/10.1021/nn203702r
450. Ma R, Wu D, Liu Y, Ye H, Sutherland D (2020) Copper plasmonic metamaterial glazing for directional thermal energy management. Mater Des 188:108407. https://doi.org/10.1016/j.matdes.2019.108407
451. Zhou Z, Hu K, Ma R, Yan Y, Ni B, Zhang Y, Wen L (2016) Dendritic platinum – copper alloy nanoparticles as theranostic agents for multimodal imaging and combined chemophotothermal therapy. Adv Funct Mater 26:5971–5978. https://doi.org/10.1002/adfm.201601754
452. Zhang Y, Zhang J, Li Z, Qin Z, Sharma S, Li G (2023) Atomically precise copper dopants in metal clusters boost up stability, fluorescence, and photocatalytic activity. Commun Chem 6:1–8. https://doi.org/10.1038/s42004-023-00817-5
453. Song Y, Li Y, Zhou M, Liu X, Li H, Wang H, Shen Y (2021) Ultrabright Au@Cu14 nanoclusters: 71.3 % phosphorescence quantum yield in non-degassed solution at room temperature. Sci Adv 7:eabd2091. https://doi.org/10.1126/sciadv.abd2091
454. Wu Y (2011) The optical properties of Cu-Ni nanoparticles produced via pulsed laser dewetting of ultrathin fi lms : the effect of nanoparticle size and composition on the plasmon response 26:277–287. https://doi.org/10.1557/jmr.2010.9
455. Manna G, Bose R, Pradhan N (2013) Semiconducting and plasmonic copper phosphide platelets. Angew Chem Int Ed 26:6762–6766. https://doi.org/10.1002/anie.201210277
456. De Trizio L, Gaspari R, Bertoni G, Kriegel I, Moretti L, Scotognella F, Maserati L, Zhang Y, Messina GC, Prato M, Marras S, Cavalli A, Manna L (2015) Cu3- xP nanocrystals as a material platform for near-infrared plasmonics and cation exchange reactions. Chem Mater 27:1120–1128. https://doi.org/10.1021/cm5044792
457. Cu P, Colloidal P, Sun T, Wang Y, Yu W, Wang Y, Dai Z, Liu Z (2017) Flexible broadband graphene photodetectors enhanced by plasmonic Cu3−xP colloidal nanocrystals. Small 13:1701881. https://doi.org/10.1002/smll.201701881
458. Bertoni G, Ramasse Q, Brescia R, de Trizio L, de Donato F, Manna L (2019) Direct quantification of Cu vacancies and spatial localization of surface plasmon resonances in copper phosphide nanocrystals. ACS Mater Lett 1:665–670. https://doi.org/10.1021/acsmaterialslett.9b00412
459. Schmidt F, Ditlbacher H, Hohenester U, Hohenau A, Hofer F, Krenn JR (2012) Dark plasmonic breathing modes in silver nanodisks. Nano Lett 12:5780–5783. https://doi.org/10.1021/nl3030938
460. Liu Z, Mu H, Xiao S, Wang R, Wang Z, Wang W, Wang Y, Zhu X, Lu K, Zhang H, Lee ST, Bao Q, Ma W (2016) Pulsed lasers employing solution-processed plasmonic Cu3-xP colloidal nanocrystals. Adv Mater 18:3535–3542. https://doi.org/10.1002/adma.201504927 (Epub 2016 Mar 10)
461. Tahir M, Tahir B, Nawawi MGM, Hussain M, Muhammad A (2019) Applied Surface Science Cu-NPs embedded 1D / 2D CNTs / pCN heterojunction composite towards enhanced and continuous photocatalytic CO 2 reduction to fuels. Appl Surf Sci 485:450–461. https://doi.org/10.1016/j.apsusc.2019.04.220
462. Wei Z, Wang Z, Fan G, Xu C, Shi G, Zhang G, Liu Y, Fan R (2021) Low-frequency plasmonic state and negative permittivity in copper/titanium dioxide percolating composites. Ceram Int 47:2208–2213. https://doi.org/10.1016/j.ceramint.2020.09.060
463. Wang Z, Sun K, Xie P, Liu Y, Gu Q, Fan R, Wang J (2020) Epsilon-negative BaTiO3/Cu composites with high thermal conductivity and yet low electrical conductivity. J Mater 6:145–151. https://doi.org/10.1016/j.jmat.2020.01.007
464. Tsutaoka T, Fukuyama K, Kinoshita H, Kasagi T, Yamamoto S, Hatakeyama K (2013) Negative permittivity and permeability spectra of Cu/yttrium iron garnet hybrid granular composite materials in the microwave frequency range. Appl Phys Lett 103:10–15. https://doi.org/10.1063/1.4858976
465. Massango H, Kono K, Tsutaoka T, Kasagi T, Yamamoto S, Hatakeyama K (2018) Percolation-induced plasmonic state and double negative electromagnetic properties of Ni-Zn Ferrite/Cu granular composite materials. J Magn Magn Mater 454:320–326. https://doi.org/10.1016/j.jmmm.2018.01.058
466. Tsutaoka T, Kasagi T, Yamamoto S, Hatakeyama K (2013) Low frequency plasmonic state and negative permittivity spectra of coagulated Cu granular composite materials in the percolation threshold. Appl Phys Lett 102:1–5. https://doi.org/10.1063/1.4804379
467. Harding GL (2014) Sputtered metal carbide solarselective absorbing surfaces 1070:10–13. https://doi.org/10.1116/1.569075
468. Content R (1982) Surface texturing of copper by sputter etching with applications for solar selective absorbing surfaces 1325:1320–1325
469. Harding GL, Window B (1979) Graded metal carbide solar selective surfaces coated onto glass tubes by a magnetron sputtering system. J Vac Sci Technol 16:2101–2104. https://doi.org/10.1116/1.570348
470. Harding GL, Craig S (1979) Magnetron-sputtered metal carbide solar selective absorbing surfaces. J Vac Sci Technol 16:857–862. https://doi.org/10.1116/1.570100
471. Harding GL (1978) Sputtered metal silicide solar selective absorbing surfaces. J Vac Sci Technol 15:65–69. https://doi.org/10.1116/1.569439
472. Harding GL, McKenzie DR, Window B (1976) Dc Sputter coating of solar-selective surfaces onto tubes. J Vac Sci Technol 13:1073–1075. https://doi.org/10.1116/1.569076
473. Teixeira V, Sousa E, Costa MF, Nunes C, Rosa L, Carvalho MJ, Collares-Pereira M, Roman E, Gago J (2001) Spectrally selective composite coatings of Cr-Cr2O3 and Mo-Al2O3 for solar energy applications. Thin Solid Films 392:320–326. https://doi.org/10.1016/S0040-6090(01)01051-3
474. Nunes C, Teixeira V, Prates ML, Barradas NP, Sequeira AD (2003) Graded selective coatings based on chromium and titanium oxynitride. Thin Solid Films 442:173–178. https://doi.org/10.1016/S0040-6090(03)00967-2
475. Barshilia HC, Kumar P, Rajam KS, Biswas A (2011) Structure and optical properties of AgAl2O3 nanocermet solar selective coatings prepared using unbalanced magnetron sputtering. Sol Energy Mater Sol Cells 95:1707–1715. https://doi.org/10.1016/j.solmat.2011.01.034
476. Graf W, Brucker F, Köhl M, Tröscher T, Wittwer V, Herlitze L (1997) Development of large area sputtered solar absorber coatings. J Non Cryst Solids 218:380–387. https://doi.org/10.1016/S0022-3093(97)00283-4
477. Kresin VZ, Morawitz H (1988) Plasmon and phonon mechanisms of superconductivity in the layered high Tc copper-oxides. Phys C Supercond Its Appl 153–155:1327–1328. https://doi.org/10.1016/0921-4534(88)90304-8
478. Kyamo MJ, Alsalhin AA, Premkumar N, Miao S, Lail BA (2021) Ultrahigh mid-infrared electric field enhancement via nanoantenna plasmonic resonance coupled to a novel hyperbolic metalens. J Mod Opt 68:394–402. https://doi.org/10.1080/09500340.2021.1900438
479. Li Y, Hao Z, Cao H, Wei S, Jiao T, Wang M (2023) Study on annealed graphene oxide nano-sheets for improving the surface

enhanced fluorescence of silver nanoparticles. Opt Laser Technol 160:109054. https://doi.org/10.1016/j.optlastec.2022.109054
480. Alsalhin A, Finch MF, Lail BA (2018) Coupling between metallic structure and phonon polaritons for sensing applications. Metamaterials, metadevices, and metasystems 2018, vol 10719. SPIE, pp 84–93. https://doi.org/10.1117/12.2321293
481. Song X, Wang M, Wang S, Cheng Z, Zhang T, Zhu T, Song H, Yu L, Xu J, Chen K (2022) A wide temperature solid-state Li–S battery enabled by a plasmon-enhanced copper–silicon nanowire photothermal current collector. J Mater Chem A 10:22584–22591. https://doi.org/10.1039/D2TA04343B
482. Chung JS, Sohn HJ (2002) Electrochemical behaviors of CuS as a cathode material for lithium secondary batteries. J Power Sources 108:226–231. https://doi.org/10.1016/S0378-7753(02)00024-1
483. Amiri IS, Alwi SAK, Raya SA, Zainuddin NAAM, Rohizat NS, Rajan MSM, Zakaria R (2023) Graphene oxide effect on improvement of silver surface plasmon resonance D-shaped optical fiber sensor. J Opt Commun 44:53–60. https://doi.org/10.1515/joc-2019-0094
484. Alsalhin AA, Lail BA (2021) A systematic investigation of coupling between dark and bright polaritons for infrared sensing design. IEEE Sens J 21:14899–14905. https://doi.org/10.1109/JSEN.2021.3074177